Developing a Thermodynamic Model for the U-Pd-Rh-Ru Quaternary System for Use in the Modelling of Nuclear Fuel

by

Lian Cheng Wang

A thesis submitted to the
School of Graduate and Postdoctoral Studies in partial
fulfillment of the requirements for the degree of

Doctor of Philosophy in Nuclear Engineering

The Faculty of Energy Systems and Nuclear Science

University of Ontario Institute of Technology

Oshawa, Ontario, Canada

December 2018

THESIS EXAMINATION INFORMATION

Submitted by: **Lian Cheng Wang**

Doctor of Philosophy in **Nuclear Engineering**

Thesis title: Developing a Thermodynamic Model for the U-Pd-Rh-Ru Quaternary System for Use in the Modelling of the Nuclear Fuel

An oral defense of this thesis took place on November 28, 2018 in front of the following examining committee:

Examining Committee:

Chair of Examining Committee	Dr. Jennifer McKellar
Research Supervisor	Dr. Matthew Kaye
Examining Committee Member	Dr. Brian Ikeda
Examining Committee Member	Dr. Anthony Waker
University Examiner	Dr. Benjamin Rouben
External Examiner	Dr. Michael Welland, Canadian Nuclear Laboratories

The above committee determined that the thesis is acceptable in form and content and that a satisfactory knowledge of the field covered by the thesis was demonstrated by the candidate during an oral examination. A signed copy of the Certificate of Approval is available from the School of Graduate and Postdoctoral Studies.

Author's Declaration

I hereby declare that this thesis consists of original work of which I have authored. This is a true copy of the thesis, including any required final revisions, as accepted by my examiners.

I authorize the University of Ontario Institute of Technology to lend this thesis to other institutions or individuals for the purpose of scholarly research. I further authorize University of Ontario Institute of Technology to reproduce this thesis by photocopying or by other means, in total or in part, at the request of other institutions or individuals for the purpose of scholarly research. I understand that my thesis will be made electronically available to the public.

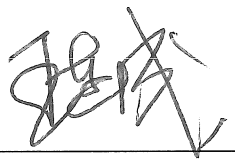

Lian Cheng Wang

December 19, 2018

Abstract

Ruthenium, rhodium, and palladium are fission products in nuclear fuels. These elements and their compounds change the properties of fuel pellets. Phase diagrams involving uranium have been constructed experimentally to study fission product behaviour, specifically diagrams containing the very stable UMe_3 (where Me = Ru, Rh, or Pd) compounds. Discrepancies such as enthalpies of formation of U_xMe_y compounds exist in both experimental binary phase diagram constructions and thermodynamic property determinations. To model the behaviour of fission products in irradiated nuclear fuels, codes (*e.g.*, BISON or RNFTT (RMC Nuclear Fuel Thermochemical Treatment) have been developed. For quantitative studies, existing experimental data are insufficient for such tasks because of difficulties determining data in ranges of composition and temperature. Experimental binary phase diagrams provide phase equilibrium information, yet if not thermodynamically evaluated, the data will be limited in application. Because industrial processes usually involve multicomponent systems that vary in wide ranges of composition and temperature. For some elements with potential catalytic functions (*e.g.*, Pd), the U-Pd phase diagrams presented in the literature were inconsistent so it was a challenge to choose which experimental data should be used for a thermodynamic evaluation. Post irradiation examinations showed that the composition of irradiated nuclear fuels are complicated. For such complex systems, experimental determination of a full set of data is practically impossible. Nevertheless, the possibility of constructing such complex systems by means of thermodynamic evaluation exists. In this work, thermodynamic evaluations of the U-Ru, U-Rh, and U-Pd binary phase diagrams were assessed or re-assessed (*e.g.*, the U-Ru system). In combination with three binary systems previously assessed, a self-consistent quaternary system (U-Pd-Rh-Ru) was constructed. An alternative strategy in optimizing the Gibbs energy functions of various phases, capable of identifying experimental fallacies in hand drawn U-Rh and U-Pd phase diagrams, was proposed. With this quaternary model, two existing ternary experimental phase diagrams were critically evaluated. Results show that without thermodynamic evaluations some experimental data were wrongly interpreted. The establishment of the quaternary model enriches thermodynamic databases and will potentially improve the performance of the RNFTT treatment and codes such as BISON.

Keywords: Phase diagrams; Thermodynamic modelling; Nuclear fuel safety; Fission product inventory.

Statement of Contributions

Some of the results in this thesis were published in conference proceedings, under the direction of my thesis supervisor Dr. M.H. Kaye. These five papers are detailed here and referenced in the thesis where appropriate:

L. Wang and M.H. Kaye, "A re-examination of thermodynamic modelling of U-Ru phase diagram", in *35th Annual Conference of the Canadian Nuclear Society*, Saint John, (2015).

M.H. Kaye and L. Wang, "U-Ru-Rh-Pd quaternary system: Thermodynamic calculations and experimental explorations", in *Proceedings of the 36th Annual Conference of the Canadian Nuclear Society*, Toronto, 2016.

M.H. Kaye and L. Wang, "An alternative strategy for thermodynamic evaluations of experimental U-Me phase diagrams to resolve considerable experimental discrepancies", in *Proceedings of the 36th Annual Conference of the Canadian Nuclear Society*, Toronto, 2016.

L. Wang and M.H. Kaye, "The Other Metallic Phase in Spent Nuclear Fuel - A Complete Thermodynamic Evaluation of the U-Pd-Rh-Ru System", *Proceedings of the 13th International Conference on CANDU Fuel*, Kingston, ON, (2016).

M.H. Kaye and L. Wang, "A Proposed Catalytic Mechanism of Pd on the Formation of UBe_{13} in Experimental Construction of U-Pd Phase Diagrams", in *Proceedings of the 37th Annual Conference of the Canadian Nuclear Society*, Niagara Falls, (June 2017).

I have used standard referencing practices to acknowledge ideas, research techniques, or other materials that belong to others. Furthermore, I hereby certify that I am the sole source of the creative works and/or inventive knowledge described in this thesis.

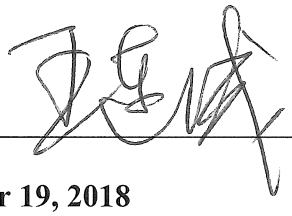

Lian Cheng Wang

December 19, 2018

Table of Contents

List of Figures

List of Tables

List of Symbols

a	Lattice parameter of a crystal (in pm).
a_i	Chemical activity of species *i*.
a_i	Parameter in the Margules expression; associated with enthalpy.
A	Area of a specific lattice plane in substitutional interdiffusion.
A_i	Parameter in the Redlich-Kister expression; associated with enthalpy.
α	Designation given to the crystal structure of the lowest temperature form for an element with several allotropic forms.
α1 and α2	Two immiscible *fcc* phases in U-Rh-Ru ternary phase diagram specified by Kleykamp and Kang [37].
α_{12}	Interaction parameter used by Kleykamp and Kang [37].
b_i	Parameter in the Margules expression; associated with entropy.
B_i	A parameter in the Redlich-Kister expression; associated with entropy.
β	Designation given to the crystal structure of the second lowest temperature form for an element with several allotropic forms.
C_P	Heat capacity ($J \cdot mol^{-1} \cdot K^{-1}$).
C_0	The total number of atoms per unit volume as a constant.
C_i	Concentration of atom type *i*.
E or Ex	Excess, especially used for excess Gibbs energy.
ϕ	An arbitrary phase.
G	Gibbs energy.
G_A	Molar Gibbs energy of component A.
G(Added)	A Gibbs energy difference defined in FactSage for energy referencing.
G^{Excess}	Excess Gibbs energy of mixing.
G_i^{Excess}	Excess Gibbs energy of component *i*.
G_i^{ϕ}	Gibbs energy of species *i* in phase ϕ.
G_p^{Excess}	Excess Gibbs energy at point p (a composition in a ternary system).
G^{ideal}	Ideal Gibbs energy.
$G^{M,ideal}$	Ideal Gibbs energy of mixing.
G_A°	Gibbs energy of component A; also called the lattice stability of A.
$G_A^{\circ,\phi}$	Gibbs energy of component A in phase ϕ.
$\bar{G}_i^{\phi}$	Partial Gibbs energy of species *i* in phase ϕ.
$\bar{G}_i^{E,\phi}$	Partial Excess Gibbs energy of species *i* in phase ϕ.
ΔG_{ϕ}^{M}	Change of Gibbs energy of mixing in phase ϕ.
γ	Designation given to the crystal structure of the third lowest temperature form for an element with several allotropic forms.

γ_i	Activity coefficient of species *i*, which represents the deviation from ideal behaviour.
h_n	Enthalpy contribution from the n^{th} term of an excess Gibbs Energy series ($J \cdot mol^{-1}$).
H	Enthalpy ($J \cdot mol^{-1}$).
$\Delta H^{\circ}_{298\ K}$	Standard enthalpy of formation at 298 K ($J \cdot mol^{-1}$).
$H°$	Standard enthalpy ($J \cdot mol^{-1}$).
ΔH°_{A}	Standard enthalpy change of A ($J \cdot mol^{-1}$).
J_i	Flux of atom type *i*.
J'_A	The flux across a thin layer of the material.
L^{ϕ}_{AB}	Interaction parameter between component A and B for phase ϕ.
L^{n}_{ij}	The n^{th} interaction parameter between species *ij*.
Liq.	*Liquid* (phase).
M_e	Metal; in this work, a subgroup of platinum metals (*i.e.*, Pd, Rh, or Ru).
μ	Chemical potential.
μ_A	Chemical potential of component A.
μ_i^{ϕ}	Chemical potential of component *i* in phase ϕ.
n_i	Number of moles for species *i*.
p_i	The shortened expression of $a_i + b_i T$, in which *a* and *b* represent the coefficients of species *i* in an interaction parameter.
P	Pressure
R	Molar gas constant; value depends on the units of volume and pressure, *e.g.*, $R=8.314\ J \cdot mol^{-1} \cdot K^{-1}$.
S_n	Entropy contribution in n^{th} term of excess Gibbs energy series ($J \cdot mol^{-1} \cdot K^{-1}$).
S	Entropy ($J \cdot mol^{-1} \cdot K^{-1}$).
$S°$	Standard entropy ($J \cdot mol^{-1} \cdot K^{-1}$).
$S^{\circ}_{298\ K}$	Standard entropy at 298 K ($J \cdot mol^{-1} \cdot K^{-1}$).
T	Temperature; unless otherwise stated, temperature is measured in Kelvin.
T_B	Boiling temperature.
T_{eu}	Eutectic temperature.
T_M	Melting temperature.
X_i	Mole fraction of species *i*.
Z	Atomic number of elements.

List of Acronyms

ACTINET	The Europe Actinide Network.
ASM	American Society for Metals (since 1913, now ASM International).
ASTEC-SOPHAEROS	A severe accident and aerosol transport code developed by the French.
BISON	Code developed by the Idaho National Laboratory.
CALPHAD	CALculation of PHAse Diagrams.
CANDU	Canadian Deuterium Uranium.
ChemSage	A thermochemical database which was incorporated into FactSage in 2001.
CMA	Complex metallic alloys.
CNS	Canadian Nuclear Society.
cph	Close packed hexagonal.
CRP	A coordinated research program conducted by IAEA since 1993.
dhcp	Or dcph, a derivative cph crystal structure.
DTA	Differential Thermal Analysis.
EPMA	Electron probe micro-analysis.
fcc	Face centred cubic.
FACT	Facility for the Analysis of Chemical Thermodynamics.
FactSage	A merged name of FACT and ChemSage since 2001.
FP	Fission Product (plural is FPs for Fission Products).
FUMEX	Fuel modelling at extended burnup, CRP programs by IAEA.
HRMECS	High-resolution medium energy chopper spectrometer.
IAEA	International Atomic Energy Agency.
INL	Idaho National Laboratory.
K&K	Kleykamp and Kang (when used in tables).
LDA	The local-density approximation.
LMTO	Linear muffin tin orbital.
LOCA	Loss-of-coolant accident.
LSDA	The local-spin-density approximation.
LWR	Light water reactor.
MOX	Mixed Oxide nuclear fuel (*e.g.*, UO_2/PuO_2).
NIST	National Institute of Standards and Technology.
ORIGEN-2	Oak Ridge Isotope GENeration – a code to calculate the fission product inventory at a specified reactor condition and time.
RK	Redlich-Kister formalism.
RLDA	The relativistic local-density approximation.

RMCC	Royal Military College of Canada.
RNFTT	Royal Military College of Canada Nuclear Fuel Thermochemical Treatment.
SCALES-5	The ORIGEN code, adapted for use with CANDU fuels and reactors.
ScRLDA	The scalar-relativistic local-density approximation.
SEM	Scanning electron microscope.
SGTE	Scientific Group Thermodata Europe.
TA	Thermal analysis.
XRD	X-ray diffractometry.

1 Introduction

Nuclear energy is considered to be one of the cleanest energy forms. While CO_2 emissions are minimised in the energy production process, fission products are generated as the fissile nuclides split and radioactive fission products decay. As the fission products accumulate, their distribution within different phases in the fuel changes depending on the operating conditions and the fuel used. There are various forms of the fission products in used fuels including fission gases, metallic inclusions, and solid solutions (either metallic or oxides) formed within the fuel pellet. These affect the fuel chemistry and may change the volume or the shape of the fuel pellets, as well as the heat transfer efficiency of the reactors. Furthermore, understanding the changes in chemistry of the fuel is the first step to the studies of potential accident scenarios (*e.g.*, a LOCA or loss-of-coolant accident).

Except for the severe impact of the generation of the gaseous fission products, solid fission products in UO_2 fuel also contribute to deformation of the fuel pellets, such as swelling and sagging of the pellets caused by the change of physical and chemical properties in different locations. The "bambooing" and "hourglassing" of the pellets exert stress and strain on the zirconium cladding. Over time, in combination with the formation of gaseous fission products and corrosion of cladding, serious deformation or even breach of cladding, may, occur and the consequences can be potentially fatal to the safety of the nuclear plant operation [1].

Thermochemistry involves reactions of various solution phases which must be treated properly, and the best way to do this often is achieved by the assessment of equilibrium phase diagrams of the constituent elements of those solution phases. Since the 1940s, many phase diagrams involving uranium have been constructed for developing

nuclear weapons, and then after the war for the peaceful harnessing of nuclear fission for energy production. The process involves radioactive elements and many transition elements, which may cause obstacles in high temperature measurements. In practice, multicomponent systems are usually involved and an experimental determination of the phase diagrams is usually costly, time consuming, and includes careful handling of the materials to avoid exposure to radiation.

To construct a multicomponent phase diagram by means of thermodynamic evaluation, the binary experimental subsystems have to be evaluated (*i.e.*, described thermodynamically) prior to a multicomponent model can be established. In practice, for many systems, high temperature measurements become one of the obstacles to precisely determining features such as the liquidus of the refractory element rich part of the diagram. For instance, the accepted melting point of Ru is 2607 ± 3 K (2334 ± 3 ºC). To measure such a high temperature is difficult using thermocouples as this temperatures is either beyond or pushing the upper limits of the operating range of most thermocouples (*e.g.*, K-type (chromel-alumel) T_{max} 1372 ºC; Type B (70%Pt/30%Rh–94%Pt/6%Rh, by mass) T_{max} = 1820 ºC; and Type C (95%W/5%Re–74%W/26%Re, by mass) T_{max} = 2350 ºC [2,3]). Thus, thermocouples are not suitable for determining the Ru-rich liquidus in an alloy system involving Ru (*e.g.*, Ru–U) at high (or elevated) temperatures. Pyrometers, often a good alternative for these purposes, can also be problematic. For example, in the work on the Ru-U system, Mason and El-Genk [4] had to use their eyes (the so-called "spot method") as the instrument failed to judge the liquidus boundary automatically. In addition, in any phase diagram determination, a container for the samples (*e.g.*, a crucible) is needed. For some refractory elements, it is difficult to eliminate the possibility of

reactions of the constituents in a sample with that of a crucible (in other words the crucible becomes part of an even more complicated system) at high temperatures. All these factors have led to discrepancies in experimental data from different research groups, and will be discussed as part of this work.

Studies of the U-Pd-Rh-Ru quaternary system exhibit all these problems, and this is especially true for the U-Pd system. For example, a contamination reaction catalyzed by the noble elements involved in the quaternary system may introduce false phase boundaries into the phase diagrams. All the six platinum metals (Ru, Rh, Pd, Os, Ir, and Pt) are effective catalysts for various processes, and Pd is the best candidate for nanoparticle catalysts [5]. This aspect is so important for this work that a special section in this thesis (See Section 6.6.2 in Chapter 0) is devoted to it.

To study future nuclear fuel fabrication and fission product behaviour, various thermodynamic databases have been utilized or are in development. Considering the potential application of the models for the U-Pd-Rh-Ru quaternary system and thermodynamic databases in the future industry codes, a quick summary of these follows.

The SGTE (Scientific Group Thermodata Europe) database [6] provides basic data and Gibbs energy functions for 78 elements used in thermodynamic assessments. Fuelbase [7,8] is a database of binary and ternary systems related to nuclear fuel designs with multicomponent systems under development within the European Actinide Network (ACTINET). The RNFTT (the Royal Military College of Canada Nuclear Fuel Thermochemical Treatment) [9-11] is a comprehensive thermodynamic database including an U-O binary system, solutes in UO_2, noble metals (the so-called “white” or “five metal”

inclusions, specifically Mo-Tc-Ru-Rh-Pd), non-fluorite oxide phases, a rhombohedral oxide phase, and the "other metallic phase" (UPd_3-URh_3-URu_3) [9,10]. In this database, the U-O binary system and Mo-Tc-Ru-Rh-Pd system are well developed, but some of the other systems are not. For example, the "other metallic phase" (UPd_3-URh_3-URu_3) is described only with three Gibbs energy functions for the solid phases of the three compounds. Without thermodynamically assessed binary phase diagrams for U-Ru, U-Rh, and U-Pd, equilibrium calculations with the present RNFTT database, while possible, are not necessarily accurate, and therefore, the application of the database is open to potential error (See Section 1.1). This work aims to expand the database by establishing thermodynamic models of the U-Pd, U-Rh, and U-Ru binary systems, combine them with the existing models for Pd-Rh-Ru, and extrapolate to the U-Pd-Rh-Ru quaternary system. By this means, many non-existing thermodynamic properties and other data can be obtained and used in future industry codes.

While solving the complicated thermochemistry is an achievement in itself, much of the value in being as accurate as possible with the thermochemistry is so that these models and treatments can be incorporated into other industrial codes that try to predict complex behaviour (*e.g.*, fuel performance). According to an IAEA report [12], dozens of nuclear industrial codes are now available. One of the more prominent codes is the BISON code developed by the Idaho National Laboratory (INL). BISON is a finite element based code that attempts to explain nuclear fuel behaviour by solving, in parallel, a series of coupled non-linear partial differential equations [13]. According to the authors of this paper, although it is a next-generation multidimensional fuel performance code [13], so far it is mainly limited to LWR fuel rod calculations. The validation results of the code show

that in the early life of the fuel, the code over-predicts the clad diameter reduction; while when fuel expansion controls the mechanical response, which is later in the life of the fuel, the code significantly over-predicts the diameter increase in the cladding [13]. Possible reasons for this are that neither a thermodynamic database is included nor thermodynamic equations are used in the code. To make the code better, more thermodynamic information of related systems should be developed and added to these codes because the deformation of the fuel rods is not merely caused by the generation of the gaseous phase, but also the thermal and mechanical deformation because of the generation of various solid phases in the spent nuclear fuel.

Due to the development of advanced computing tools, mathematical modelling and computational thermodynamics during the past two decades has progressed rapidly. However, it is still an ongoing task to get a complete treatment of all related systems for calculations of a nuclear industrial code concerning fission products. The developments of the Fuelbase, a special thermodynamic database developing by a group of French scientist [7, 8], the RNFTT treatment [9-11], and other similar databases are only the first (but significant) step in developing codes for the final application into industrial codes (*e.g.*, BISON [13] or ASTEC-SOPHAEROS [14]). Thus, the thermochemical evaluation of the U-Pd-Rh-Ru quaternary system is an important part of this mission.

Previous work that has been included in the RNFTT treatment [9-11], includes a model for the noble metal Mo-Pd-Rh-Ru-Tc quinary system [15,16]. This model includes the Pd-Rh-Ru ternary system, which is a subsystem of the U-Pd-Rh-Ru quaternary system. This adds a complication to the modelling efforts for the U-Pd-Rh-Ru quaternary system as both models must be internally consistent. Since the development of the Fuelbase, many

U related binary phase diagrams have been thermodynamically evaluated, including: U-Ti [17,18], U-W [17], U-Mo [17], U-Cr [17], U-Re [17], U-Ru [17], U-Pu [19-21], U-Ga [21], U-V [22], U-Zr [19,20]. However, the U-Pd and U-Rh phase diagrams have never been thermodynamically evaluated before this work, and the model for U-Ru [17] is not consistent with the noble metal model [15,16]. Recently, the developers of the Fuelbase have published a new evaluation of the Pd-Rh-Ru system [23], at roughly the same time as the presentation of the results of this work at the 36th CNS annual conference [24,25], and the 13th International Conference on CANDU Fuel [26]. However, the new evaluation of the Pd-Rh-Ru system is inconsistent with the model for the Mo-Pd-Rh-Ru-Tc quinary system [15,16].

Also complicating the modelling efforts are discrepancies in the experimental data for the U-Pd, U-Rh, and U-Ru binary systems. In particular, experimental measurements in the U-Pd system present a challenge since Pd acts as an efficient catalyst for other side reactions. For this reason, an alternative strategy is planned and used to establish the U-Pd and U-Rh thermodynamic evaluations by means of the FactSage software [25]. To further clarify the goals of this work, the context, objectives, originality, and significance are presented in the following sections.

1.1 Context of This Work

There are different methods for classifying fission products (FPs). In analyzing loss-of-coolant accidents, Prussin *et al*. [27] divided the FPs into three distinct groups based on their significant radioactive characteristics, their degree of volatility, and their chemical properties. These groups are:

1. Inert or noble gases - Xe and Kr;
2. Volatile fission products - I, Br, Cs, Rb, Te, Se, and Sb
3. Non-volatile fission products (not-so-volatile) - Ba, Sr, Mo, Tc, Ru, Rh, Pd, Y, La, Ce, Pr, Nd, Pm, Sm, Eu, Np, Pu, Zr, and Nb.

Kleykamp [28-30], and others [31] used the chemical state of the fission products to provide a more specific classification which had the following four classes:

1. Fission gases and other volatile fission products - Kr, Xe, Br, and I;
2. Metallic precipitates - Mo, Tc, Ru, Rh, Pd[*], Ag, Cd, In, Sn, Sb, and Te;
3. Oxide precipitates - Rb, Cs, Ba, Zr, Nb, Mo, and Te;
4. Dissolved as oxides in the fuel matrix - Sr, Zr, Nb, Y, La, Ce, Pr, Nd, Pm, Sm, and Eu.

One of the important points to realize concerning the classification scheme proposed by Kleykamp is that it places some elements (*e.g.*, Mo and Nb) in more than one category. This is because transitions between the classifications are based on solubility limits of the given fission products and changes in oxygen potential during fuel burnup.

Olander [32] has described the transformation of fresh fuel as a result of burnup in a reactor. Schematically this is shown in Figure 1-1.

[*] These five elements are the main constituents of the so-called "white inclusion" and "the other metallic inclusions". The former was thermodynamically evaluated by Kaye *et al.* [15,16], and the latter is the object of this study with the addition to the element U.

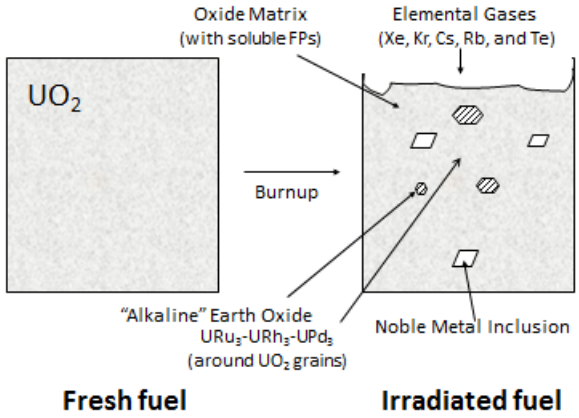

Figure 1-1. The transformation of fresh UO_2 fuel as a result of burnup [32].

In summary Olander shows that several distinct phases can be produced, namely:

1. A matrix of UO_2 with dissolved fission products;
2. A gas phase – predominantly composed of Kr and Xe;
3. The white metallic inclusions – composed of the noble metals of Mo, Ru, Rh, Pd, and Tc;
4. A complex grey oxide inclusion;
5. The other metallic inclusion; a solution of UPd_3, URh_3, and URu_3.

Considerable work at the Royal Military College of Canada (RMCC) under the supervision of Lewis and Thompson, and later expanded upon by others, has led to the construction of the RMCC Nuclear Fuel Thermochemical Treatment (RNFTT) [11,15,16, 33-35].* The purpose of the RNFTT is to thermodynamically predict the chemical behaviour of irradiated fuel by appropriately treating the various product phases. This has been done in the following manner:

1. The uranium-oxygen phase diagram was evaluated [9,34]. This model allows for dissolved fission products being present in the matrix of UO_2 and

* In this work, in keeping with the convention adopted in Corcoran *et al*. [11], the term "model" is used to refer to a particular phase, whereas "treatment" indicates an assemblage of models that together represent a system. Thus, a model is a subset of a treatment.

also allows for deviations from stoichiometry for UO_2 (in other words, models $UO_{2\pm x}$).

2. Fission products that can be dissolved are oxides of: Cs, Rb, Sr, Ba, Ce, Dy, Ho, La, Nd, Pr, Sm, Y, Ce, Mo, Nb, Np, Pu, Te, and Zr;
3. The gas phase is treated as an ideal gas [9];
4. The quinary Noble Metals system of Mo, Ru, Rh, Pd, and Tc was modelled by Kaye *et al*. [15,16];
5. The complex grey oxide phases are approximated by ideal solutions of similar oxides, taken from the following list: $(Rb,Cs)_2ZrO_3$; $(Sr,Ba)ZrO_3$; $(Rb,Cs)_2UO_4$; $(Sr,Ba)UO_4$; and $(Rb,Cs)_2MoO_4$;
6. The UPd_3-URh_3-URu_3 system is treated as an ideal solution of these three components at 2000 K. In other words, their chemical activity was given by their mole fraction (or relative proportion available) [9].

In a typical calculation to determine the chemical composition of fuel, for a CANDU fuel bundle, the approximated elemental composition (in moles) is given by the reaction (The products of this reaction are very complicated, parts of the results are shown in Figure 1-2):

79.95107 **U** + 0.29738 **Pu** + 0.16719 **Zr** + 0.19846 **Xe** + 0.12592 **Mo** + 0.10593 **Ce** + 0.11598 **Ru** + 0.09257 **Nd** + 0.05189 **Sr** + 0.08325 **Cs** + 0.01607 **Np** + 0.04518 **Ba** + 0.03903 **La** + 0.02548 **Y** + 0.03739 **Tc** + 0.02832 **Pr** + 0.01635 **Rb** + 0.01744 **Te** + 0.04029 **Pd** + 0.00971 **I** + 0.01653 **Rh** + 0.00009 **H** + 80.85685 $\mathbf{O_2}$ =

where, mole numbers were computed using the SCALES-5 code [36]. Burnup conditions were: 175 $MWh \cdot kgU^{-1}$ (irradiated for 143 days), in a flux of 2.16×10^{14} $n \cdot cm^{-2} \cdot s^{-1}$, and a power of 980.3 $kW(f) \cdot bundle^{-1}$.

The results of a fuel treatment calculation shown in Figure 1-2 represent the results of its development over at least ten years. At the time of this calculation, a model for the

U-Pd-Rh-Ru quaternary system had not been developed, and so the other metallic inclusions were treated as an ideal solution of the compounds UPd_3, URh_3, and URu_3. This represents a potential deficiency in the fuel treatment and a potential area for improvement.

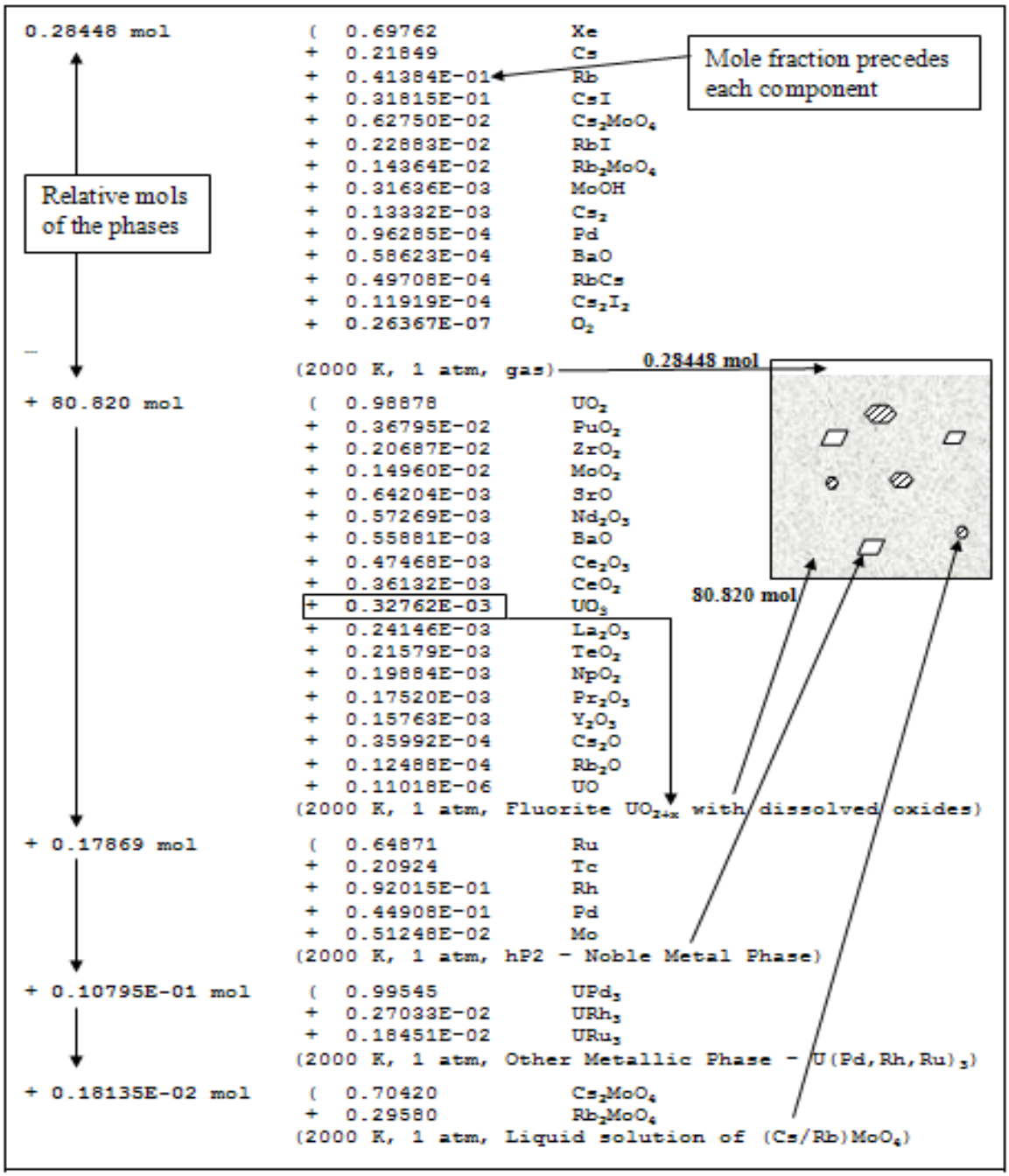

Figure 1-2. The results of a typical burnup calculation (175 $MWh \cdot kgU^{-1}$) based on the atomic proportions shown in the complex reaction shown in the previous page [9].

1.2 Objectives

The objective of this thesis is to thermodynamically assess the U-Pd-Rh-Ru quaternary system in order to enrich the nuclear fuel databases and ultimately improve the industry codes which use them.

To achieve this objective, the following three steps were taken:

i. Develop thermochemical models for the U-Pd, U-Rh, and U-Ru binary phase diagrams by critically evaluating these three systems;
ii. Construct a complete quaternary (U-Pd-Rh-Ru) system by the incorporation of the compound and solution databases of the six subsystems, and establish and optimize the necessary ternary interaction parameters so that reasonable ternary isothermal sections and various isopleths can be obtained;
iii. Compare the calculated results with existing ternary experimental phase diagrams, *e.g.*, U-Rh-Pd isothermal section [37] and the UPd_3-URu_3-URh_3 isothermal section [38], in order to assess the model.

In performing the thermodynamic evaluations of the binary systems, discrepancies and inconsistencies within the experimental evidence were revealed. These comparisons will not only demonstrate the value of these thermodynamic calculations, but may possibly lead to conclusions as to the necessity of other potential thermodynamic and dynamic "improvements".

1.3 Significance of This Study

Once a U-Pd-Rh-Ru quaternary model is established, it can provide thermodynamic data for the whole composition and temperature ranges of the system. That is to say, the missing thermodynamic properties can be calculated by the model. Although these calculated data are not obtained directly from experiments, they are extrapolated on the

basis of all available experimental data of the subsystems by well-established thermodynamic principles. Moreover, the calculated thermodynamic data and phase boundaries can be used as guidance for further experimental explorations. The new optimization scheme targeted on controversial U-Me binary systems provides an approach to other similar systems. In the meantime, the models developed in this work can be incorporated into industrial computer codes that need equilibrium thermodynamic data for these four elements.

1.4 Originality of This Work

To establish the U-Pd-Rh-Ru quaternary thermodynamic model, evaluations of the six binary subsystems are essential. Table 1-1 shows originality status of the six binary models, three ternary and the overall quaternary models that are necessary for this work.

Table 1-1. Information concerning the originality of this work

Multicomponent System	System	Experimental Phase Diagram	Thermodynamic Evaluations
Pd-Rh-Ru	**Ru-Rh**	Paschoal *et al*. [39]	Kaye and Kaye *et al*. [15, 16]
	Rh-Pd	Raub *et al*. [40]	
	Pd-Ru	Rudnitskii and Polyakova [41]	
U-Pd-Rh-Ru	**U-Ru**	Park [42]	Berche *et al*. [17] (Reviewed and modified in this work)
	U-Rh	Park [42]	Original to this work
	U-Pd	Kleykamp and Kang [37]	Original to this work
	U-Pd-Rh	Kleykamp and Kang [37]	Original to this work
	U-Rh-Ru	NA	Original to this work
	U-Pd-Ru	NA	Original to this work
	UPd_3-URh_3-URu_3	Kurosaki and Uno [38]	Original to this work

As specified in the steps of this project (Section 1.2), the U-Pd-Rh-Ru quaternary model will provide thermodynamic properties over the complete range of composition and at all temperatures. It is these data that will be used in more complicated industrial codes.

1.5 Outline of This Thesis

In Chapter 2, the basic theory of Gibbs energy minimization will be reviewed and the relationship of Gibbs energy minimization with phase diagram construction will be introduced. Chapter 3 reviews the literature for previous experimental work in the U-Pd-Rh-Ru quaternary system. Thermodynamic properties of the elements are listed first, and then the data for the six binary systems are introduced.

In Chapter 4, the methodology of assessing and evaluating the thermodynamic data is given and the procedures for phase diagram evaluation will be illustrated. Chapter 5 will present the thermodynamic evaluation results of the three U-related binary systems and some important ternary isothermal sections and isopleths. Chapter 6 will be an in-depth discussion of the evaluation results with focuses on three connotation phenomena found in the thermodynamic evaluation. Chapter 7 will summarize the enrichment of this work to the existing RNFTT treatment. Conclusions will be given in Chapter 8, while future work and references cited in this thesis will be listed in Chapter 9 and 10, respectively.

2 Theory of Gibbs Energy Minimization and Phase Diagram Development

2.1 Preliminary Remarks

Only a few decades ago, all phase diagrams were drawn by hand to capture features determined by experimental measurements. For example, by heating a series of samples with known compositions to various temperatures and quenching them; then by using metallographic techniques one could show whether the sample at an elevated temperature is a one phase or a two phase solid; if a sample is melted (or partially melted), then it exhibits liquid behaviour or a liquid in equilibrium with a solid. This technique, and others classically used to determine phase diagram features, is reviewed by Kaye *et al*. [43], and suggests how phase diagrams can be sketched.

In recent years, with the rapid growth of the capability of computers, Gibbs energy minimization techniques have been developed that allow complex calculations to be performed rapidly. One application is for phase diagram construction and validation.

In this chapter, the theory of Gibbs energy minimization and its applications in thermodynamic phase diagram construction will be introduced, and the mathematics which enables phase diagrams to be calculated and predicted from the experimental data will be illustrated.

2.2 Thermodynamic Basics of Gibbs Energy Minimization

For a system in achieving an equilibrium state, the core of computational thermodynamics is the principle of Gibbs energy minimization, *i.e.*, at a constant pressure and temperature a system drives toward a configuration at which it has the lowest Gibbs

energy (G). In computational thermodynamics, the Gibbs energy in each phase is optimized and compared. The Gibbs energy of the system is at the minimum only when the phases are at equilibrium. Therefore, the system Gibbs energy can be represented by Equation 1.

$$G = \sum_{i=1}^{p} n_i G_i^{\phi} = minimum \quad (1)$$

In the above equation, G_i^{ϕ} is a function of composition and temperature with variable coefficients; n_i represents the number of moles of species i in a phase ϕ, respectively; i represents a constituent in the phase ϕ.

The molar Gibbs energy, G, of a solution can be expressed as:

$$G = G^{ideal} + G^{Excess} \quad (2)$$

where G^{ideal} represents the molar Gibbs energy that the solution would have if it were ideal, and G^{Excess} represents the excess Gibbs energy or in other words the difference of Gibbs energy between ideal behaviour and actual behaviour.

2.2.1 Gibbs Energy Expression for Binary Systems

The G^{ideal} term in Equation 2 can be split into two parts as shown in Equation 3.

$$G = \left(X_A G_A^{\circ} + X_B G_B^{\circ}\right) + \Delta G^{M,ideal} + G^{Excess} \quad (3)$$

where X_A and X_B represent the mole fractions of A and B (note $X_A + X_B = 1$), G_A° and G_B° the Gibbs energy of components A and B, respectively, and $\Delta G^{M,ideal}$ represents the ideal Gibbs energy of mixing of A and B.

Accordingly, $\Delta G^{M,ideal}$, the ideal Gibbs energy of mixing, can be represented as a function of the mole fractions of A and B, multiplied by the gas constant *R* and the temperature *T*, as shown in Equations 4a and 4b.

$$\Delta G^{M,ideal} = RT(X_A lnX_A + X_B lnX_B) \quad (4a)$$

$$G^{Excess} = \sum X_A X_B [(h_n - s_n T) X_B^n] \quad (4b)$$

In Equation 4b, the index n represents the number of terms of a polynomial. Then, by referencing the Gibbs expression in Equations 4a and 4b to a particular reference phase (often for convenience this is the *Liquid* phase), an expression for the Gibbs energy of mixing for a particular phase can be obtained. Thus, for each phase, ϕ, in a binary system, a Gibbs energy expression as a function of composition and temperature can be derived. The complete expression for this Gibbs energy of mixing is presented in Equation 5, for the generic binary system A-B.

$$G = X_A \cdot \underbrace{\left(H_A^\circ - TS_A^\circ\right)}_{lattice\ stability\ for\ A} + X_B \cdot \underbrace{\left(H_B^\circ - TS_B^\circ\right)}_{lattice\ stability\ for\ B} + \underbrace{RT(X_A lnX_A + X_B lnX_B)}_{ideal\ mixing\ term} + \underbrace{\sum X_A X_B [(h_n - s_n T) X_B^n]}_{excess\ Gibbs\ energy} \quad (5)$$

where X_A and X_B represent the mole fractions of A and B (again, note $X_A + X_B = 1$), *T* the absolute temperature, *R* the molar gas constant, H° and S° the standard enthalpy and entropy contributions to the lattice energy, and h_n and s_n the enthalpy and entropy contributions in the excess Gibbs energy series.

2.2.1.1 Lattice Stabilities

In Equation 5 the first two terms represent the energy components attributable to the lattice stabilities of A and B, respectively; the third term represents the contribution from ideal mixing of A and B as a function of temperature; and the fourth term represents

the excess energy term, and is often expressed as an expansion series in both composition and temperature. The excess term represents the deviation from ideal behaviour.

The concept of "lattice stabilities" describes the energy required to transition from one phase to another, either a liquid-solid transition (*i.e.*, melting/solidification) or a solid-solid transition (*i.e.*, from a solid of one crystal structure to that of another). Lattice stabilities usually take the form of an enthalpy and entropy, and the lattice stabilities for a component in a system can be either real or hypothetical.

Real lattice stabilities are established directly from experimental measurements and relate to transitions between phases that exist in nature. For example, Ru solid only has a close-packed hexagonal (*cph*[*]) crystal structure. At the melting temperature (2607 K), ruthenium melts and becomes a liquid. While difficult to measure for U-Me systems, there is a measurable heat of melting at a specific temperature, and hence a real lattice stability representing this transition can be reported.

However, in some situations, it is necessary to imagine that ruthenium solid exists in a crystal structure other than a close packed hexagonal structure, for example a face-centred cubic structure. This situation represents a hypothetical crystal structure for Ru; it does not exist in nature. Nevertheless, an imagined enthalpy and melting temperature can be "assigned", and then used to describe the phase behaviour via Equation 5. The hypothetical properties set references for specific hypothetical phases, but they do not affect the real phase boundaries.

[*] In some references it is also named as *hcp* phase; both of them refer to "hexagonal close packed" or "close packed hexagonal" crystal structure. In this paper, *cph* is adopted, for consistency.

2.2.1.2 Excess Gibbs Energy Properties

In Equation 5, the excess term can be considered as two parts: the product of the mole fractions and the interaction portion in the square brackets. In computational thermodynamics, many empirical expressions of thermodynamic properties, such as Gibbs energy, enthalpy, entropy, and heat capacity of the constituents or a collection of them are needed. To describe the excess properties there are two main equations used: the Margules Power Series Formalism [44] which is preferred in this work instead of the alternative Redlich-Kister Expansion [45].

As mentioned previously, the interaction parameters of a phase (L_{AB}^{ϕ}) is used to represent the square bracketed term in the excess portion of Equation 5. This is shown in Equation 6 for the two component system A and B.

$$\sum X_A X_B\left[(h_i - s_i T)X_B^{\phi}\right] = X_A X_B\left(L_{AB}^{\phi}\right) \tag{6}$$

In the Redlich-Kister (RK) Formalism, L_{AB}^{ϕ} is given by Equation (7) [45].

$$L_{AB}^{\phi} = (A_0 + B_0 T) + (A_1 + B_1 T)(X_A - X_B) + (A_2 + B_2 T)(X_A - X_B)^2 + (A_3 + B_3 T)(X_A - X_B)^3 \ldots \tag{7}$$

where A_i and B_i represent parameters in the Redlich-Kister expression (not to be confused with components A and B), and can be considered as an enthalpy and entropy terms, respectively. The term X_i represents the mole fraction of either component A or B, with their sum being unity since it is a binary system.

Equation 8 shows the interaction parameter (L_{AB}^{ϕ}) in the Margules Formalism [44].

$$L_{AB}^{\phi} = (a_0 + b_0 T) + (a_1 + b_1 T)X_B + (a_2 + b_2 T)X_B^2 + (a_3 + b_3 T)X_B^3 \cdots \tag{8}$$

where a_n and b_n (n = 1, 2, 3…) represent parameters in the Margules expression, and also can be considered an enthalpy and entropy term, respectively, and *A* and *B* are the two components. Again the term X_i represents the mole fraction of either component A or B.

Theoretically, both RK and Margules expressions are infinitely long polynomials, but in practice, usually less than four terms are used in optimization, since raising the mole fraction to a large number makes the contribution of the associated term negligible unless the values for the parameters become ridiculously large[*]. A conversion scheme between these two expressions, when there are up to cubic terms in the excess Gibbs energy expression, is provided in Table 2-1.

Table 2-1. The conversion schemes from RK formalism to Margules formalism.

n	a_n	b_n
0	$A_0 + A_1 + A_2 + A_3$	$B_0 + B_1 + B_2 + B_3$
1	$-2A_1 - 4A_2 - 6A_3$	$-2B_1 - 4B_2 - 6B_3$
2	$4A_2 + 12A_3$	$4B_2 + 12B_3$
3	$-8A_3$	$-8B_3$

Alternatively, coefficients provided by the Margules formalism can be converted to RK formalism as shown in Table 2-2.

Table 2-2. The conversion schemes from Margules formalism to RK formalism.

n	A_n	B_n
0	$a_0 - {}^1/_2\, a_1 + {}^3/_4\, a_2 + {}^1/_2\, a_3$	$b_0 - {}^1/_2\, b_1 + {}^3/_4\, b_2 + {}^1/_2\, b_3$
1	${}^1/_2\, a_1 + a_2 + {}^3/_4\, a_3$	${}^1/_2\, b_1 + b_2 + {}^3/_4\, b_3$
2	${}^1/_4\, a_2 + {}^3/_8\, a_3$	${}^1/_4\, b_2 + {}^3/_8\, b_3$
3	$-{}^1/_8\, a_3$	$-{}^1/_8\, b_3$

[*] Very large values for these parameters typically indicates a poorly fitting model.

For example, the interaction parameters of the U-Ru solution phases optimized by Berche *et al.* [17] have a maximum of three terms as shown in Table 2-3.

Table 2-3. The interaction parameters in RK formalism by Berche *et al.* [17].

Phase	RK Interaction Parameters Optimized by Berche *et al.* [17]
Liquid	$L_{Ru,U}^{liquid} = -173587 + 10.82T - 63720(X_{Ru} - X_U)$
bcc	$L_{Ru,U}^{bcc} = -164020 + 43.68T - 19280(X_{Ru} - X_U)$
β-U	$G_{Ru}^{\beta-U} - G_{Ru}^{fcc} = 18800$
	$L_{Ru,U}^{\beta-U} = -105000$

The interaction parameter of the liquid phase established by Berche *et al.* [17] was transformed from RK formalism to Margules formalism and used as a standard liquidus in this work (Table 5-10). Table 2-4 shows a comparison of the interaction parameters of the liquid phase in U-Ru system, which are equivalent using either method. In this case the Margules values were derived from the literature RK values using the conversion scheme in Table 2-1. Note that higher order terms (*i.e.*, A_2, A_3, B_1, B_2, and B_3 equal 0).

Table 2-4. A comparison of the interaction parameters of liquid phase in U-Ru system expressed as Margules formalism and RK formalism.

Formalism	Interaction Parameters of liquid phase in U-Ru system
Margules	$L_{Ru,U}^{liquid} = -237307 + 10.82T + 127440X_U$
RK	$L_{Ru,U}^{liquid} = -173587 + 10.82T - 63720(X_{Ru} - X_U)$

In this thesis, the optimized interaction parameters for solution phases have a maximum number of terms of four (Chapter 5).

2.2.1.3 Stoichiometric Compounds

A further complicating factor in a phase diagram evaluation is the presence of stoichiometric compounds. These solid compound phases are not modelled with Equation

5, instead, they require three pieces of thermodynamic data: $\Delta H^{\circ}_{298\,K}$ (the standard enthalpy of formation at 298 K); $S^{\circ}_{298\,K}$ (the standard entropy at 298 K); and C_P (an expression for the heat capacity as a function of temperature at constant pressure).

The U-Me systems, where Me represents Pd, Rh, or Ru, are characterized by the existing of solid solutions on the uranium side of the diagram, and a series of intermetallic compounds, the most notable being UMe_3, with increasing amounts of Me being present. For the U-Me systems, some thermodynamic data are unavailable, especially for many of the intermetallic compounds (the exception being the UMe_3 compounds). In spite of these challenges, the thermodynamic computations can still be applied to evaluate these systems.

2.2.2 Gibbs Energy Expressions for Ternary Systems

The purpose of thermodynamic evaluation of binary systems is not limited to creating electronic versions of the phase diagrams or to justify the experimental data. Because of the huge amount of experimental work needed in constructing ternary or higher order phase diagrams, interpolation to ternary or higher order phase diagrams from related binary phase diagrams can provide reasonable and useful information of multicomponent phase diagrams. These calculated phase diagrams can serve at least as guidance for experimental measurements. For systems confronting experimental difficulties, for example, when high temperature measurements are involved (*e.g.*, this is often the case when at least one component is a transition metal), the information provided by calculated phase diagrams becomes more important. As the lattice parameters of elements become more and more sophisticated, *e.g.*, many successful U and Me related (but not U-Me

systems) thermodynamic assessment had been performed, the authenticity of extrapolated phase diagrams increases.

To calculate the properties at a given composition (a point *p*) in a ternary system[*], properties from the surrounding binary systems are weighted via an interpolation scheme in order to estimate the key properties at point *p*.

During the past few decades, different kinds of interpolation formalisms have been developed. The most frequently used equations are referred as Muggianu's equation [46], Kohler's equation [47] and Toop's equation [48]. How these interpolation schemes weight the properties of the binary systems is discussed in the next three sub-sections.

2.2.2.1 Muggianu's Equation

The equation was derived geometrically by Muggianu, Gambino, and Bros [46] in 1975. The position of points *c*, *b*, and *a* on Figure 2-1 are determined by lines running normal to edges *AB*, *AC*, and *BC* that pass through at point *p*. Figure 2-1 is a geometric representation of Muggianu Equation [46].

[*] The principle can be applied to higher order systems too.

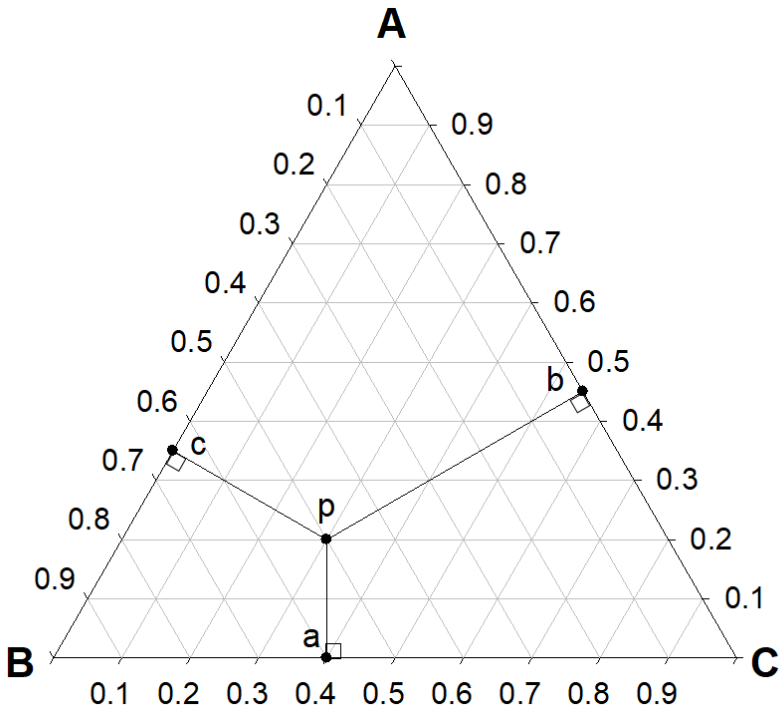

Figure 2-1. A geometric representation of Muggianu interpolation scheme [46].

For a sub-regular solution phase*, the Muggianu equation can be written as:

$$G_p^{Excess} = X_A X_B\{L_{AB}^0 + L_{AB}^1(X_A - X_B)\} + X_B X_C\{L_{BC}^0 + L_{BC}^1(X_B - X_C)\} + X_A X_C\{L_{AC}^0 + L_{AC}^1(X_A - X_C)\} \quad (9)$$

2.2.2.2 Kohler's Equation

An equation was derived by Kohler [47] based on binary excess Gibbs energy equations and a set of experimental data of the methylethylketone – *n*-heptane - toluene ternary system. The Kohler equation is given by Equation 10.

$$G_p^{Excess} = (1 - X_C)^2 G_a^{Excess} + (1 - X_A)^2 G_b^{Excess} + (1 - X_B)^2 G_c^{Excess} \quad (10)$$

* A regular solution behavior is more close to that of the ideal solution phase; a sub-regular solutions is more non-ideal.

In Equation 10 the excess Gibbs energy (G_p^{Excess}) at a point p, is calculated extending three straight lines from the composition values for the three binary systems, *i.e.*, point a, b, and c, to the three apexes, A, B, and C, as illustrated in Figure 2-2. The focus of the three straight lines is the ternary composition "p".

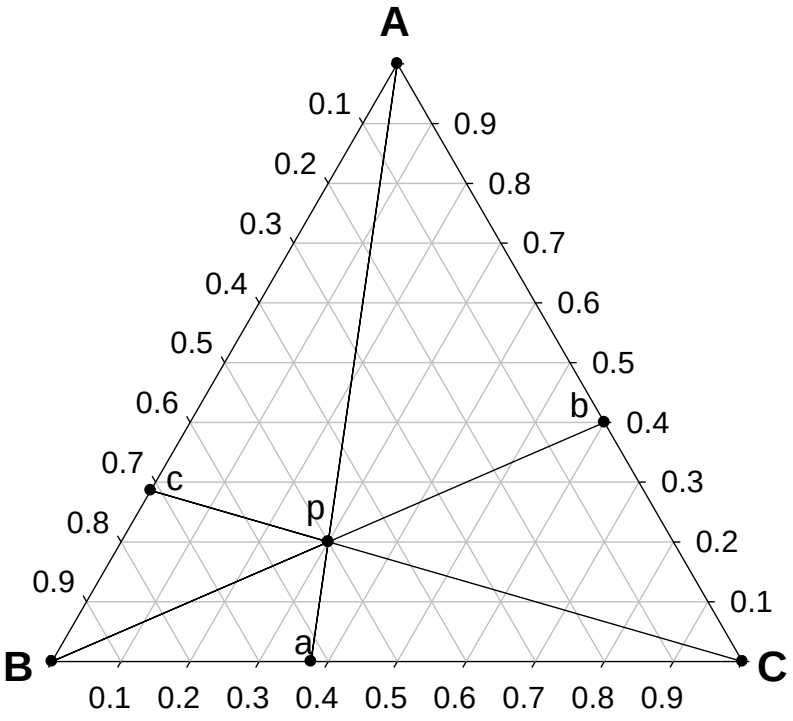

Figure 2-2. A geometric representation of Kohler interpolation scheme [47].

Equation 10 can be expressed in alternative ways without changing the total excess Gibbs energy. For example, in *CALPHAD: A Comprehensive Guide*, it is written in terms of mole fractions of binary systems involved in a ternary system [49].

$$G_p^{Excess} = (X_A + X_B)^2 \frac{X_A}{X_A + X_B} \cdot \frac{X_B}{X + X_B} \left\{ L_{AB}^0 + L_{AB}^1 \left(\frac{X_A - X_B}{X_A + X_B} \right) \right\}$$
$$+ (X_B + X_C)^2 \frac{X_B}{X_B + X_C} \cdot \frac{X_C}{X_B + X_C} \left\{ L_{BC}^0 + L_{BC}^1 \left(\frac{X_B - X_C}{X_B + X_C} \right) \right\}$$
$$+ (X_A + X_C)^2 \frac{X_A}{X_A + X_C} \cdot \frac{X_C}{X_A + X_C} \left\{ L_{AC}^0 + L_{AC}^1 \left(\frac{X_A - X_C}{X_A + X_C} \right) \right\} \quad (11)$$

where L_{ij}^n represents the *n*th interaction parameter between species *ij* (in this case, species A, B, and C) and X_i represents the mole fraction of component *i*.

2.2.2.3 Toop's Equation

Unlike Muggianu and Kohler equations, Toop's equation was derived from previous work [50-53] in combination with known experimental data from the Cd-Pb-Bi, Pb-Sn-Cd, and CaO-FeO-SiO_2 ternary systems. Toop's Equation is often used when one component (in this case *A*) is different from the other two (*i.e.*, *B* and *C*). A line is drawn from vertex *A*, through p to side *BC* (as in the Kohler method), but the other two points (*b* and *c*) are determined by a line parallel to *BC* running from side *AB* to side *AC*. Graphically, the Toop equation is shown in Figure 2-3 [50-53].

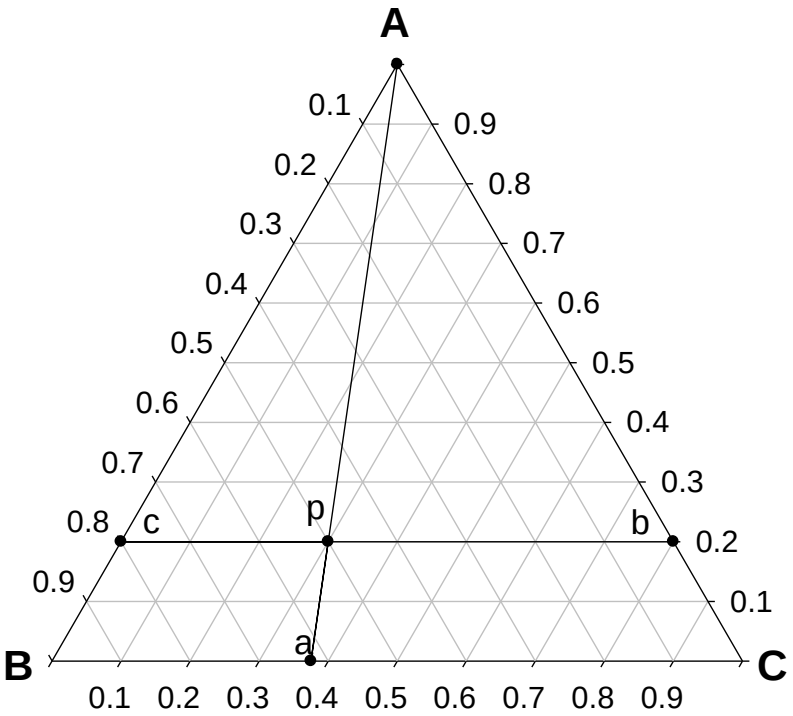

Figure 2-3. A geometric representation of Toop interpolation scheme [50-53].

As the original equations proposed by Toop were derived in terms of specific solution phases, the method was generalized by Hillert in 1980 [54]. The following equation is consistent with Figure 2-3 [49].

$$G_p^{Excess} = X_A X_B\{L_{AB}^0 + L_{AB}^1(X_A - X_B - X_c)\} + X_A X_C\{L_{AC}^0 + L_{AC}^1(X_A - X_c - X_B)\} + X_B X_C\left\{L_{BC}^0 + L_{BC}^1\left(X_B - X_C - \frac{X_B - X_C}{X_B + X_C}X_A\right)\right\} \quad (12)$$

where once again L_{ij}^n represents the *n*th interaction parameter between species *ij* (with *i* and *j* representing components A, B, or C) and X_i represents the mole fraction of component *i* at point *p*. It should be noted that the values of L_{ij}^n in Equation 12 are distinct from those of Equation 11.

All the three ternary excess Gibbs energy equations can be reduced to binary subsystems when one of the three mole fractions in a system becomes zero. The Muggianu and Kohler equations are relatively homogeneous when extrapolating binary systems that have similar properties. It is reported in [49] that these two equations provide comparable results [55]. In contrast, Toop's equation is more favorable to systems with miscibility gaps, for example, the *fcc* miscibility gap between Rh and Pd in U-Rh-Pd systems, which will be discussed in detail of the quaternary model of this program. In fact, Toop derived the equation by comparing the calculated results with three sets of ternary experimental data. In the cases of Cd-Pb-Bi and Pb-Sn-Cd systems, the temperatures are the same: 500 ºC, which is well above the melting points of the constituent elements. As a result, the equation was used for liquid solutions (with immiscible liquids). In the third system (CaO-FeO-SiO_2), the temperature (1600 ºC) is lower than the melting point of CaO and is at the melting point of SiO_2. This means that the effects of the existing solid phase were omitted in the calculation. Toop emphasized the influence of the choice of component 2 (the three components are represented as 1, 2, and 3 respectively), but the results showed that only in the CaO-FeO-SiO_2 system the obvious differences are illustrated. In addition, in all the three systems the measured excess Gibbs energy curves are very close to the positions of the calculated curves, which implies that the deviations from different choices are acceptable considering the distinctive positions of the three elements in the periodic table. Pelton [56] and Chartrand and Pelton [57] presented detailed explanations regarding the feasibility of the choice between these two interpolation schemes. In this work, the Kohler scheme has been selected since it provides a balanced weighting of properties from the binary systems when being interpolated into the relevant ternary diagram.

2.3 Relating Gibbs Energy of Mixing Curves and Phase Diagrams

In mapping a traditional phase diagram (*i.e.*, composition as the horizontal axis and temperature as the vertical axis) by the computational method for a system at specified temperatures and pressure (usually 1 atm), the Gibbs energy curves of each phase are calculated, *e.g.*, Gibbs energy curves of the *Liquid* phase, all solid solution phases, as well as what could be considered Gibbs energy lines for the compound phases[*]. As was indicated by Equation 5, the Gibbs energy for a solution phase is a function of temperature and composition, with any pressure and magnetic effects being ignored for condensed systems, especially when the system pressure is close to standard pressure (*i.e.*, 1 atm).

If in calculating the Gibbs energy of mixing curves for the various solutions, one curve is lower than the other curves over the whole composition range (*i.e.*, when $0 \leq X_B \leq 1$), then that phase possesses a minimum Gibbs energy. On the phase diagram, this would represent a single phase region that stretches across the whole composition range of the diagram. Typically, for metallic systems, this situation occurs at a relatively high temperature range when there is only one *Liquid* phase, without any miscibility issues, or when the two components have identical crystal structures (*e.g.*, Ru and Tc – both are *cph* [16]) and exhibit complete solid-solid miscibility.

When two (or more) Gibbs energy curves of mixing intersect, it means that a two (or three) phase equilibrium exists, as illustrated in Figure 2-4 [58]. When the two phases each have a local minimum (*e.g.*, for T_1, T_2, or T_4 in Figure 2-4), the equilibrium

[*] In the general discussion that follows, the phrase "Gibbs Energy Curve" will be used to indicate both the curves for solution phases, and the Gibbs energy lines for compounds. For stoichiometric compounds, these lines are vertical lines.

concentrations of the two phases is determined by drawing a tangent the two lowest points of the Gibbs energy curves of mixing. Should the tangent touch three curves (*e.g.*, T_3 in Figure 2-4), then a critical temperature is being illustrated where a specific reaction (in the example, a eutectic reaction: $L \rightarrow \alpha + \beta$) occurs.

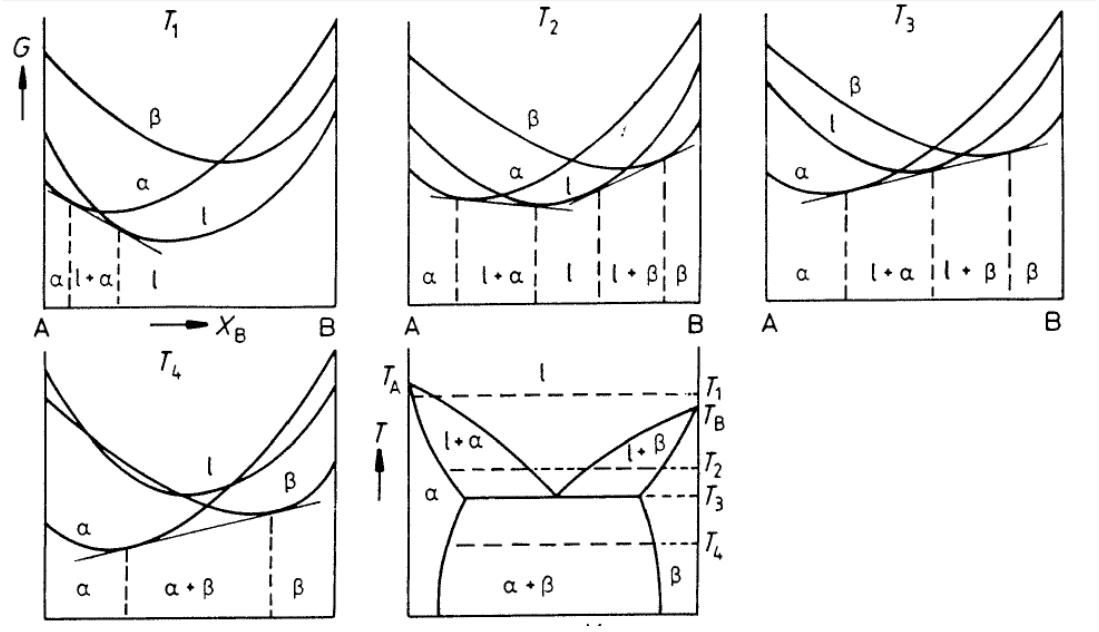

Figure 2-4. A copy of Gibbs energy of mixing curves and their relationship with a hypothetical binary phase diagram of A and B from [58].

From the Gibbs energy curves of mixing, illustrated in Figure 2-4, the points of tangency are mapped directly onto the phase diagram at each temperature. Thus, by computing the Gibbs energy curves of mixing at every temperature, a complete diagram can be generated. In theory, this process works in the opposite direction as well, but is harder to apply. One can examine the phase diagram and suggest that at a given temperature these two phases will be in equilibrium.

A phase diagram is usually sketched according to experimental data. Such a sketch is an interpretation of the experimental data by the experimentalists, and sometimes is an attempt to reconcile conflicting measurements. From the perspective of computational thermodynamics, boundaries on a phase diagram represent equilibrium concentrations as a function of temperature, and are governed by the chemical potentials of the constituents in the system [58]. For example, for a binary system with pure components A and B and with two phases α and β, the following equalities are true for the two components [58]:

$$\mu_A^{\alpha} = \left(\frac{\partial G}{\partial n_A}\right)^{\alpha}_{T,P,n_B} \text{ and } \mu_A^{\beta} = \left(\frac{\partial G}{\partial n_A}\right)^{\beta}_{T,P,n_B} \quad (13)$$

$$\mu_B^{\alpha} = \left(\frac{\partial G}{\partial n_B}\right)^{\alpha}_{T,P,n_A} \text{ and } \mu_B^{\beta} = \left(\frac{\partial G}{\partial n_B}\right)^{\beta}_{T,P,n_A} \quad (14)$$

where μ_A^{α} represents the chemical potential of component A in phase α; μ_A^{β} the chemical potential of component A in phase β; μ_B^{α} the chemical potential of component B in phase α; μ_B^{β} the chemical potential of component B in phase β; n_i the number of moles of component *i*; and T and P represent temperature and pressure, respectively.

In general, the chemical potential for a particular component A in any phase can be expressed by Equation 15 [58]:

$$\mu_A = G_A + RT\ln(a_A) \quad (15)$$

where G_A stands for the molar Gibbs energy of pure A; and a_A the activity of component A in the phase. In terms of the mole fraction of A, chemical activity can be introduced by Equation 16, in which γ_A represents the deviation from ideal behaviour [58]:

$$a_A = \gamma_A(X_A) \quad (16)$$

Expanding Equation 15 and substituting the activity from Equation 16, gives:

$$\mu_A = G_A + RT\ln(X_A) + RT\ln(\gamma_A) \quad (17)$$

In this equation, the first term still represents the molar Gibbs energy of pure A; the second term represents the ideal mixing term when A is mixed with another species; and the third term represents the excess mixing term, similar to the terms in Equation 5.

Schematically, the relationships between the Gibbs energies of mixing, chemical potentials, and the activities of components A and B, related to the tangency, are shown in Figure 2-5 [58].

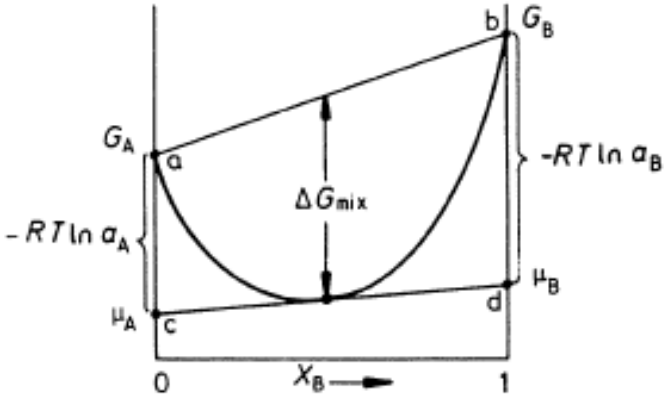

Figure 2-5. The relationship between the Gibbs energy of mixing and the activities of components A and B [58].

When two (or more) phases are in equilibrium, as indicated on a binary phase diagram either by a two phase region or a reaction at a critical temperature (*e.g.*, a peritectic or eutectic reaction), then the phases in question will have a common tangent as illustrated in Figure 2-4, and then the chemical potentials of each component in both phases are equal with respect to a common reference value. This last phrase is important as it will position the points "c" and "d" of Figure 2-5 on an absolute scale at the same value for the two (or three) phases in question.

This means that the following equalities simultaneously apply:

$$\mu_A^{\alpha} = \mu_A^{\beta} \quad \text{and} \quad \mu_B^{\alpha} = \mu_B^{\beta} \tag{18}$$

Schematically this is shown in Figure 2-6 (adapted from [58]).

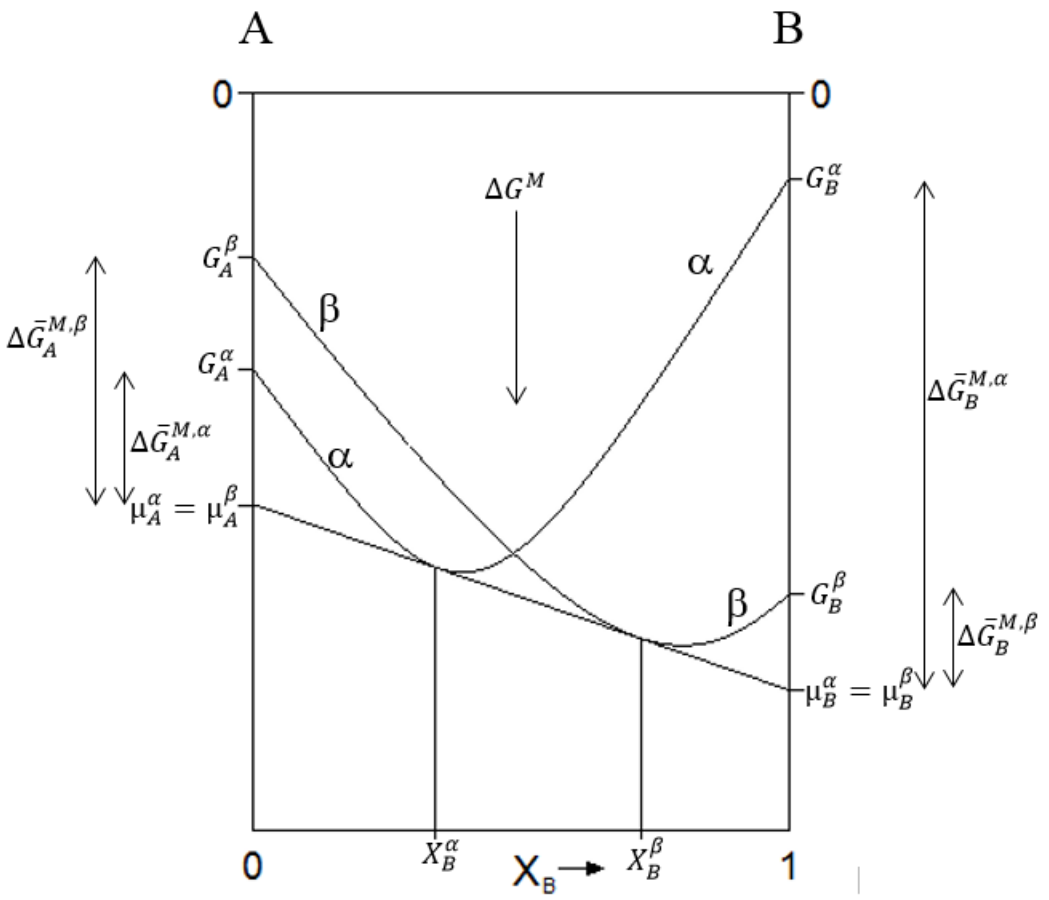

Figure 2-6. Diagram showing the common tangent method applied to two phases, α and β, for a binary system A-B (adapted from [58]).

The two equalities expressed in Equation 18 and illustrated in Figure 2-6 can be utilized to determine the parameters in Equation 4 and Equation 5 and correlate the parameters for different phases. The figure shows that, for compositions X_B^{α} and X_B^{β}, the partial Gibbs energies of each component ($\bar{G}_i^{\phi}$) are equal in the two phases because the α and β phases are in equilibrium. So, at X_B^{α} and X_B^{β}:

$$\bar{G}_A^{\alpha} = \bar{G}_A^{\beta} \tag{19}$$

$$\bar{G}_B^{\alpha} = \bar{G}_B^{\beta} \tag{20}$$

The partial Gibbs energy is expressed as the sum of three terms: the Gibbs energy of the pure component (which relates to a lattice stability term); a term for ideal Gibbs energy of mixing; and a term for excess Gibbs energy of mixing. The general form for this expression is shown as Equation 21, where X_i^{ϕ} represents the composition of component *i* in phase ϕ (ϕ = α, β...) at equilibrium.

$$\bar{G}_A^{\alpha} = G_A^{\circ,\alpha} + RT\ln(X_A^{\alpha}) + \bar{G}_A^{E,\alpha} \tag{21}$$

Using the general form expressed in Equation 21, Equations 19 and 20 can be rewritten as Equations 22 and 23:

$$G_A^{\circ,\alpha} + RT\ln(X_A^{\alpha}) + \bar{G}_A^{E,\alpha} = G_A^{\circ,\beta} + RT\ln\left(X_A^{\beta}\right) + \bar{G}_A^{E,\beta} \tag{22}$$

$$G_B^{\circ,\alpha} + RT\ln(X_B^{\alpha}) + \bar{G}_B^{E,\alpha} = G_B^{\circ,\beta} + RT\ln\left(X_B^{\beta}\right) + \bar{G}_B^{E,\beta} \tag{23}$$

where $X_A^{\alpha} + X_A^{\beta} = 1$ and $X_B^{\alpha} + X_B^{\beta} = 1$. Therefore, these two equations can be re-written as:

$$\bar{G}_A^{E,\alpha} = \left(G_A^{\circ,\beta} - G_A^{\circ,\alpha}\right) + RT\ln\left(X_A^{\beta}\right) - RT\ln(X_A^{\alpha}) + \bar{G}_A^{E,\beta} \tag{24}$$

$$\bar{G}_B^{E,\alpha} = \left(G_B^{\circ,\beta} - G_B^{\circ,\alpha}\right) + RT\ln\left(X_B^{\beta}\right) - RT\ln(X_B^{\alpha}) + \bar{G}_B^{E,\beta} \tag{25}$$

Equations 24 and 25 directly relate the partial excess Gibbs energy properties of one phase to those of a second phase with which it is at equilibrium. These equations can be used in calculations of an unknown excess property when the corresponding excess property of the other species is known.

A small simplification can be made on Equation 8 for notational brevity. Replacing each $a_i + b_iT$ term with p_i, the excess Gibbs energy can be written as:

$$G^{Excess} = X_A X_B\big((p_0) + (p_1)X_B + (p_2)X_B^2 + (p_3)X_B^3 \cdots\big) \tag{26}$$

From Equation 26, the partial excess Gibbs energies of components A and B can be derived by partial differentiation with respect to X_A and X_B. The results are shown in Equations 27 and 28, respectively. As mentioned in Section 2.2, it is sufficient to truncate Equation 26 at the p_3 term for most purposes.

$$\bar{G}_A^{Excess} = X_B^2[(p_0 - p_1) + (2p_1 - 2p_2)X_B + (3p_2 - 3p_3)X_B^2 + (4p_3)X_B^3] \tag{27}$$

$$\bar{G}_B^{Excess} = X_A^2[(p_0) + (2p_1)X_B + (3p_2)X_B^2 + (4p_3)X_B^3] \tag{28}$$

Some of the p_i values in Equations 27 and 28 have the same values for a specific phase (*e.g.*, liquid phase, α, β, γ phase etc.); therefore, they can be cancelled by establishing an equality at equilibrium condition. Then, by substituting $a_i + b_iT = p_i$, a series of equations can be generated at various temperatures and systematically solved. In this process, choosing temperatures and compositions where two-phase equilibrium exists is important. It should be noted that small variations in the chosen composition of a species can drastically change the placement of the common tangent, which, in turn, changes the excess properties. Although a series of mathematical equations are used, the final phase boundaries of a phase diagram cannot typically be fulfilled in one calculation. The purpose of introducing these equations is to present the principles behind the thermodynamic approach. For simple systems, for example, binary systems without intermetallic compounds or with only one or two compounds at relatively low temperatures, this method is efficient. For U-Me systems with four or five compounds, this method does not work well nor efficiently. This is why a new approach was proposed in Section 4.2 of this thesis.

However, once the Gibbs energy of mixing curves have been determined, the method of tangents will, of course, generate an appropriate phase diagram. A pair of Gibbs energy curves for the uranium-ruthenium binary system at 1200 K is shown in Figure 2-7.

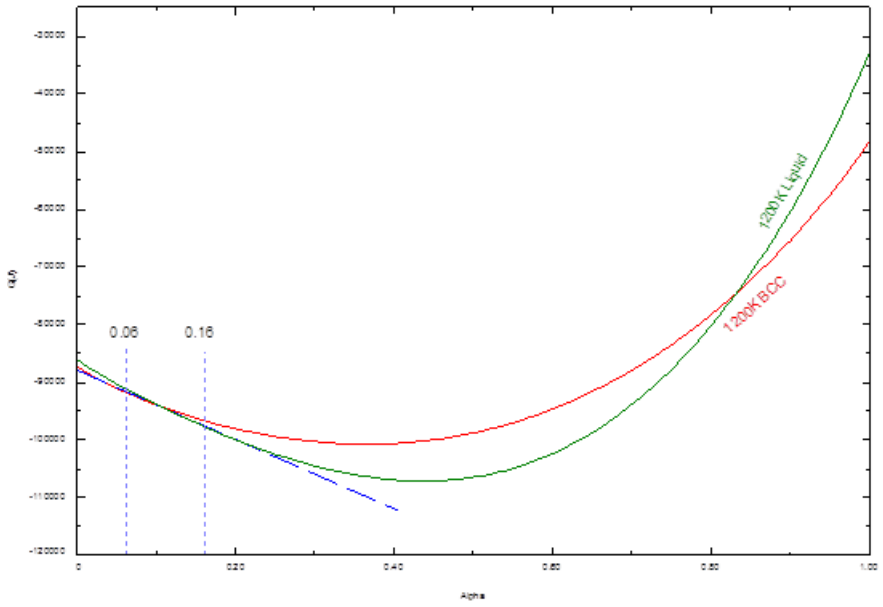

Figure 2-7. Gibbs energy curves for the *Liquid* phase (green) and *bcc* phase (red) in the U-Ru system at 1 atm and 1200 K.

The correlation between the Gibbs energy of mixing curves (Figure 2-7) and the calculated phase diagram shown in Figure 2-8 is explained briefly for the uranium-ruthenium system. On the U-rich part of the figure, the two Gibbs energy curves cross and a common tangent can be found. On Figure 2-7, the composition of the liquidus (mole fraction in terms of Ru is 0.16) and the solidus of the *bcc* phase (mole fraction in terms of Ru is 0.06) are calculated and illustrated. The compositions and the equilibrium tie line of *bcc* and *Liquid* phases (the dotted blue lines) are shown on the U-Ru phase diagram in Figure 2-8. In contrast, the crossing of the two Gibbs energy curves on the Ru-rich side (right side) of Figure 2-7 has no practical meaning because the *Liquid-bcc* equilibrium is

hypothetical. In Berche *et al*. [17], the solubility of U in Ru was supposed to be zero, therefore, no *cph* solution phase is shown in Figure 2-8. In this work the *cph* solid solution phase has been added and the *Liquid-cph* two-phase equilibrium has been shown in [59]. Figure 2-7 and Figure 2-8, however, show clearly how a hypothetical lattice stability functions and why it is necessary for thermodynamic calculations: the crossing of the two Gibbs energy curves on right part of Figure 2-7 does not coincide with the liquidus on the right part of the U-Ru phase diagram (Figure 2-8), which means the hypothetical lattice stabilities do not affect the real shape of the calculated phase diagram.

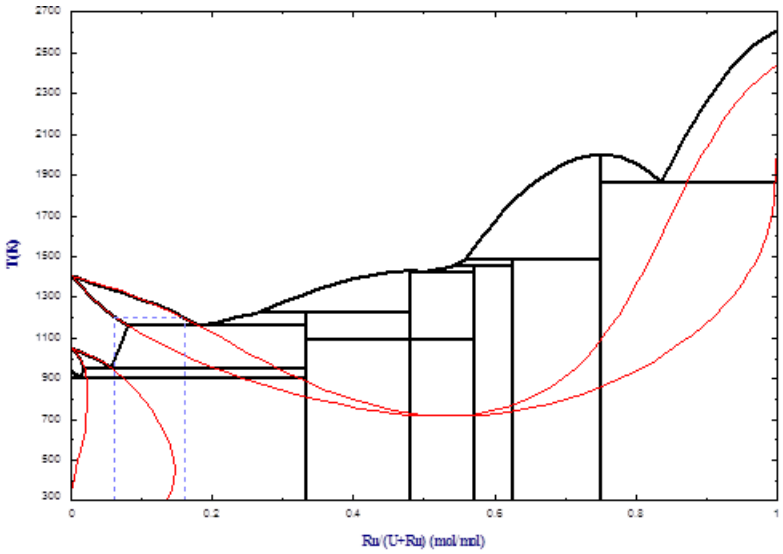

Figure 2-8. A calculated U-Ru phase diagram with metastable phases*. The vertical dash lines show equilibrium compositions of *bcc* and *Liquid* phases and the horizontal dash line shows the two phase equilibrium at 1200 K.

* Please note that in this phase diagram the *cph* phase is not added.

3 Previous Experimental Work — A Literature Review

3.1 Preliminary Remarks

The quaternary system U-Pd-Rh-Ru consists of six binary systems (Pd-Rh, Pd-Ru, Rh-Ru, U-Pd, U-Rh, and U-Ru), four ternary systems (Pd-Rh-Ru, U-Pd-Rh, U-Pd-Ru, and U-Rh-Ru) and the important pseudo-ternary system UPd_3-URh_3-URu_3. As mentioned in Table 1-1, some of these systems have been previously modelled, but the majority have not and original evaluations will be presented in the results of this work (See Chapter 5). This does not mean that there has not been experimental work performed in the quaternary system. On the contrary, there is a modest amount of experimental work that can be used to complete self-consistent thermodynamic evaluations.

As an introduction to the six binary systems, the latest phase diagrams are presented here.

3.1.1 Pd-Rh, Pd-Ru, and Rh-Ru Systems

The evaluation for the Pd-Rh system has been accepted from the work of Kaye [15] and Kaye *et al*. [16]. Figure 3-1 shows the evaluated phase diagram at a system pressure of 1 atm. Note the absence of metallic compounds, and the presence of a solid-state miscibility gap.

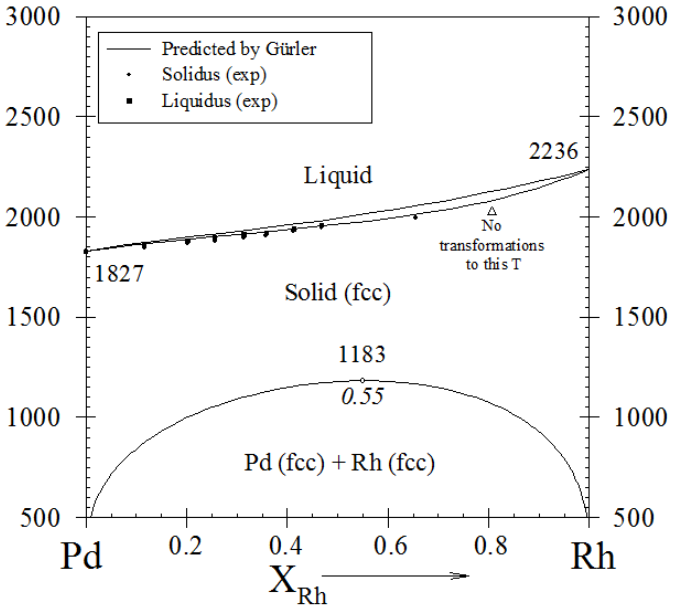

Figure 3-1. Pd-Rh phase diagram [15,16].

Figure 3-2 shows the Pd-Ru system from the work of Kaye *et al*. [15,16]. Again note the absence of metallic compounds.

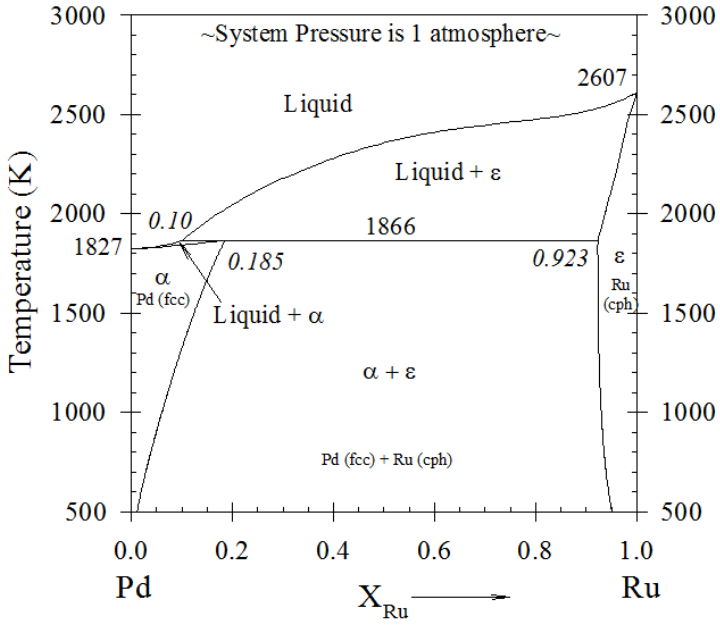

Figure 3-2. Pd-Ru phase diagram [15,16].

Figure 3-3 shows the Rh-Ru system from the work of Kaye *et al*. [15,16]. This diagram is also without metallic compounds.

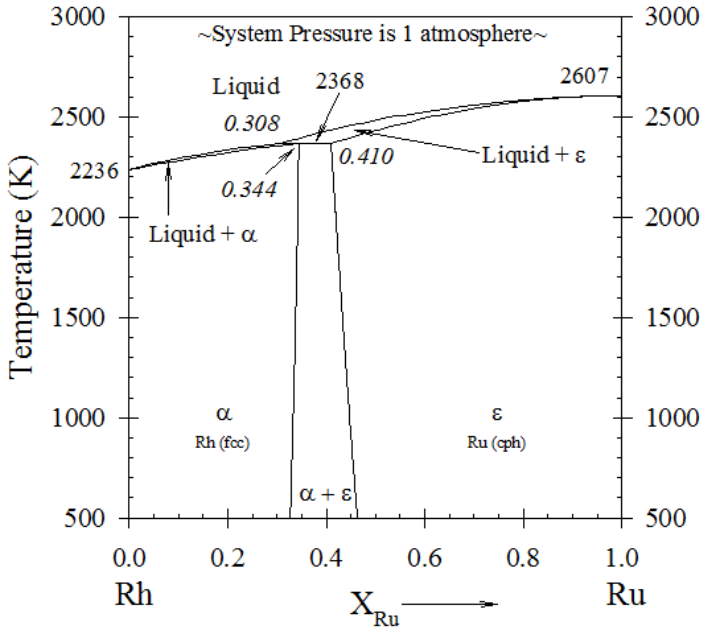

Figure 3-3. Rh-Ru phase diagram [15,16].

3.1.2 The Latest Experimental U-Pd, U-Rh, and U-Ru Phase Diagrams

The latest binary phase diagrams involving uranium are markedly different from the first three binary phase diagrams presented in Section 3.1.1. Firstly, uranium has three allotropic crystal structures and secondly the U-related binary phase diagrams are characterized by the existence of many intermetallic compounds. The latest U-Pd phase diagram was compiled by Kleykamp and Kang [37], which also appeared in the *ASM Handbook* [60] is shown in Figure 3-4.

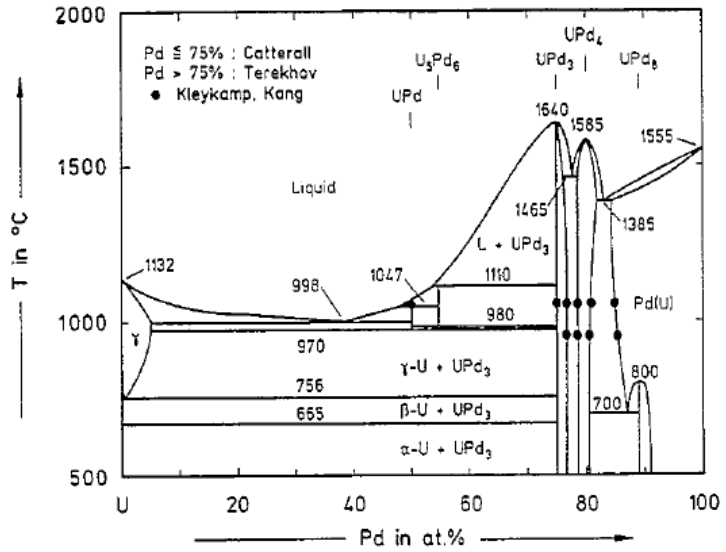

Figure 3-4. The U-Pd phase diagram edited by Kleykamp and Kang [37].

The latest U-Rh phase diagram, taken from the *ASM Handbook* [60], is shown in Figure 3-5.

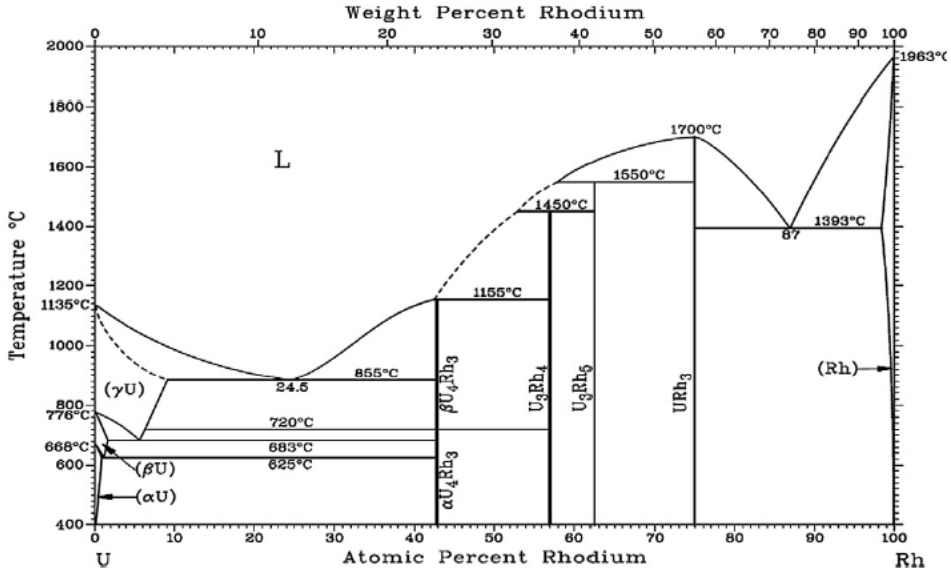

Figure 3-5. U-Rh phase diagram by Park, as shown in *ASM Handbook* [60].

The latest U-Ru phase diagram, taken from [17] is shown in Figure 3-6. This is the only one in three of the U-Me phase diagrams that was thermodynamically evaluated by a CALPHAD software—Thermo-Calc.

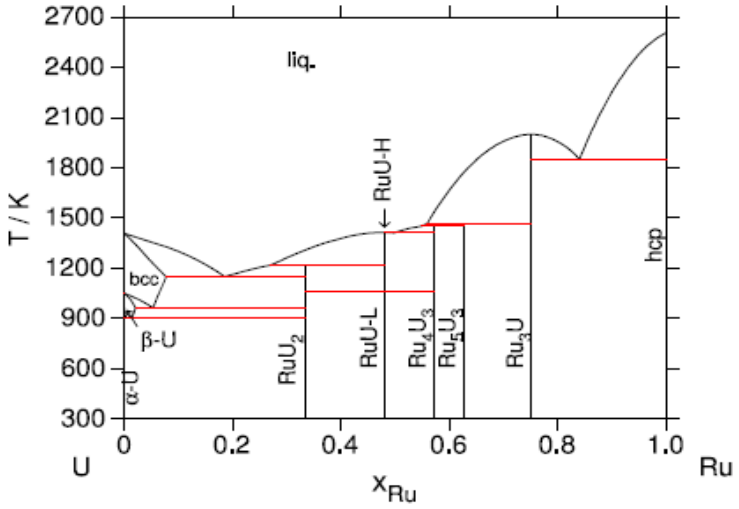

Figure 3-6. The first thermodynamic description of U-Ru system by Berche *et al.* [17].

3.1.3 Outline for Chapter 3

In the following sections of this chapter, the thermodynamic data from the literature for the U-Pd-Rh-Ru quaternary system will be presented. First, the properties of the component elements (U, Pd, Rh, and Ru) will be examined; compounds in the U-Pd, U-Rh, and U-Ru system will be introduced; properties for solution phases from previous thermodynamic modelling will be listed (*e.g.*, the Pd-Rh-Ru ternary system and its constituent binary systems); and finally experimental work from the other ternary and pseudo-ternary system will be illustrated.

3.2 Thermodynamic Properties of the Elements: Pd, Rh, Ru, and U

Basic thermodynamic data for the elements Pd, Rh, Ru, and U have been well described in the literature [61-65] and the enthalpies of formation, entropies, and heat capacities of elements related to this work are listed in Table 3-1.

Table 3-1. Thermodynamic data of U, Pd, Rh, and Ru [61-65].

Element	ΔH°_{298}	S°_{298}	$c_P = a + bT + cT^{-2} + dT^2$ $(J \cdot mol^{-1} \cdot K^{-1})$				T_{min}	T_{max}
	$(J{\cdot}mol^{-1})$	$(J{\cdot}mol^{-1}{\cdot}K^{-1})$	a	b x 10^3	c	d x 10^6	(K)	(K)
U-α	0	50.29	26.919	-2.5020	-76985	0.2656	298	942
U-β	2790.7	53.25	26.919	-2.5020	-76985	0.2656	942	1049
U-γ	3231.1	47.97	42.928	0	0	0	1049	1405
U-*Liq.*	4375.2	44.24	48.660	0	0	0	1405	4407
Pd-*fcc*	0	37.82	25.028	5.4404	-67548	0	298	3000
Pd-*Liq.*	16480.0	46.84	25.028	5.4404	-67548	0	298	3000
Rh-*fcc*	0	31.51	20.811	13.400	33942	-2.268	298	3000
Rh-*Liq.*	26568.0	43.39	20.811	13.400	33942	-2.268	298	3000
Ru-*cph*	0	28.53	22.236	4.1437	40607	1.6015	298	3000
Ru-*Liq.*	38589.0	43.34	22.236	4.1437	40607	1.6015	298	3000

Table 3-1 shows that U has three allotropic crystal structures: α-U has a crystal structure of *orthorhombic*_A20, which transforms to β-U (*tetragonal* crystal structure) at 669 ºC. The β-U is the crystal structure stable for only a range of temperature of 107 ºC, before transforming at 776 ºC to γ-U with a *bcc* crystal structure, which melts at 1132 ºC [61]. The other three elements have only one stable crystal structure: *fcc*-Pd, *fcc*-Rh, and *cph*-Ru, respectively.

However, in evaluating the solid solutions in the six binary systems involving U, Ru, Rh, and Pd, it is necessary to consider some hypothetical crystal structures of these elements (See Table 3-2). On the basis of a critical evaluation of the literature, a quinary solution model of the Mo-Pd-Rh-Ru-Tc system has been thermodynamically established by Kaye *et al*. [15,16], from which the Pd-Rh, Pd-Ru, and Rh-Ru subsystems will be used in this research. The Gibbs energy expressions for the elements in each phase (real or hypothetical) are given as the energy required to transition from a particular phase into the *Liquid* state. The values for these lattice stabilities are summarised in Table 3-2:

Table 3-2. Lattice stabilities for the components.

Phase	Gibbs energy (J·mol^{-1})	Comment	Reference
Pd (*Liquid*)	0	Reference phase	
Pd (*fcc*)	-16480 + 9.02T	Stable	[66-69]
Pd (*cph*)	-12300 + 14.88T	Hypothetical	[66,68,69]
Pd (*bcc*)	-12300 + 12.37T	Hypothetical	[66]
Rh (*Liquid*)	0	Reference phase	
Rh (*fcc*)	-26568 + 11.88T	Stable	[67,68,70]
Rh (*cph*)	-25910 + 12.51T	Hypothetical	[68,70]
Rh (*bcc*)	-19664 + 16.27T	Hypothetical	[70]
Ru (*Liquid*)	0	Reference phase	
Ru (*fcc*)	-21019 + 8.94T	Hypothetical	[68,69]
Ru (*cph*)	-38589 + 14.80T	Stable	[68]
Ru (*bcc*)	-30420 + 12.51T	Hypothetical	[69]

3.3 Thermodynamic Properties of the Compounds

3.3.1 UMe_3 Compounds

For the compounds UPd_3, URh_3, and URu_3 there have been various studies [71-76]. For example, Huang *et al.* [77] chose ΔH°_{298} = -524 kJ·mol^{-1} and established a Gibbs energy expression for UPd_3, which has been tested in the thermodynamic evaluation of the U-Pd phase diagram. Here the calculated entropy at 298 K was as low as 66.091 J·mol^{-1}·K^{-1}, only about ⅓ of the accepted value (176.35 J·mol^{-1}·K^{-1}) and lower than those of URh_3 and URu_3. This suggests that ΔH°_{298} = -524 kJ·mol^{-1} might not be reasonable. Further, for URu_3, URh_3, UPd_3, the distribution of experimental data gets larger, as shown in Table 3-3 and Figure 3-7.

Table 3-3. A summary of standard enthalpy of formation values from different authors.

Authors	$\Delta H^{\circ}_{298}\ (kJ \cdot mol^{-1})$		
	UPd_3	**URh_3**	**URu_3**
Jung and Kleppa [74]	-294.7	-278.8	-124.0
Wijbenga [72]	-524.0	-301.2	-153.2
Lorenzelli and Marcon [71]	-260.0		
de Boer *et al.* [73]	-244.0	-192.0	-152.0
Holleck and Kleykamp [75]		-256.7	-224.9
Edwards *et al.* [76]			-195.0

Jung and Kleppa measured enthalpies of formation of the compounds by means of (solute + solvent) drop calorimetry and compared them with previous studies [74]. The values that were listed in Table 3-3 are reproduced in Figure 3-7 in the manner of Jung and Kleppa [74].

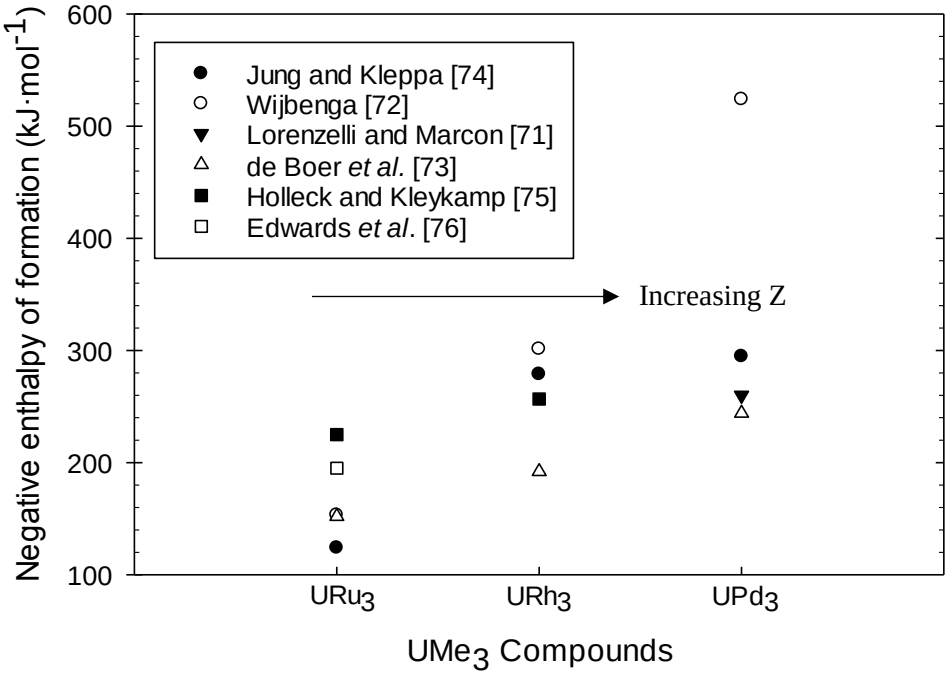

Figure 3-7. A summary of enthalpy of formation data from Jung and Kleppa [74].

In this figure, Z represents the atomic number of Ru, Rh and Pd elements. It is well known that to determine a reasonable liquidus position in a thermodynamic assessment some experimental data of thermodynamic properties are needed (*i.e.*, the mixing enthalpy or activity values as a function of composition or temperature). Otherwise, a similar phase diagram may be calculated, but with a completely wrong set of thermodynamic properties for the compounds or phases. Unfortunately, for systems involving uranium and refractory metals, these thermodynamic properties are often unavailable because even temperature measurements become problematic at high temperatures. In this research, as the liquidus of the three U-Me systems will be optimized, the enthalpies of the UMe_3 compounds will be re-evaluated thermodynamically, and all the enthalpies and entropies of other compounds will be estimated.

3.3.2 Other properties of UMe_3 compounds

3.3.2.1 Dissolution analysis

In order to study the properties of UMe_3 compounds in used fuels, dissolution of the spent fuel samples is necessary [78,79]. The process involves dissolution of the samples, separation of the insoluble residue, and non-destructive and/or destructive analysis of the insoluble residue. Non-destructive analyses include X-ray diffractometry (XRD), scanning electron microscopy (SEM), electron probe microanalysis (EPMA), and Gamma-ray spectroscopic measurements. In this process, the destructive study refers to further dissolution of the residue by a stronger acid mixture. However, one may not properly separate the UMe_3 compounds from the residue and did not obtain any thermodynamic values for these compounds.

3.3.2.2 Sample-crucible interaction in lattice parameter determination

Erdmann and Keller [80] measured lattice parameters of many actinide (lanthanide)-noble metal alloy phases and noticed a sample-crucible interaction phenomena. Although they sealed the crucibles of alumina, iridium or nickel in an alumina tube respectively, they found the some uranium were reduced to valences less than four.

3.3.2.3 Characteristic electronic structures and molar volume change

Johansson et al. [81] theoretically studied the actinide intermetallic compounds, especially UMe_3, with the scalar relativistic linear muffin tin orbital (LMTO) energy bands method, and found the "sudden localization" of the 5f electrons in UPd_3 in comparison to that of URh_3. In Figure 3 of the paper [81], UPd_3 shows a dramatic increase in molar volume change relative to that of URu_3 and URh_3. This was accounted for by the interaction of the 5f electrons of uranium and the 4d electrons of the transition metals. Thermodynamic evaluation in this work shows very similar abnormal effects among the U-Me systems, but not limited to molar volume change. McEwen *et al*. [82] preceded neutron inelastic scattering studies by means of high-resolution medium energy chopper spectrometer (HRMECS), and obtained the lattice constants/mole fraction curves for $U(Pd_{1-x}Pt_x)_3$ mixtures.

3.3.2.4 Thermal conductivities

Kurosaki *et al*. [83] evaluated the thermal conductivities of the UMe_3 compounds in the temperature range of 300-1200 K (27-927 °C). They found that the thermal conductivity of URu_3 is higher than those of URh_3 and UPd_3 over the whole temperature range.

3.3.2.5 Thermal expansion coefficient, longitudinal/shear sound velocities and hardness

Yamanaka *et al*. [84] examined some more mechanical and thermal properties of the UMe_3 compounds. UPd_3 had the highest thermal expansion coefficient, which is consistent with the theoretical study of molar volume changes by Johansson et al. [81] (See Section 3.3.2.3).

3.3.2.6 A μSR study of UPd_3 at an extremely low temperature range

Schenck *et al*. [85] carried out a μSR (Muon Spin Resonance) investigation on a single crystal of dhcp*-UPd_3 and reported an anomalous temperature dependence of the μ^+ Knight shift and provided a "phase diagram" at extremely low temperatures. From a completely different perspective, the authors proved that UPd_3 compound is different from other UMe_3 compounds and all other actinide/noble metal compounds. However, they pointed out at the end of the paper that the anomaly is similar to that of UPt_3. It is not an accident that the U-rich eutectic features of U-Pd and U-Pt were found to be similar in this work (See Section 6.2.3).

To sum up, these non-thermodynamic UMe_3 related studies are complementary with the present work. In other words, using the data provided in the papers one may correlate with the thermodynamically optimized Gibbs energy, enthalpy or other properties to establish equations useful in industrial processes in the future.

3.3.3 Heat capacity expressions of the UMe_3 compounds

For the intermetallic compounds in the U-Me systems, only a few compounds had been experimentally determined the heat capacity values over limited temperature ranges.

* A derivative hcp crystal structure.

Cordfunke *et al*. [86] measured the heat capacities of URu_3 and URh_3 from 5 to 850 K and Burriel *et al*. [87] measured the heat capacity of UPd_3 from 8 to 850 K. These results were gathered in a book by Cordfunke and Konings [61]. A summary of the heat capacities for the UMe_3 species over a wider temperature range are listed in Table 3-4 and illustrated in Figure 3-8.

Table 3-4. Heat capacity expressions used in this work.

Compound	**Heat capacity expression (C_p in $J \cdot mol^{-1} \cdot K^{-1}$)**	**Reference**
URu_3	$101.224 + 0.0185T - 471814T^{-2}$	[17], RMCC database
URh_3	$104.45 + 0.0182T - 610033T^{-2}$	RMCC database
UPd_3	$98.688 + 0.0114T$	Fact PS and RMCC base

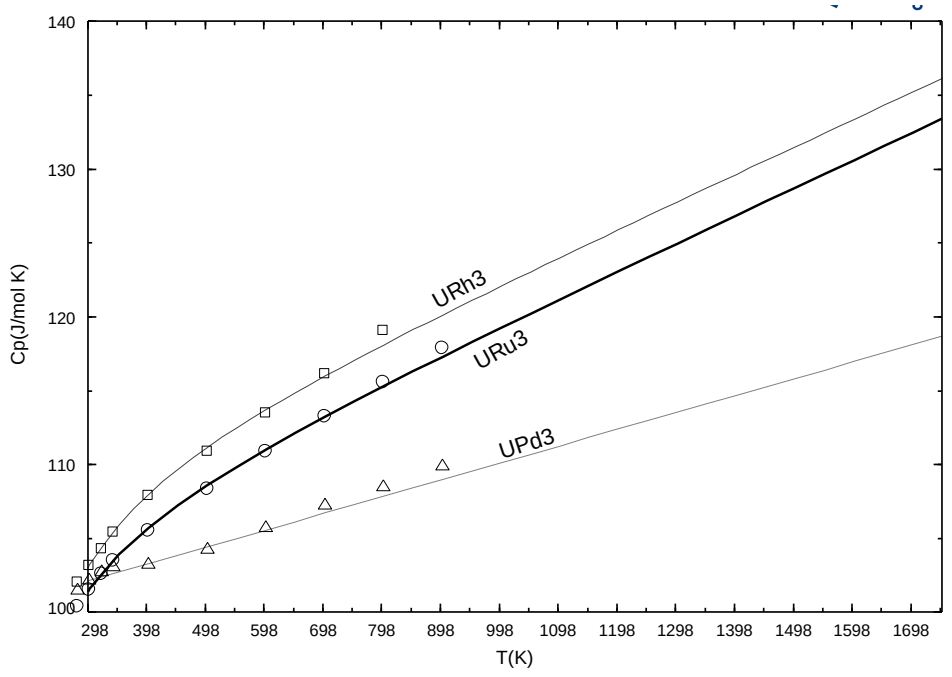

Figure 3-8. Calculated and experimental C_p curves for the UMe_3 compounds [86,87].

For other compounds, the heat capacities are calculated by the Kopp-Neumann rule [88,89]. As pointed out before, one of the main obstacles in any thermodynamic

evaluation, which is also true of the U-Me systems, occurs when thermodynamic data are not available in the literature. The use of the Kopp-Neumann rule is an approximation, but it provides a means to estimate linearly the heat capacities of a compound from those of its constituent elements. Thus, it provides a very good "first guess" when the data are not available. Although this introduces some uncertainties for heat capacities, the advantages provide useful Gibbs energy expressions that are proportional to the known UMe_3 compounds in each of the three systems. Because the Gibbs energy expressions are determined under many phase equilibrium conditions in the phase diagrams, these results can provide guidance for future experimental work. The heat capacity curves of UMe_3 compounds fit well with available experimental data and it is supposed can be extrapolate to about 2000 K, a temperature to which the compounds are stable.

There is considerable experimental work regarding for the UMe_3 compounds, namely: UPd_3 [61,71-74,77,87,]; URh_3 [61,73-75,77,86,91]; and URu_3 [61,73,74,76,77,86, 91]. Finally, experimental enthalpies of formation for UMe_3 compounds are available, but with large discrepancies [74]. Because these properties are re-examined in the thermodynamic evaluations, they will be discussed in detail later in this thesis.

3.3.4 Other Compounds in U-Me System

Except for the UMe_3 compounds introduced above, many other U_xMe_y compounds had been proved to exist or suggested during the experimental construction of the U-Me binary phase diagrams. These are summarized briefly in the following three sub-sections.

3.3.4.1 Compounds in U-Pd System

Due to the influence of the strongest catalytic property of Pd among the three Me elements considered in this work, the experimental determinations of the intermediate compounds in U-Pd system from different groups of scientist are extremely diverse. Catterall, Grogan, and Pleasance [92] found only three intermetallic compounds in their experiments. They are UPd, U_5Pd_6, and UPd_3, and they found no compounds beyond UPd_3 in the Pd-rich side.

Pells, however, declared in 1963 that there are four more compounds beyond UPd_3 namely: UPd_4, UPd_5, U_2Pd_{11}, and U_2Pd_{17} [100]. Five years later, Terekhov *et al.* [93] questioned the existence of U_2Pd_{11} and U_2Pd_{17}, and proposed the existence of only UPd_8. After this, the compounds in U-Pd system were accepted as UPd, U_5Pd_6, UPd_3, and UPd_8, among which the thermodynamic properties and crystal structures remain unknown before this work, except for UPd_3.

3.3.4.2 Compounds in U-Rh System

The first partial experimental phase diagram (U-rich part) was obtained by Chiswik *et al.* [94] and they found two intermetallic compounds: U_2Rh and URh. The only complete experimental phase diagram of U-Rh system was compiled by Park [42,95], in which the four intermetallic compounds determined were: U_4Rh_3 (in two crystal structures L-U_4Rh_3 and H-U_4Rh_3), U_3Rh_4, U_3Rh_5, and URh_3. In 1974, Naraine and Bell [96] suggested the existence of U_2Rh and URh at the U-rich side, but did not propose a phase diagram.

3.3.4.3 Compounds in U-Ru System

Although there are several experimental explorations of the U-Ru binary system, there is only one complete phase diagram, which was proposed by Park [42,95]. Compared

to the other two U-Me binary systems, there are no computations of the types of intermetallic compounds in U-Ru system. The five compounds are: U_2Ru, URu, U_3Ru_4, U_3Ru_5, and URu_3.

3.4 Thermodynamic Properties of Solution Phases

Previous experimental work and a thermodynamic evaluation exist for the three binary systems of the Pd-Rh-Ru ternary system. This work will be presented first. Experimental work on the other three uranium related ternary systems will be presented after that, followed by the work from the pseudo-ternary UPd_3-URh_3-URu_3.

3.4.1 Properties of Solution Phases in Pd-Rh, Pd-Ru, and Rh-Ru Binary Systems

The Pd-Rh-Ru ternary system has three binary subsystems. For the Pd-Rh, Pd-Ru, and Rh-Ru subsystems, the excess properties were taken from Kaye *et al*. [15,16], and the expressions are shown in Table 3-5 (X_i represents the mole fraction of species *i*).

Table 3-5. Excess properties for the binary subsystems.

Phase	**Subsystem**	**Expression for the excess Gibbs energy (*i.e.*, ΔG^E) ($J \cdot mol^{-1}$)**
Liquid	Pd-Rh	$X_{Pd}X_{Rh}[20027 - 2260X_{Rh} - (2.74 - 0.56X_{Rh})T]$
bcc	Pd-Rh	$X_{Pd}X_{Rh}[20920]$ (hypothetical)
cph	Pd-Rh	$X_{Pd}X_{Rh}[20920]$ (hypothetical)
fcc	Pd-Rh	$X_{Pd}X_{Rh}[21247 + 2199X_{Rh} - (2.74 - 0.56X_{Rh})T]$
Liquid	Pd-Ru	$X_{Pd}X_{Ru}[187564.062 - 62169.281X_{Pd} - (63.661 - 6.64X_{Pd})T]$
bcc	Pd-Ru	$X_{Pd}X_{Ru}[20000]$ (hypothetical)
cph	Pd-Ru	$X_{Pd}X_{Ru}[-1524.818 + 14.933T]$
fcc	Pd-Ru	$X_{Pd}X_{Ru}[-5049.035 + 17.59T]$
Liquid	Rh-Ru	$X_{Rh}X_{Ru}[-35739.32 + 16.369T]$
bcc	Rh-Ru	0 (hypothetical)
cph	Rh-Ru	$X_{Rh}X_{Ru}[-26440.004 + 10.445T]$
fcc	Rh-Ru	$X_{Rh}X_{Ru}[-53477.07 + 21.738T]$

The three calculated phase diagrams are quoted in this research in the next section.

3.4.2 Pd-Rh-Ru Ternary System

From the three subsystems shown, isothermal sections of the Pd-Rh-Ru ternary system have been obtained at various temperatures by thermodynamic interpolations. These enabled the ternary excess Gibbs energy terms to be calculated as explained previously by Kaye *et al.* [15,16]. These parameters are given in Table 3-6.

Table 3-6. Ternary excess Gibbs energy terms for Pd-Rh-Ru ternary system [15,16].

Phase	**Components**	**Ternary excess Gibbs energy term ($J \cdot mol^{-1}$)**
Liquid	Pd-Rh-Ru	$X_{Pd}X_{Rh}X_{Ru}(-52500)$
cph-solid	Pd-Rh-Ru	$X_{Pd}X_{Rh}X_{Ru}(-90000)$
fcc-solid	Pd-Rh-Ru	$X_{Pd}X_{Rh}X_{Ru}(-40000)$

A comparison of the experimental work of Paschoal *et al.* [97] with the evaluated ternary model at 1973 K, taken from [15,16], shows agreement between the model and the experimental values. This is illustrated in Figure 3-9.

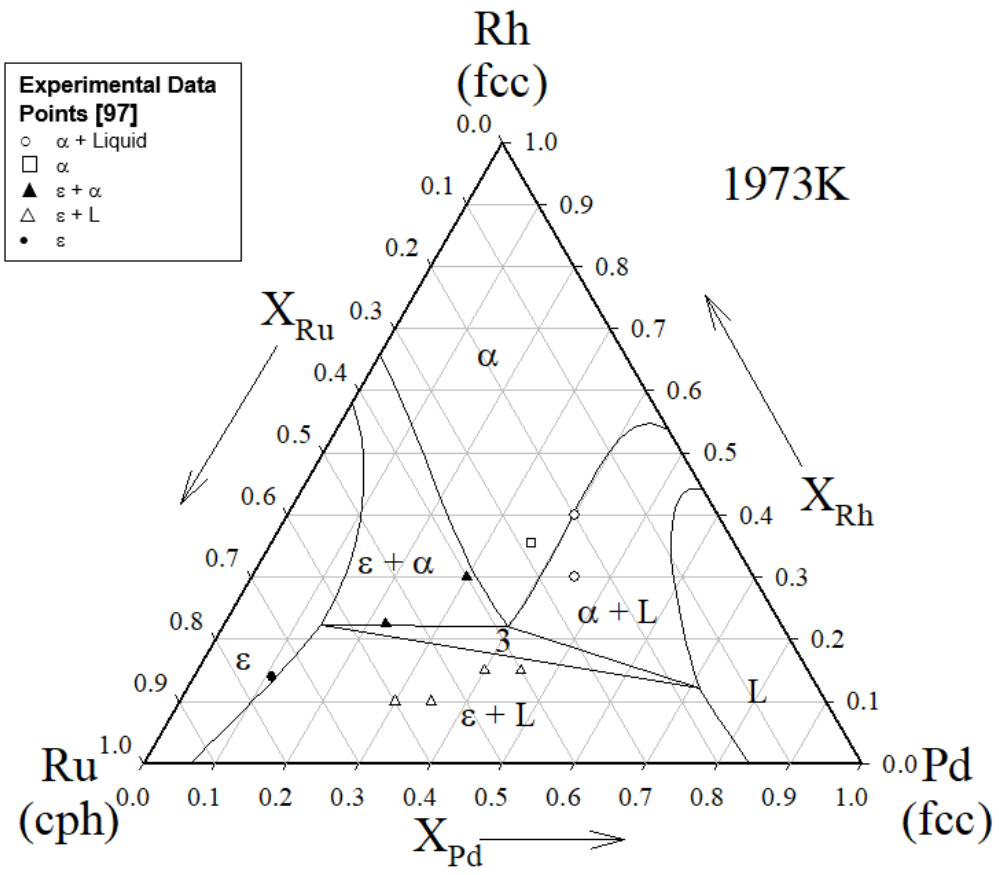

Figure 3-9. Rh-Ru-Pd ternary isothermal section interpolated from Rh-Ru, Rh-Pd, and Ru-Pd subsystems at 1973 K [15,16,97].

The establishment of the ternary excess Gibbs energy terms is necessary because without adequate adjustments, the calculated phase boundaries do not fit with the experimental data, as illustrated in Figure 3-10. Figure 3-10 shows a ternary isothermal section without establishing the ternary interaction parameters. In Figure 3-10, one ε + α phase data point falls into an α phase region and another into a three phase region, while one ε phase data point falls into ε + L phase field. It should be noted that the ternary excess terms are relatively small and the adjustments of the phase relations are slight, but significant as they now account for the experimental observations of Paschoal *et al*. [97]

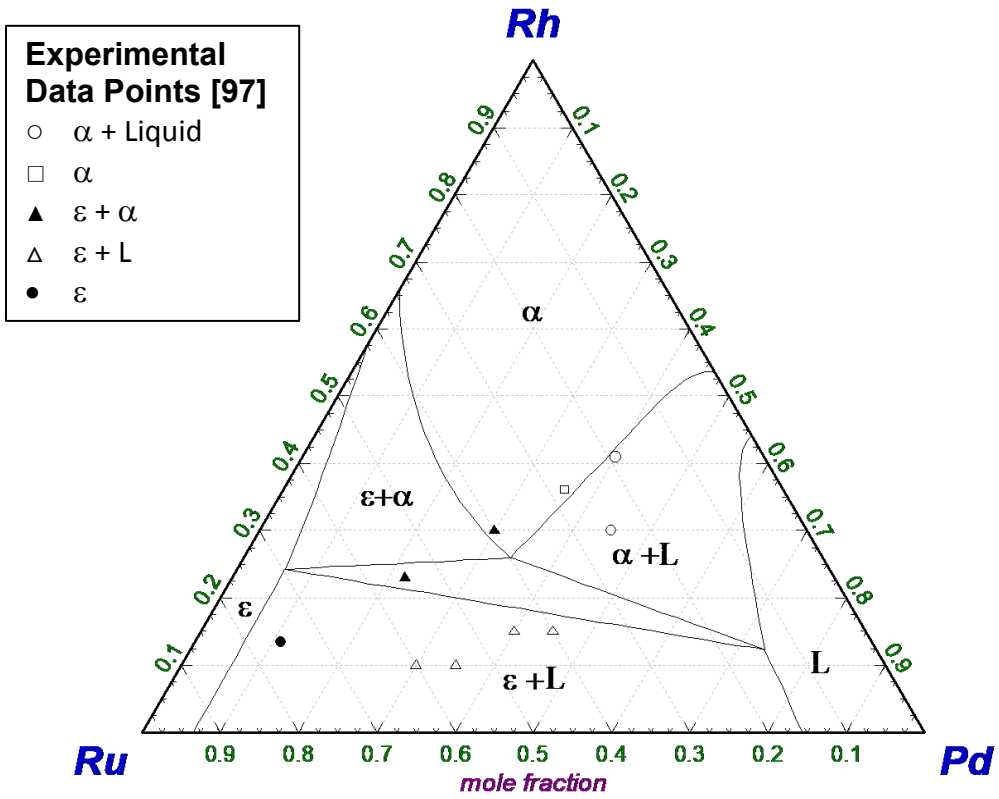

Figure 3-10. Calculated Rh-Ru-Pd ternary diagram at 1 atm, 1973 ºC without ternary excess parameters [15]; note poor agreement with experimental data [97].

3.5 Previous Binary U-Me Experimental Phase Diagrams

In Section 3.1.2, the latest U-Me phase diagrams are illustrated. In the following three sub-sections, a summary of the development of the U-Pd, U-Rh, and U-Ru phase diagrams will be presented.

3.5.1 U-Pd Binary System

There have been several experimental descriptions of the U-Pd binary system [37, 92,93,98-100]. In 1956 the first U-Pd phase diagram (Figure 3-11) over the whole composition range was proposed by Catterall, Grogan, and Pleasance [92], but with great uncertainty in the region from 75 to 100 at.% Pd.

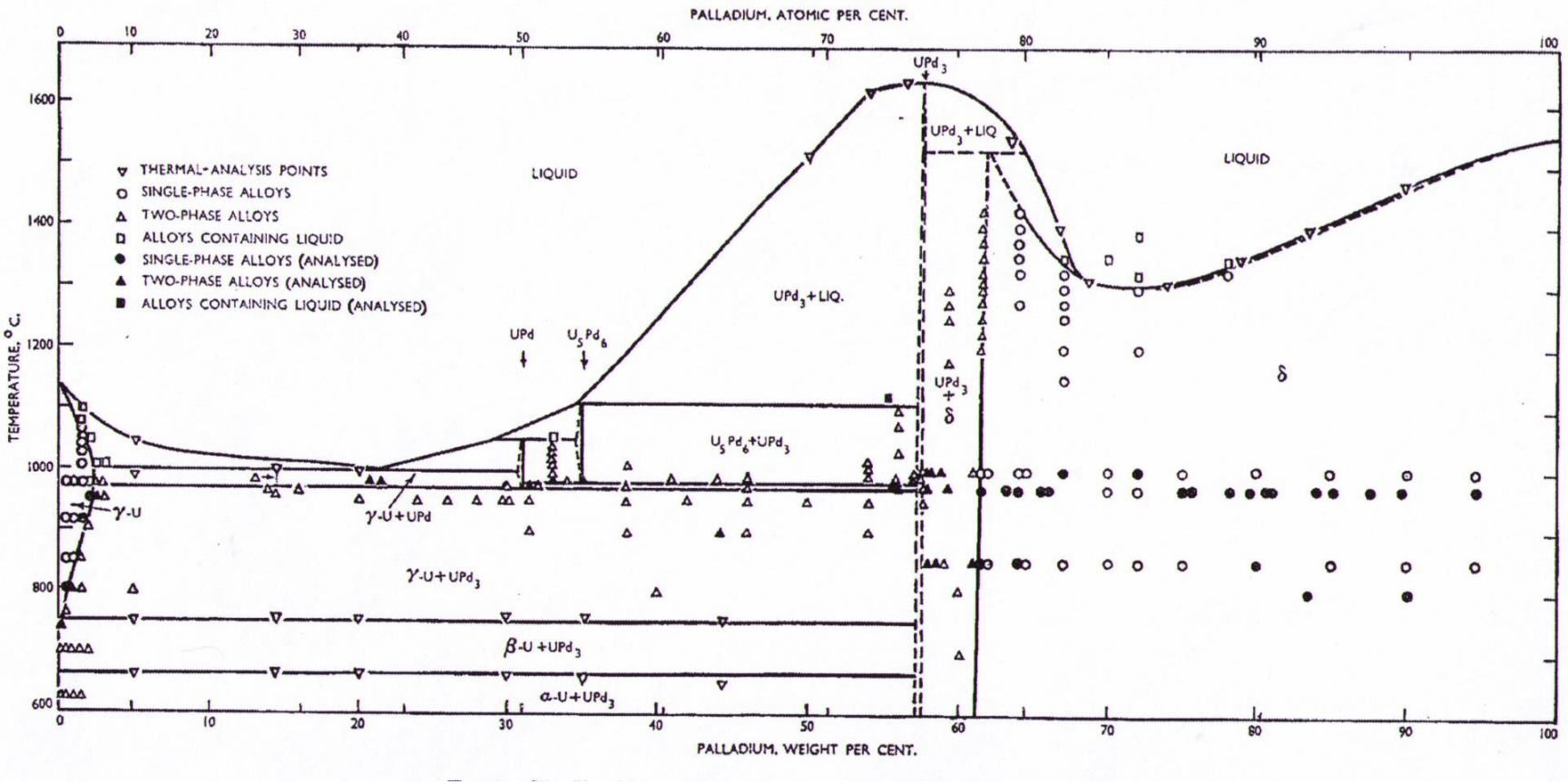

Figure 3-11. An early U-Pd phase diagram by Catterall, Grogan, and Pleasance [92].

In the same year, Park and Buzzard presented a report [98] at a Metallurgy Information Meeting, in which the progress developing phase diagrams of uranium with all the six platinum metal elements (Ru, Rh, Pd, Os, Ir, and Pt) was presented. The preliminary diagram for U-Pd had two distinctive features:

i. The *bcc* eutectic composition was much lower than the one detected by Catterall, Grogan, and Pleasance (13.7 wt.% Pd < 21 wt.% Pd) [92]; and
ii. The two compounds detected by Catterall, Grogan, and Pleasance were not detected at all within 30-35 wt.% Pd, and only a few features on the right part of the phase diagram were mentioned in the texts of the report without giving the phase boundaries [92].

In 1963, Park, Fickle, and Mullen submitted a complete report of their research on the U-Pd system, shown in Figure 3-12, without publishing it in a journal [99].

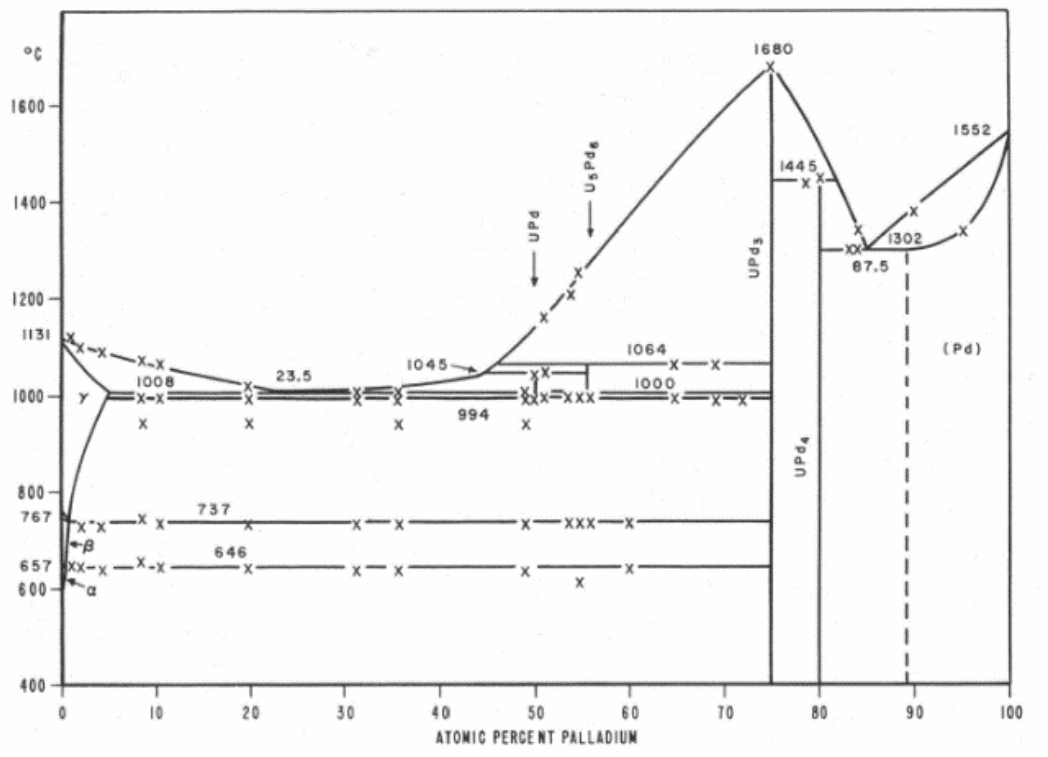

Figure 3-12. The complete U-Pd phase diagram by Park, Fickle, and Mullen [99].

The compounds and liquidus within 75 to 100 at.% Pd were experimentally investigated by Pells [100] in 1963 (Figure 3-13). In this partial phase diagram, the following five compounds were specified: UPd_3, UPd_4, UPd_5, U_2Pd_{11}, and U_2Pd_{17}.

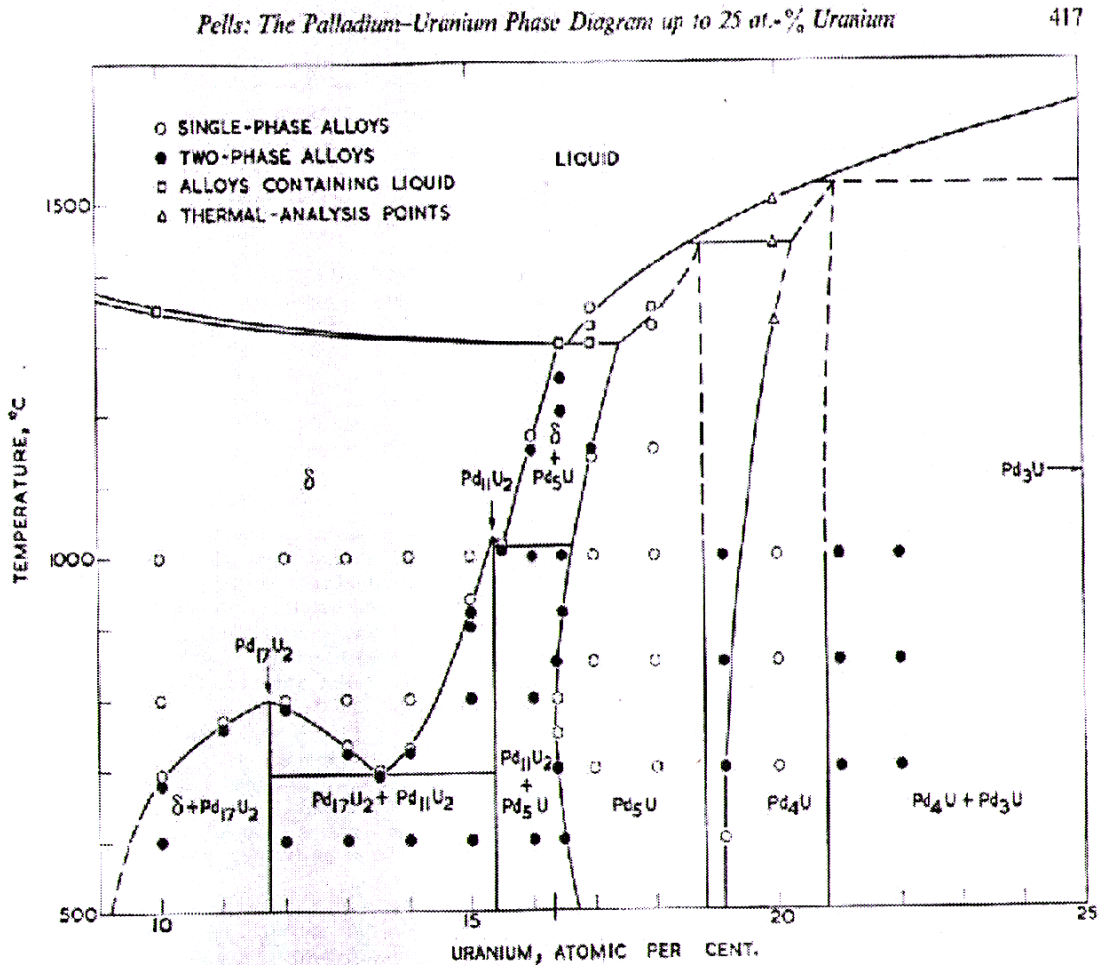

Figure 3-13. An investigation of the U-rich side of U-Pd phase diagram by Pells [100].

In 1968, a group of Soviet scientists re-examined this part of the phase diagram [93]. They refuted the existence of U_2Pd_{11} and U_2Pd_{17}, and declared the existence of UPd_8. By means of thermal analysis in combination with the XRD technique they obtained a very neatly shaped phase diagram, especially at the high temperature range (Figure 3-14). Unlike other experimentalists, they did not change from thermocouples to pyrometers even

at the high temperature range, which is very close to the limit of the application of the thermocouples.

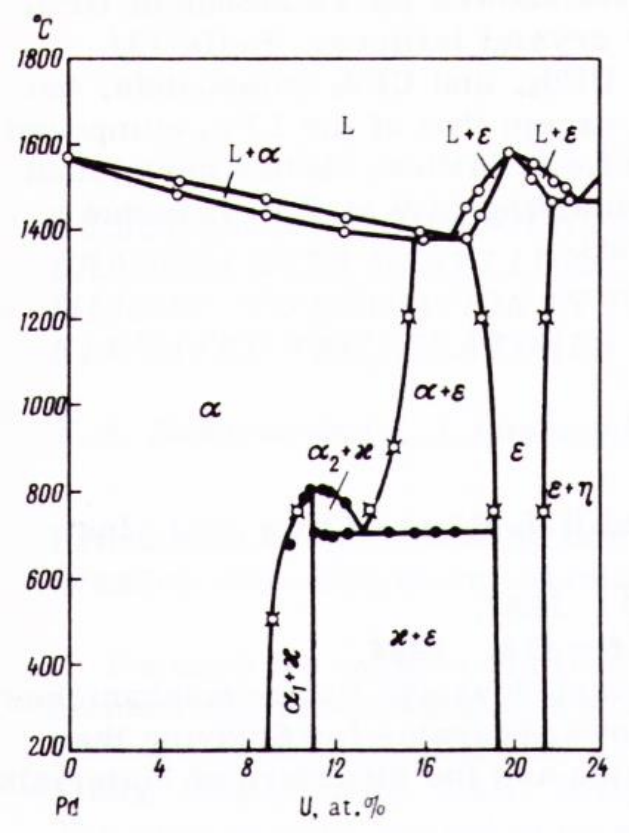

Figure 3-14. Pd-rich partial diagram by Terekhov *et al*. [93].

In 1986, a U-Pd phase diagram was constructed by combining the U-rich part of the phase diagram suggested by Catterall, Grogan, and Pleasance [92] and the Pd-rich part of the phase diagram by Pells [100], shown in Figure 3-15 [60].

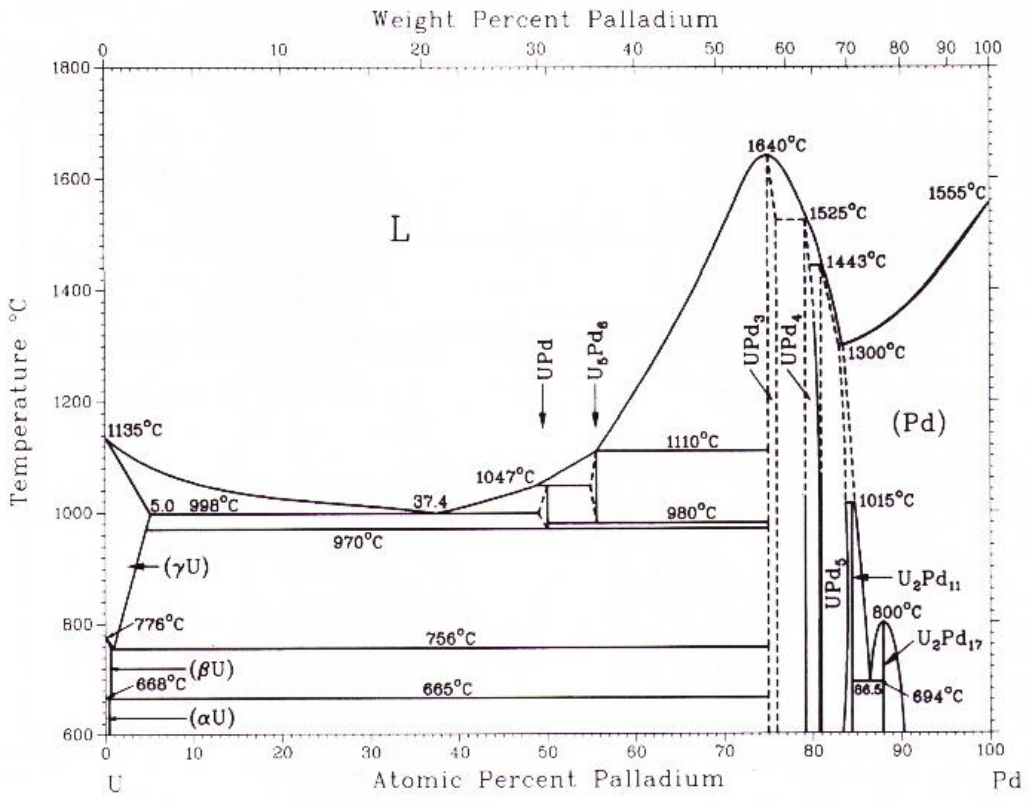

Figure 3-15. A combined phase diagram from Catterall, Grogan, and Pleasance [92] and Pells [100]. It was published in the *ASM Handbook* [60].

In 1991, Kleykamp and Kang [37] performed annealing experiments at a few selected points. The diagram that they proposed was a combination of the U-rich part by Catterall, Grogan, and Pleasance [92] and the Pd-rich part by Terekhov *et al.* [93]. This phase diagram, shown in Figure 3-4, is currently the accepted U-Pd phase diagram [37]. The U-Pd phase diagram can also be found in *ASM Handbook* [60].

3.5.2 U-Rh Binary System

There have been several experimental descriptions of the U-Rh binary system published in the literature [42,94-96]. Park presented the U-Rh system phase diagram in his PhD thesis [42] together with the U-Ru binary system that were published as two separate papers in 1968 [95]. Park's U-Rh phase diagram is the most accepted one to date

because nobody has repeated the experiments over the full composition range. However, in studies focused on some specific locations of the diagram, there were conflicting data regarding the existence of some of the compounds. For example, Chiswik *et al*. [94] showed in 1958 that instead of U_4Rh_3, two other compounds were found at about 33.3 at.% Rh (U_2Rh) and 50 at.% Rh (URh), as illustrated in Figure 3-16.

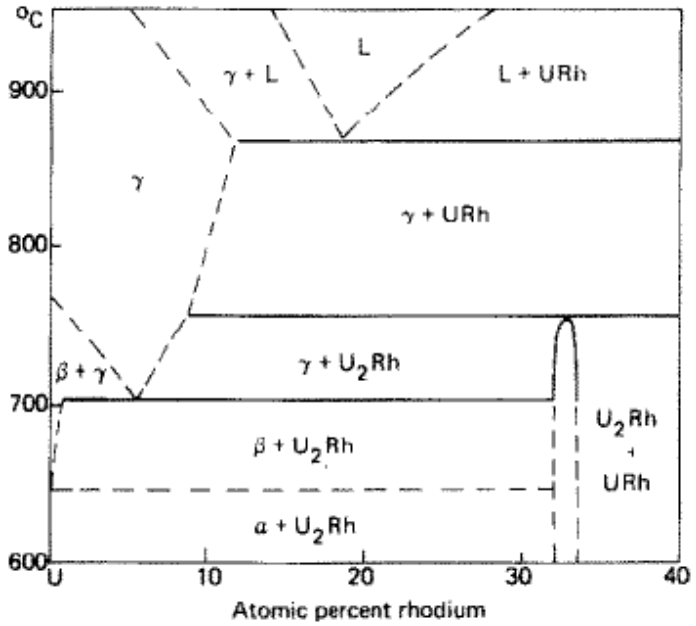

Figure 3-16. A partial U-Rh phase diagram by Chiswik *et al*. [94].

In 1974, based on the observation of Chiswik *et al.* [94], Naraine and Bell [96] experimentally re-examined the compounds using EPMA and concluded that there should be five compounds in the system (instead of four as shown by Park), namely: URh_3, U_3Rh_5, U_3Rh_4, URh, and U_2Rh. If true, the U-Rh phase diagram would be more similar to the U-Ru phase diagram. Nevertheless, because they did not measure the melting points of the compounds, liquidus, and other phase boundaries in other regions, Naraine and Bell [96] did not provide a new U-Rh phase diagram.

Therefore, the U-Rh phase diagram of Park was adopted by the *ASM Handbook* [60], shown in Figure 3-17.

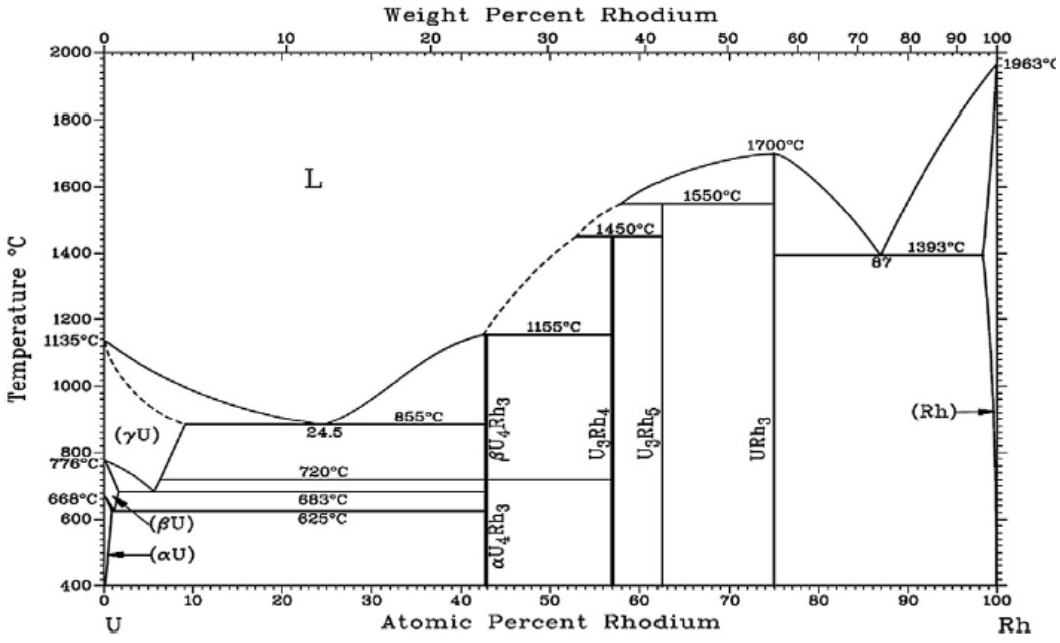

Figure 3-17. U-Rh phase diagram by Park, as shown in *ASM Handbook* [60].

The U-Rh system had not been thermodynamically evaluated before this work.

3.5.3 U-Ru Binary System

There have been several experimental descriptions of the U-Ru binary system published in the literature [4,42,95,101-103]. The earliest U-Ru phase diagram was published in 1958 [101], which is a partial phase diagram without high temperature phase boundaries. This shows that temperature measurement above 1000 ºC was difficult for this system.

Figure 3-18 shows the first complete U-Ru phase diagram obtained experimentally by J.J. Park and published in his PhD dissertation [42]. Three years later, the results were published as a journal paper [95].

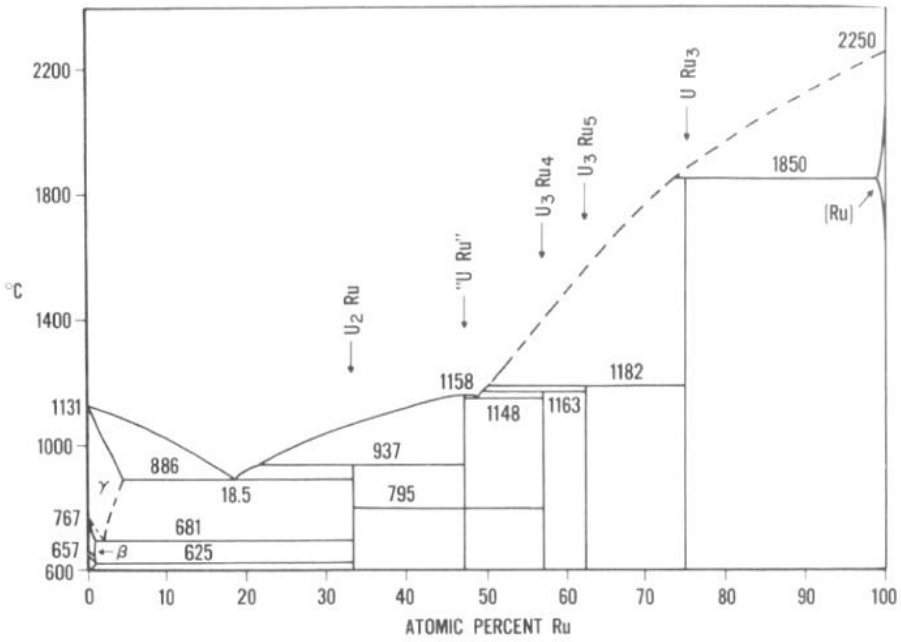

Figure 3-18. The first complete U-Ru experimental phase diagram by Park [95].

More than two decades later, Mason and El-Genk [4] re-examined the high temperature part (from 50 to 100 at.% Ru) of the system, shown in Figure 3-19. They suggested that the URu_3 melted congruently and that the reaction involving Ru and URu_3 was not peritectic, but eutectic with a eutectic isotherm at 1861 ± 20 K and a eutectic composition of 77.5 ± 1 at.% Ru [4]. The profile of the liquidus showed great difficulties (see the phase boundaries illustrated by dotted lines in [Figure 3-18]) in high temperature measurements with chemical interactions between the samples and the crucibles. In fact, it was so difficult to determine the liquidus in their experiments that they gave two possible liquidus curves on the diagram.

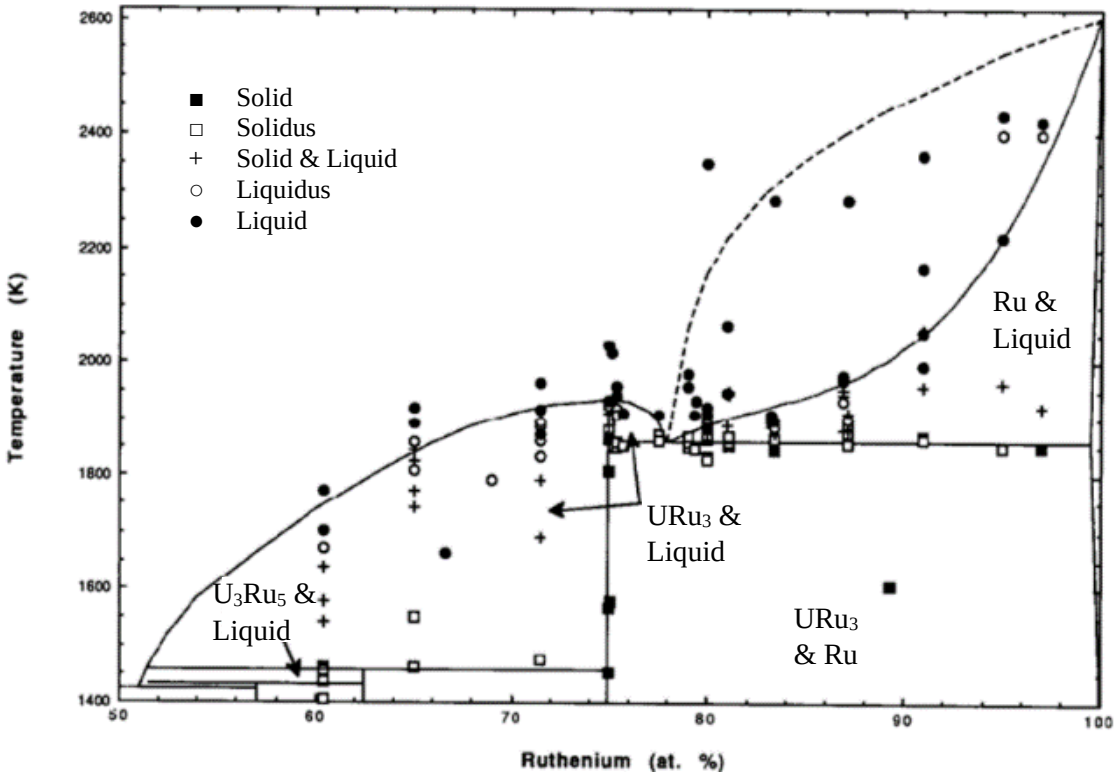

Figure 3-19. Re-examination of Ru-rich part of U-Ru system by Mason and El-Genk [4].

In 2011 the first thermodynamic assessment of U-Ru system was published by Berche *et al.* [17], in which major changes had been made on the Ru-rich side: they placed an eutectic reaction to the right of the URu_3 compound, which had a congruent melting according to experiments by Mason and El-Genk [4][*]. Nevertheless, the *cph* solution phase was missing. The diagram calculated by Berche *et al.* [17], is shown in Figure 3-6.

3.6 Ternary Experimental Isothermal Sections

The significance of establishing binary thermodynamic models lies not only in obtaining a numerical description of the experimental phase diagrams, but also in calculating some unknown thermodynamic properties and making it possible to extrapolate

[*] At this point, the result of the thermodynamic treatment is not the same as the experimental one in [4], which does not mean the thermodynamic method failed to mimic the experimental data; on the contrary, it is a sign of the latent potential of the method in identifying experimental fallacies.

to higher order systems. The establishment of a quaternary U-Pd-Rh-Ru thermodynamic model enables calculation of ternary isothermal sections of any three elements in the quaternary system and estimate quasi- or pseudo-phase diagrams, *e.g.*, U-Rh-Pd, U-Ru-Pd, U-Ru-Rh, URu_3-URh_3, URu_3-UPd_3, URh_3-UPd_3, and URu_3-URh_3- UPd_3 *etc*.

Experimental data available for the U-Ru-Pd and U-Ru-Rh ternary systems is absent from the literature. However, there is a limited amount of data for the U-Pd-Rh ternary system, as will be discussed in the following section.

3.6.1 U-Pd-Rh Isothermal Section at 1050 ºC

The U-Pd-Rh ternary systems was investigated experimentally and at only one temperature (1050 ºC) by Kleykamp and Kang [37]. They prepared 74 samples, each annealed at this temperature for at least 3 to 6 weeks. They discovered that although the single *fcc* phase of Rh and Pd solution exists at 1050 ºC on the Rh-Pd binary phase diagram, on the ternary phase diagram with U an isolated "island" or, as they named it, a "closed region" was identified at low U content region (Figure 3-20). Their acceptance of the existence of U_5Pd_6 (stable between 980-1110 ºC) as they combined U-Pd phase diagram from the two sources is contradicted by the fact that the compound is missing on their own ternary isothermal section.

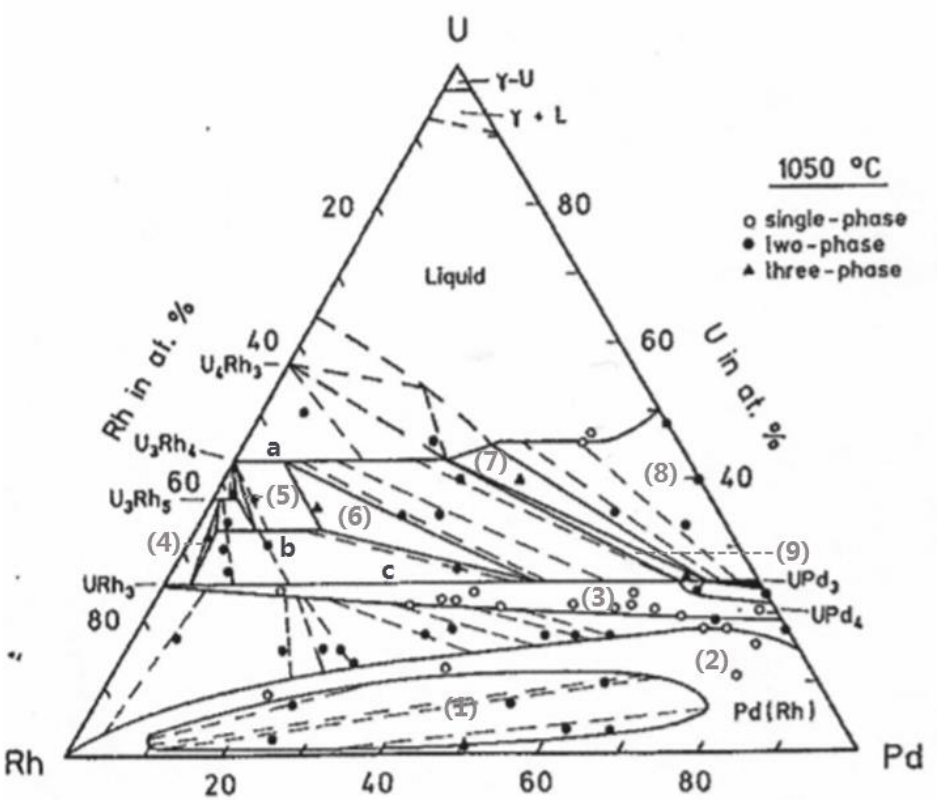

Figure 3-20. An isothermal section of U-Rh-Pd ternary system obtained experimentally by Kleykamp and Kang [37].

The numbers (1-9) on Figure 3-20 refer to problematic phase regions defined by Kleykamp and Kang and the phase areas are analysed in Table 6-8.

It is interesting that Kleykamp and Kang [37] tried to validate the presence of the "closed region" by estimating the binary interaction parameters, simplifying the symmetric equation, and calculating spinodal curves at different U-Pd interaction parameters, as shown in Figure 3-21. However, these approaches are unreasonable because thermodynamic principles suggest that only one U-Pd interaction parameter is valid for a specific phase. In addition, in this ternary system, even if multiple interaction parameters are valid, the spinodal curves should be related to the U-Rh interaction parameters as well.

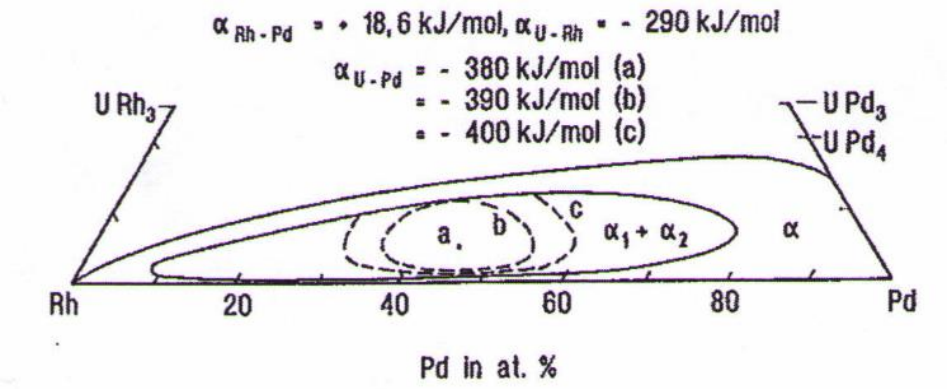

Figure 3-21. Calculated spinodal curves by Kleykamp and Kang [37].

3.6.2 An Overarching UPd_3-URh_3-URu_3 Phase Diagram

Fission products are generated in different kinds of nuclear fuels during operations. In case of uranium dioxide or uranium-plutonium oxide fuels, two typical precipitates, called "the white inclusions" and "the other metallic phase", were investigated and characterized by Bramman *et al.* [104] in 1968 and then by different groups of researchers including Kleykamp [28] and Kaye *et al.* [15,16]. In the case of uranium mononitride, a potential advanced nuclear reactor fuel, $AuCu_3$ type intermetallic compounds are also observed as a result of reaction of the platinum metals in fission products with UN [105]. Kurosaki and Uno confirmed, by means of reactions of UN + 3(Ru_x + Pd_y) [$x + y = 1$] and UN + 3(Rh_y + Pd_{1-y}) [$0.25 \leq y \leq 1$] at 1673 K under vacuum condition, the formation of UPd_3, URu_3, and URh_3 and a tentative ternary quasi-phase diagram was obtained [38,106]. As shown in Figure 3-22, the diagram has only 13 experimental points and, therefore, there is room for further experimental investigation. In addition, because of the nature of the samples, the experimentalists had difficulties in monitoring the phase equilibria at high temperatures and the samples were cooled to room temperature for XRD determinations after the reaction. For this reason, no liquid phase is shown on the ternary isothermal

section at 1673 K (1400 ºC). However, thermodynamic evaluations in this thesis will provide more detailed equilibrium phase relationships.

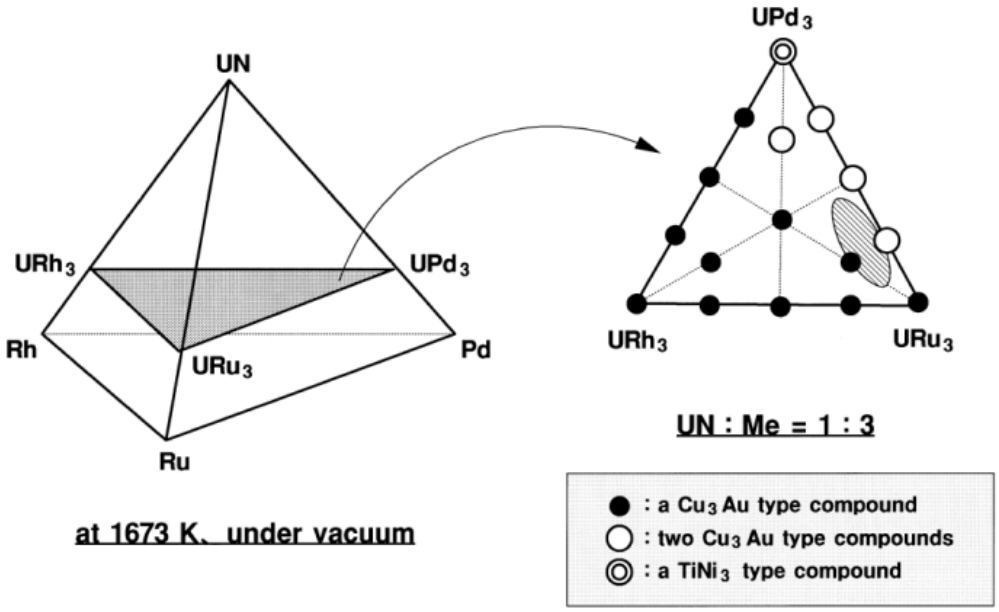

Figure 3-22. A tentative UPd_3-URh_3-URu_3 phase diagram by Kurosaki and Uno [106] at 1673 K or 1400 ºC.

4 Methodology for Evaluating Complicated Phase Diagrams

4.1 Preliminary Remarks

J.W. Gibbs was the first scientist who established thermodynamic principles for phase diagram calculations in the 19th century. He derived almost all the mathematical relations used in present computational thermodynamic studies of phase diagrams and established the phase rule [107]. Computational thermodynamics or the computer coupling of phase diagram and thermochemistry method was developed around 1970 by Kaufman and Bernstein [108] and is now extensively used for thermodynamic evaluation of experimental phase diagrams and their extrapolation to higher order systems. Furthermore, based on thermodynamic descriptions of the related binary systems, information of ternary, quaternary, or higher order systems can be obtained by adequate extrapolation schemes.

A flowchart of the thermodynamic evaluation process is shown in Figure 4-1 and summarized here. Before an evaluation of any system, a thorough search of the literature is performed to obtain any previously sketched phase diagrams and any other thermodynamic data that pertains to the system (*e.g.*, data for gas, liquid, alloys and compounds in the system; the phase transition temperatures; the heats of melting; metallographic information, *etc*.). It is also important in this step to identify any defects in the data or any data that are conflicting with other data.

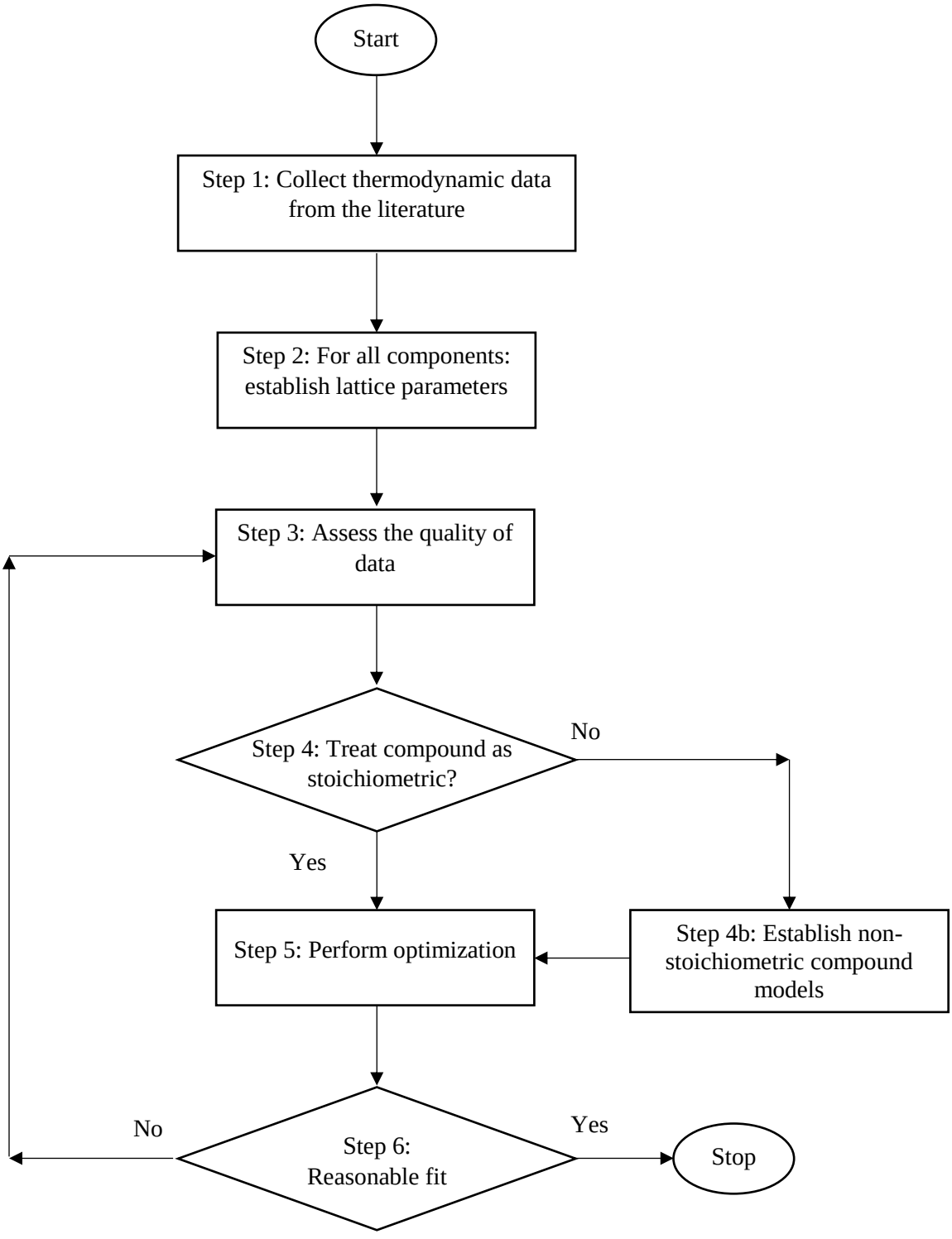

Figure 4-1. A flowchart of a general thermodynamic evaluation.

The second step is to choose lattice stabilities for the components (usually the elements). For real phases of these components, dependable (or accepted) values are usually those repeatedly used in various applications in thermodynamic calculations of other phase diagrams containing the interested elements and proved sound, *e.g.*, data from SGTE database [6]. Usually these dependable valued are those given in tables of melting temperatures and heats of fusion, or the equivalent data for heats and temperatures of transition for isotropic elements (*e.g.*, U). For metastable (or hypothetical) phases the choices represent a degree of freedom; however, the values, once selected for a particular phase of an element, must not change from diagram to diagram.

An initial assessment of the data is performed, and repeated until a sense of the diagram is obtained. At this stage, some critical features are highlighted (*e.g.*, eutectic temperatures and compositions; congruent melting points of compounds; *etc*.) and stable phase regions from the experimental phase diagram have to be shown on the diagram.

Binary compounds present a challenge because they can be treated in two ways. The first, and more common, is to assume that they are stoichiometric compounds with the exact ratio of the components present, as expressed by their Dalton numbers. In other words, a compound such as URu_3, contains 1 atom of uranium and 3 atoms of ruthenium, and is unable to accommodate any deviation from this ratio without another phase being present.

The second possibility is to treat the compound with some homogeneity of the given stoichiometry. Uranium dioxide, UO_2, is an excellent example in that at elevated temperatures, the fluorite lattice of UO_2 can accommodate the loss or gain of oxygen atoms.

This leads to an alternate terminology of the formula of UO_2, common to nuclear fuel chemists as $UO_{2\pm x}$, where *x* represents the deviation from stoichiometry. In this work, compounds included in U-Ru and U-Rh systems are all stoichiometric according to experimental observations. For compounds of U_xPd_y in U-Pd system, the phase boundaries are controversial in experimental phase diagrams from different sources. The controversies exist not only in terms of their homogeneity (the compositional range of a non-stoichiometric compound), but also of the types of some compounds. That is, different compounds were identified in different observations. For example, four compounds were identified by Park [95] in U-Rh phase diagram, but five were proposed by Naraine and Bell [96]. At the beginning, the U_xPd_y compounds were treated as stoichiometric for the sake of simplification, and finally they had been remained so because the most recent (in fact, in 1963) experimental results by Park, Fickle, and Mullen [99] showed that they were treated as stoichiometric compounds against all the previous conclusions. Based on these facts, using a compound formalism, which had been employed in some systems without significant discrepancies, are not suitable to the complicated systems in this research.

Once the method for treating the compounds has been decided, optimization of the system can be performed and repeated until a satisfactory fit of the data is achieved, at which point the system can be considered thermodynamically evaluated. This cycle may be performed multiple times as new data are found or more critical examination of existing data is performed.

4.2 A Proposed Strategy for Complicated Systems in This Work

On the basis of the literature review (Chapter 3), experimental phase diagrams of U-Pd and U-Rh show significant inconsistencies and some spots of the diagrams show obvious signs of experimental fallacies. Under these circumstances, the implications of a proper treatment of the other metallic phase should be considered. Traditionally, the aim of a thermodynamic model is to match the targeted experimental phase diagram as closely as possible, but when the experimental phase diagrams of a specific system show significant discrepancies and obvious fallacies, it becomes insufficient or even unreasonable to do so. In other words, in such circumstances such a treatment is incorrect.

The implications of a correct treatment for complicated systems, such as the other metallic phase, are to find ways of dealing with these discrepancies and identifying the experimental fallacies. In this work, a direct trial and error method involving two separate cycles (shown in Figure 4-2) is designed for treatments of complicated systems with many intermetallic compounds. The methodology of the treatment is to use thermodynamic equations using sound experimental data to determine the stable solution phase and metastable solution phase boundaries and then optimise the compound database.

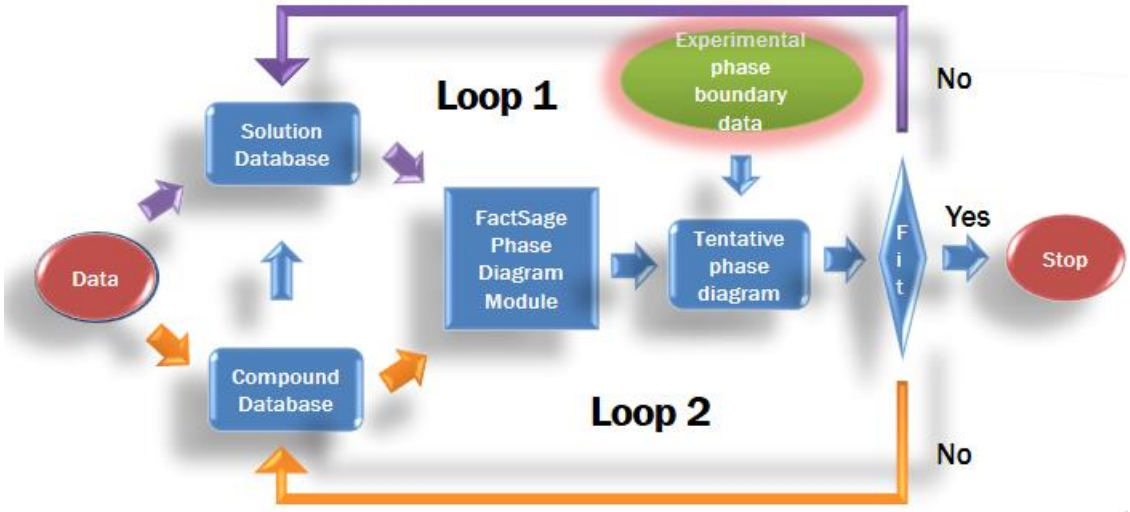

Figure 4-2. Flowchart showing the approach adopted in this work.

The procedures shown in Figure 4-2 can be described as follows. Upon establishing the compound and solution databases, the Phase Diagram module is used to searching for a tentative phase diagram. All the available experimental phase diagram data points are plotted in separate files with the same coordinates for different systems. These data points can be superimposed with the tentative phase diagram whenever a comparison is needed. Therefore, the data are not directly used in the optimization processes, but they provide information for the assessor to adjust the parameters. In this way, an assessor does not need to give any subjective weighting to any set of data before or during the optimization. Furthermore, by this means, all the existing experimental data can be reasonably considered during an optimization process.

The blue arrows in the flowchart represent directions for two sub-cycles. The purple arrows form the first cycle (Loop 1) together with some of the blue arrows for optimization of a solution phase diagram; the orange arrows form the second cycle (Loop 2) for optimization of the compound database in combination of some of the blue arrows.

In this work, FactSage software [109,110] is used because of the advantages of the design of its modules.

In summary, based on the regular procedures of thermodynamic evaluations (Figure 4-1), a new scheme for controversial U-Me phase diagrams is devised (Figure 4-2). It is shown in this work that it not only makes the evaluations possible and efficient, but also enables the location of some of the fallacies in developing the experimental phase diagrams.

5 Thermodynamic Evaluation Results

5.1 Preliminary Remarks

In applying the evaluation methodology presented in Chapter 4, phase diagrams for the U-Pd, U-Rh, and U-Ru binary system were thermodynamically created using FactSage. Starting from the binary systems and using the Kohler interpolation scheme (shown in Section 2.2.2.2), ternary and quaternary models were established as well. In this chapter, the properties of the binary systems will be presented and the corresponding phase diagrams will be illustrated.

5.2 U-Pd System

The thermodynamic data derived in this work for the U-Pd system is presented in this section. These data consist of lattice stability data, assessed interaction parameters of solution phases, and calculated compound expressions.

5.2.1 Thermodynamic properties (U-Pd binary system)

The lattice stabilities that are described in Section 2.2.1 and applied via Equation 5, are presented in Table 5-1.

Table 5-1. Lattice stabilities and energy referencing of the solution phases in U-Pd system.

Phase	U			Pd		
	ΔH°_{298} (J·mol^{-1})	S°_{298} (J·mol^{-1}·K^{-1})	G(Added) (J·mol^{-1})	ΔH°_{298} (J·mol^{-1})	S°_{298} (J·mol^{-1}·K^{-1})	G(Added) (J·mol^{-1})
Liquid	4375.22	44.24	0	16480	46.84	0
γ (*bcc*)	3231.08	47.98	0	4180	34.47	0
β	2790.73	53.25	0	0	37.82	5000
α	0	50.29	0	0	37.82	3000
fcc	0	50.29	5000	0	37.82	0

The enthalpy and entropy data in Table 5-1 are quoted from SGTE database, and

the G(Added) data are hypothetical values.

The interaction parameters for the solution phases of the U-Pd system are given in Table 5-2. These are applied via the excess term in Equation 5 and optimized in this work.

Table 5-2. Interaction parameters of solution phases.

System	Excess Gibbs energy functions in Margule's formalism (J·mol^{-1})
Liquid	$\Delta G^{E}_{Liquid} = X_{Pd}X_{U}[(-268000 + 9.60T) + 165000X_{U}]$
bcc (γ-U)	$\Delta G^{E}_{bcc} = X_{Ru}X_{U}[(-168500 + 43.68T) + 38560X_{U}]$
Tetragonal (β-U)	$\Delta G^{E}_{\beta-U} = X_{Pd}X_{U}[-101000]$ $(hypothetical)$
Orthorhombic (α-U)	$\Delta G^{E}_{\alpha-U} = X_{Pd}X_{U}[-85000]$
fcc	$\Delta G^{E}_{hcp} = X_{Pd}X_{U}[(-285000 + 6.00T + 3.00T\ln T) + 15200X_{U}]$ $(hypothetical)$

For the compounds selected as part of this evaluation of the U-Pd system, their thermodynamic properties are calculated in this work and given in Table 5-3.

Table 5-3. Thermodynamic properties of palladium-uranium compounds.

	$\Delta H^{\circ}_{298.15\,K}$	$S^{\circ}_{298.15\,K}$	$c_p = a + bT + cT^{-2} + dT^2$ *(J·mol^{-1}·K^{-1})*				
Compound	**(J·mol^{-1})**	**(J·mol^{-1}·K^{-1})**	***a***	***b x 10^3***	***c***	***d x 10^6***	***T_{max} (°C)***
UPd	-165,500	39.45	52.13	-16.75	-414510	38.08	970-1047
U_5Pd_6	-1,110,000	85.00	327.86	-97.97	-2409924	201.90	1110
UPd_3	-210,500	176.35	98.69	11.41	0	0	1680
UPd_4	-236,200	192.50	155.76	-59.47	-1426632	72.66	1445
UPd_8	-407,700	200.00	284.61	-11.64	-2776128	118.74	800

Finally the Gibbs energy expressions for the compounds in Table 5-3 are presented in Table 5-4.

Table 5-4. Gibbs energy expressions of the compounds calculated in this work.

Compound	Gibbs energy expression (J·mol^{-1})
UPd_3	$G^{UPd_3} = -240430.96 + 488.02T - 98.69T\ln T - 0.00923014T^2$
UPd	$G^{UPd} - G_U^{\alpha-U} - G_{Pd}^{fcc} = -165500 + 48.57T$
UPd_4	$G^{UPd_4} - G_U^{\alpha-U} - 4G_{Pd}^{fcc} = -236200 + 9.50T$
UPd_8	$G^{UPd_8} - 8G_{Pd}^{fcc} = -407700 + 152.78T$
U_5Pd_6	$G^{U_5Pd_6} - 5G_U^{\alpha-U} - 6G_{Pd}^{fcc} = -1110000 + 392.94T$

Figure 5-1 shows the calculated U-Pd phase diagram with extrapolated solution phases. Although the phase diagram has all the phases and compounds that the "accepted" phase diagram has, in a comparison with the thermodynamically assessed phase diagram, there are some problems in the experimental phase diagrams that need to be identified and clarified.

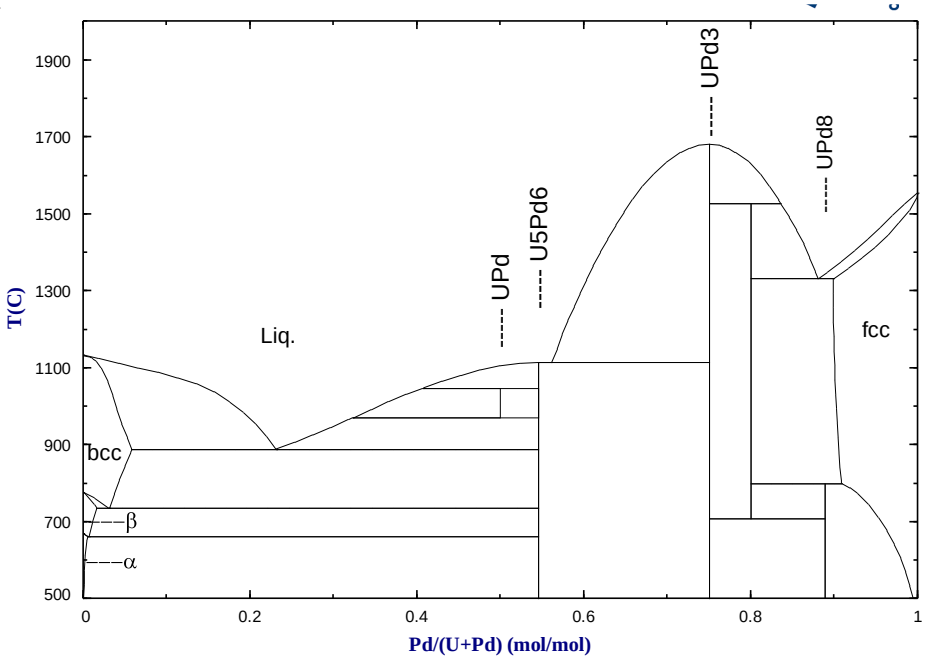

Figure 5-1. U-Pd phase diagram at 1 atm calculated in this work.

5.3 U-Rh System

The thermodynamic data derived in this work for the U-Rh system is presented in this section. These data consist of lattice stability data, assessed interaction parameter of the solution phases, and calculated intermetallic compound expressions.

5.3.1 Thermodynamic properties (U-Rh binary system)

The lattice stabilities that are described in Section 2.2.1 and applied in Equation 5 are presented in Table 5-5.

Table 5-5. Lattice stability and referencing of U-Rh system.

Phase	U			Rh		
	ΔH°_{298} (J·mol^{-1})	S°_{298} (J·mol^{-1}·K^{-1})	G(Added) (J·mol^{-1})	ΔH°_{298} (J·mol^{-1})	S°_{298} (J·mol^{-1}·K^{-1})	G(Added) (J·mol^{-1})
Liquid	4375.22	44.24	0	26568	43.39	0
γ (*bcc*)	3231.08	47.98	0	6904	27.12	0
β	2790.73	53.25	0	0	31.51	23400
α	0	50.29	0	0	31.51	28400
fcc	0	50.29	5000	0	31.51	0

The interaction parameters for the solution phases of the U-Rh system are given in Table 5-6.

Table 5-6. Interaction parameters of solution phases of U-Rh system.

System	Excess Gibbs energy functions in Margules formalism (J·mol^{-1})
Liquid	$\Delta G^{E}_{Liquid} = X_{Rh}X_{U}[(-255000 + 5.00T) + 140000X_{U}]$
bcc (γ-U)	$\Delta G^{E}_{bcc} = X_{Ru}X_{U}[(-168500 + 43.68T) + 38560X_{U}]$
Tetragonal (β-U)	$\Delta G^{E}_{\beta-U} = X_{Rh}X_{U}[-114000]$ $(hypothetical)$
Orthorhombic (α-U)	$\Delta G^{E}_{\alpha-U} = X_{Rh}X_{U}[-110000]$
fcc	$\Delta G^{E}_{hcp} = X_{Rh}X_{U}[(-160000 + 5.00T) + 15000X_{U}]$ $(hypothetical)$

For the compounds selected as part of this evaluation of the U-Rh system, their thermodynamic properties are calculated in this work and given in Table 5-7.

Table 5-7. Thermodynamic properties of rhodium-uranium compounds.

	$\Delta H^{\circ}_{298.15\,K}$	$S^{\circ}_{298.15\,K}$	$c_p = a + bT + cT^{-2} + dT^2$ *(J·mol⁻¹·K⁻¹)*				
Compound	**(J·mol⁻¹)**	**(J·mol⁻¹·K⁻¹)**	***a***	***b x 10³***	***c***	***d x 10⁶***	***T_{max} (°C)***
α-U_4Rh_3	-442,740	190.75	252.80	-67.99	-643620	109.25	720
β-U_4Rh_3	-442,740	190.69	252.80	-67.99	-643620	109.25	1115
U_3Rh_4	-461,180	196.10	274.26	-84.82	-678176	83.70	1450
U_3Rh_5	-508,540	226.60	322.64	-104.14	-789868	84.71	1550
URh_3	-194,000	153.40	104.45	18.21	-610033	0	1700

Finally the Gibbs energy expressions for the compounds in Table 5-7 are presented in Table 5-8.

Table 5-8. Gibbs energy expressions of compounds in U-Rh system.

Compound	Gibbs energy expression (J·mol^{-1})
URh_3	$G^{URh_3} = -228000 + 555.0T - 104.445T\ln T - 0.0091027T^2 + 305016.5T^{-1}$
U_3Rh_4	$G^{U_3Rh_4} - 3G_U^{\alpha-U} - 4G_{Rh}^{fcc} = -485581 + 702.05T$
U_3Rh_5	$G^{U_3Rh_5} - 3G_U^{\alpha-U} - 5G_{Rh}^{fcc} = -539033 + 858.53T$
U_4Rh_3-L	$G^{U_4Rh_3-L} - 4G_U^{\alpha-U} - 3G_{Rh}^{fcc} = -461330 + 569.68T$
U_4Rh_3-H	$G^{U_4Rh_3-H} - G^{U_4Rh_3-L} = -557.763 - 1.12T$

The calculated U-Rh phase diagram with metastable extrapolation curves is shown in Figure 5-2.

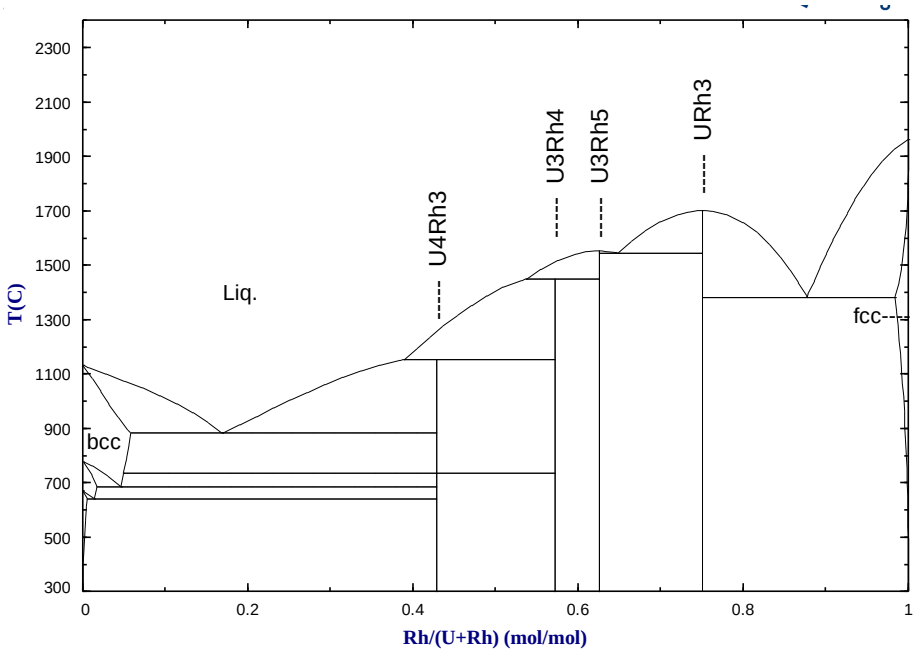

Figure 5-2. Calculated U-Rh phase diagram with four compounds (1 atm) [this work].

5.4 U-Ru System

Thermodynamic data derived in this work for the U-Ru system is presented here.

5.4.1 Thermodynamic properties (U-Ru binary system)

The lattice stabilities that are described in Section 2.2.1 and applied in Equation 5 are presented in Table 5-9.

Table 5-9. Lattice stability and energy referencing of U-Ru system.

Phase	U			Ru		
	ΔH°_{298} (J·mol^{-1})	S°_{298} (J·mol^{-1}·K^{-1})	G(Added) (J·mol^{-1})	ΔH°_{298} (J·mol^{-1})	S°_{298} (J·mol^{-1}·K^{-1})	G(Added) (J·mol^{-1})
Liquid	4375.22	44.24	0	38589	43.33	0
γ (*bcc*)	3231.08	47.98	0	8169.00	30.82	0
β	2790.73	53.25	0	0	28.53	18800
α	0	50.29	0	-	-	0
cph	0	50.29	11659.50	0	28.53	0

The interaction parameters for the solution phases of the U-Ru system are given in Table 5-10.

Table 5-10. Interaction parameters of solution phases in U-Ru system.

System	Excess Gibbs energy functions in Margules formalism (J·mol^{-1})
Liquid [17]	$\Delta G^{E}_{Liquid} = X_{Ru}X_{U}[(-237307 + 10.82T) + 127440X_{U}]$
bcc (γ-U)	$\Delta G^{E}_{bcc} = X_{Ru}X_{U}[(-168500 + 43.68T) + 38560X_{U}]$ $(hypothetical)$
Tetragonal (β-U)	$\Delta G^{E}_{\beta-U} = X_{Ru}X_{U}[-90000]$
cph	$\Delta G^{E}_{cph} = X_{Ru}X_{U}[-100000]$ $(hypothetical)$

For the compounds selected as part of this evaluation of the U-Ru system, their thermodynamic properties are given in Table 5-11.

Table 5-11. Thermodynamic properties of ruthenium-uranium compounds.

	$\Delta H^{\circ}_{298.15\,K}$	$S^{\circ}_{298.15\,K}$	$c_p = a + bT + cT^{-2} + dT^2$ ***(J·mol^{-1}·K^{-1})***				
Compound	**(J·mol^{-1})**	**(J·mol^{-1}·K^{-1})**	***a***	***b x 10^3***	***c***	***d x 10^6***	***T_{max} (°C)***
U_2Ru	-123,770	103.40	76.75	3.12	-267026	52.05	937
URu (low)	-597,660	25.16	25.00	2.60	-94233	13.32	795
URu (high)	-597,700	25.16	25.00	2.60	-94233	13.32	1158
U_3Ru_4	-375,880	196.30	172.41	24.99	-682424	75.44	1163
U_3Ru_5	-389,220	241.90	195.33	33.12	-795178	74.38	1182
URu_3	-144,700	145.30	101.22	18.46	-471814	0	1850

Finally, the Gibbs energy expressions for the compounds in Table 5-11 are calculated and presented in Table 5-12.

Table 5-12. Gibbs energy expressions of compounds in U-Ru system.

Compound	Gibbs energy expression ($J \cdot mol^{-1}$)
URu_3	$G^{URu_3} = -177240 + 540.77T - 101.224T \ln T - 0.009230T^2 + 235907T^{-1}$
U_3Ru_4	$G^{U_3Ru_4} - 3G_U^{\alpha-U} - 4G_{Ru}^{hcp} = -375879 + 68.8T$
U_3Ru_5	$G^{U_3Ru_5} - 3G_U^{\alpha-U} - 5G_{Ru}^{hcp} = -389217 + 51.8T$
URu-L	$G^{URu-L} - 0.52G_U^{\alpha-U} - 0.48G_{Ru}^{hcp} = -59766.5 + 14.68T$
URu-H	$G^{URu-H} - G^{URu-L} = -3.108 - 0.00057T$
U_2Ru	$G^{U_2Ru} - 2G_U^{\alpha-U} - G_{Ru}^{hcp} = -123773 + 25.58T$

The remaining problem is that the β-U and γ-U regions are still standing alone in the metastable phase diagram. A metastable isotherm appears as a three phase equilibrium at the Ru-rich side. In evaluations of the U-Rh and U-Pd systems, it is shown during the optimization process that the metastable isotherms should appear at the U-rich side and form an integrated solution-phase metastable phase diagram. To realize this, a new set of interaction parameters has to be calculated. Although the area of such a phase (in this case, *cph* phase) is small, its effect on higher order phase diagrams must be considerable [111].

Figure 5-3 is a U-Ru phase diagram thermodynamically assessed in this work with the *hcp* phase region added.

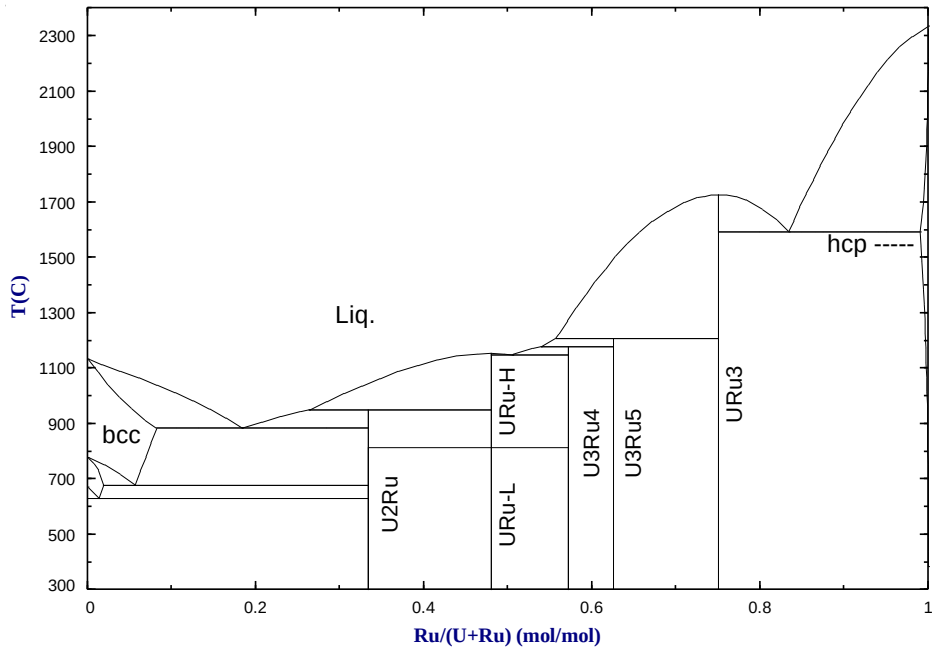

Figure 5-3. U-Ru phase diagram with *hcp* phase region is added.

5.5 Ternary and Pseudo Ternary Phase Diagrams

The optimized ternary interaction parameters are listed in Table 5-13.

Table 5-13. Ternary interaction parameters.

Phase	Interaction	i*	j	k	A	B	Reference
Liquid	Pd Ru Rh	1	1	1	-525000	0	[16]
	U Rh Pd	1	1	1	-234000	0	This work
	U Rh Ru	1	1	1	-124000	0	This work
	U Ru Pd	1	1	1	-300000	0	This work
fcc	Pd Ru Rh	1	1	1	-40000	0	[16]
	U Rh Pd	1	1	1	-223000	0	This work
cph	Pd Ru Rh	1	1	1	-90000	0	[16]

*i, j, and k are index of the interaction constituents used in the excess Gibbs energy expression

5.5.1 Calculated U-Rh-Pd phase diagram at 1050 °C

After the ternary interaction parameters were established, the U-Rh-Pd phase diagram is shown in Figure 5-4, in which all the solution phases and compound phases are labelled by numbers and summarized in Table 5-14 for clarity sake.

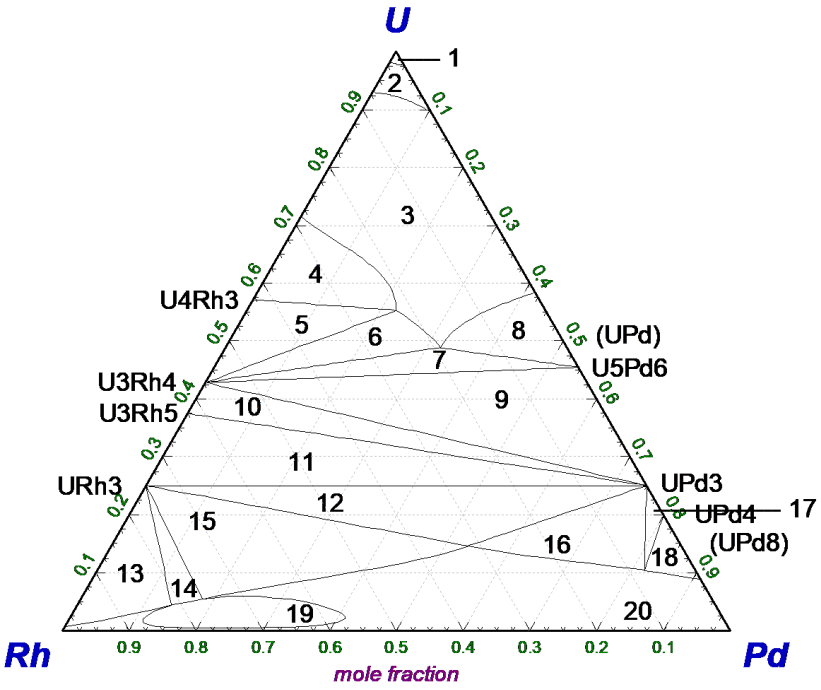

Figure 5-4. Adjusted U-Rh-Pd phase diagram at 1050 °C, 1 atm.

The detailed list of phase from Figure 5-4 are presented in Table 5-14, below.

Table 5-14. A detailed list of phases in different phase regions for Figure 5-4.

Phase Region	Phases	Phase Region	Phases
1	*bcc*	11	U_3Rh_5 + URh_3 + UPd_3
2	*bcc* + *Liquid*	12	URh_3 + UPd_3 + *fcc*
3	*Liquid*	13	URh_3 + *fcc*
4	U_4Rh_3 + *Liquid*	14	URh_3 + *fcc* + *fcc*#2
5	U_4Rh_3 + U_3Rh_4 + *Liquid*	15	URh_3 + *fcc*
6	U_3Rh_4 + *Liquid*	16	UPd_3 + *fcc*
7	U_3Rh_4 + U_5Pd_6 + *Liquid*	17	UPd_3 + UPd_4 + *fcc*
8	U_5Pd_6 + *Liquid*	18	UPd_4 + *fcc*
9	U_5Pd_6 + U_3Rh_4 + UPd_3	19	*fcc* + *fcc*#2
10	U_3Rh_4 + U_3Rh_5 + UPd_3	20	*fcc*

5.5.2 Calculated UMe_3 Binary Phase Diagrams

After the establishment of the U-Pd-Rh-Ru quaternary system and based on the re-assessed thermodynamic data for the UMe_3 compounds (UPd_3, URh_3, and UPd_3), quasi-

binary phase diagrams that were not available before this work can be calculated.

The calculated URu_3-URh_3 phase diagram is shown in Figure 5-5.

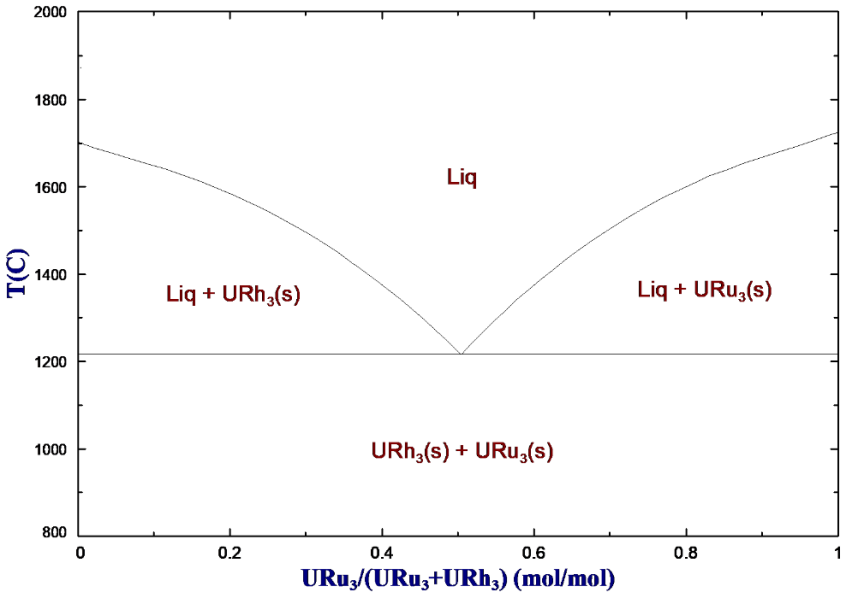

Figure 5-5. Calculated URu_3-URh_3 phase diagram.

The calculated URu_3-UPd_3 phase diagram is shown in Figure 5-6.

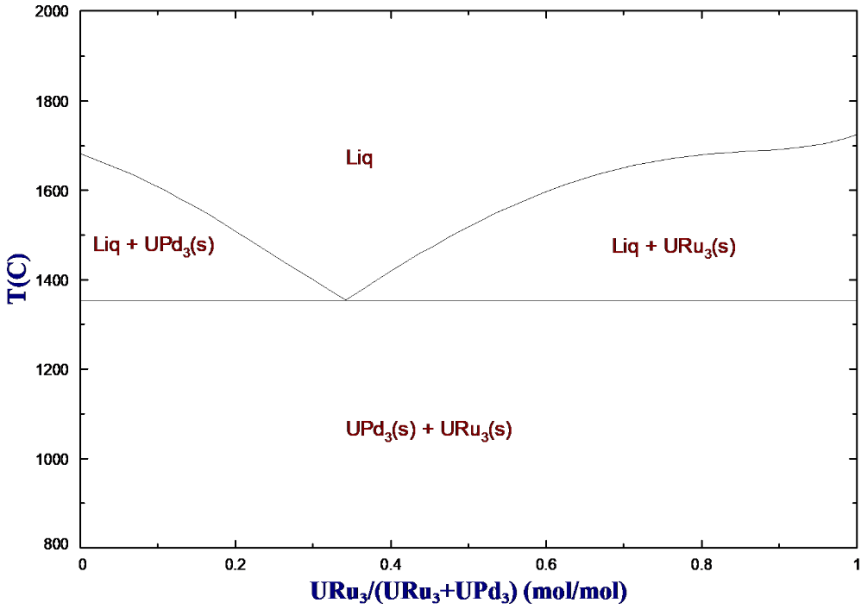

Figure 5-6. Calculated URu_3-UPd_3 phase diagram.

The calculated URh_3-UPd_3 phase diagram is shown in Figure 5-7.

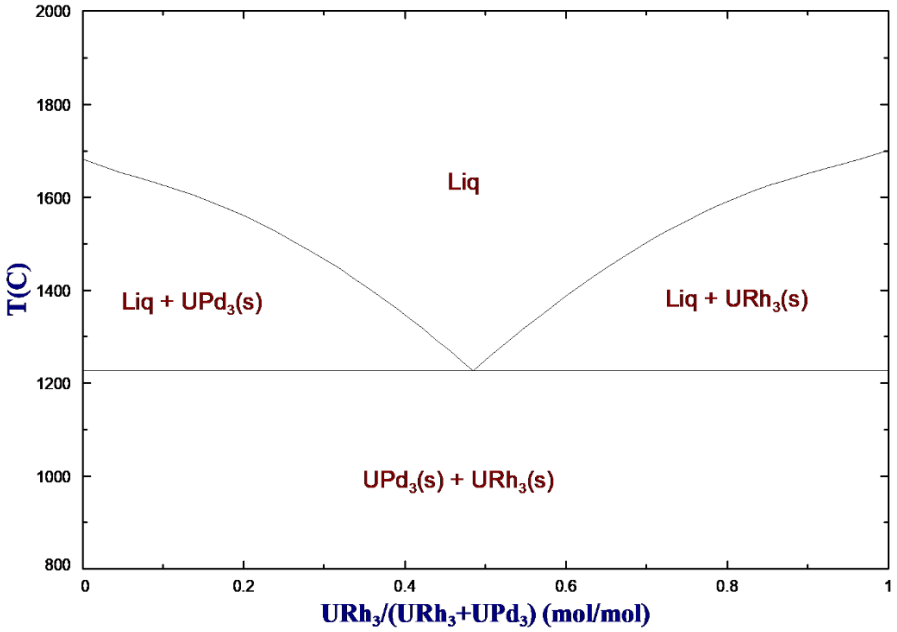

Figure 5-7. Calculated URh_3-UPd_3 phase diagram.

Although all the three quasi-phase diagrams are simple in form, they predict phase boundaries, eutectic compositions and eutectic temperatures of the binary systems (Table 5-15) and can be used in URu_3-URh_3-UPd_3 phase diagram calculations.

Table 5-15. Calculated eutectic compositions and temperatures for binary UMe_3 Systems.

System		**Melting point of compounds (°C)**		**Eutectic properties**	
A	B	A	B	X_A	T_{eu} (°C)
URu_3	UPd_3	1725	1680	0.340	1354
URu_3	URh_3	1725	1700	0.504	1217
URh_3	UPd_3	1700	1680	0.485	1227

5.5.3 Calculated URu_3-URh_3-UPd_3 phase diagrams

The U-Pd-Rh-Ru thermodynamic model provides equilibrium isothermal sections and isopleths at any temperature or composition. For instance, in comparison with the

experimental UPd_3-URh_3-URu_3 diagram constructed by Kurosaki and Uno [38] (see Figure 3-22), an equilibrium isothermal section at 1400 °C (1673 K) can be readily calculated and plotted (Figure 5-8). In this phase diagram, a *Liquid*-phase region is reasonably illustrated, which was missing in Figure 3-22 [38], due to the extreme difficulty in phase-equilibrium observation at the high temperature measurement.

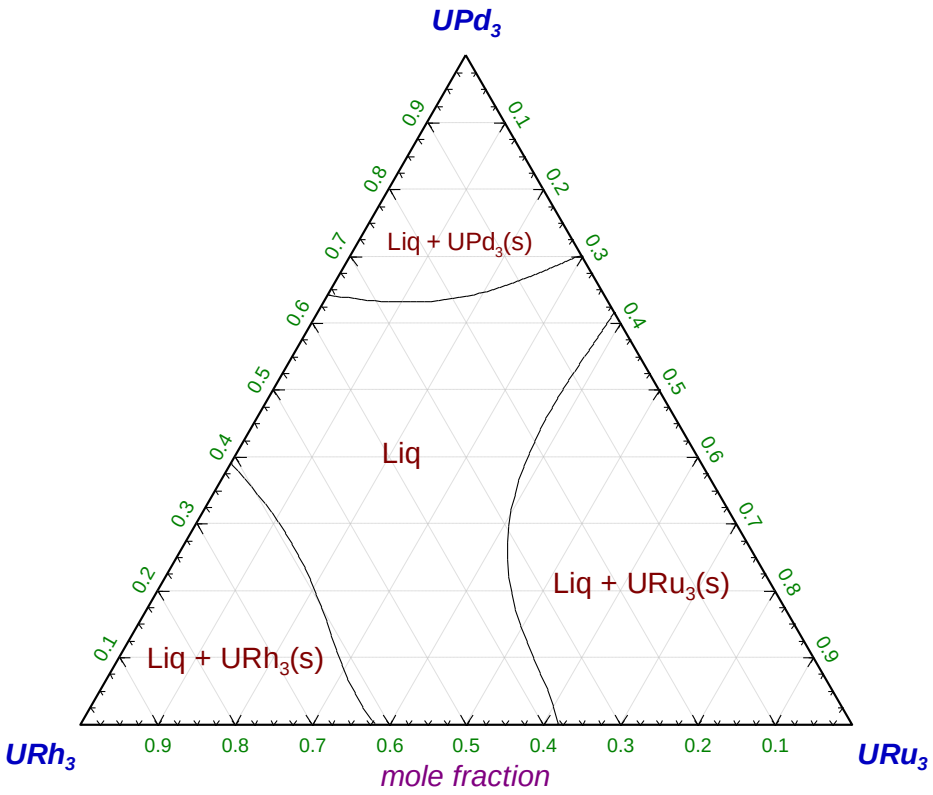

Figure 5-8. Calculated UPd_3-URh_3-URu_3 isothermal section at 1400 °C, 1 atm.

A liquidus projection above the eutectic temperatures of the three binary system is shown in Figure 5-9 in which the contraction or expansion of the contours of liquidus can be examined.

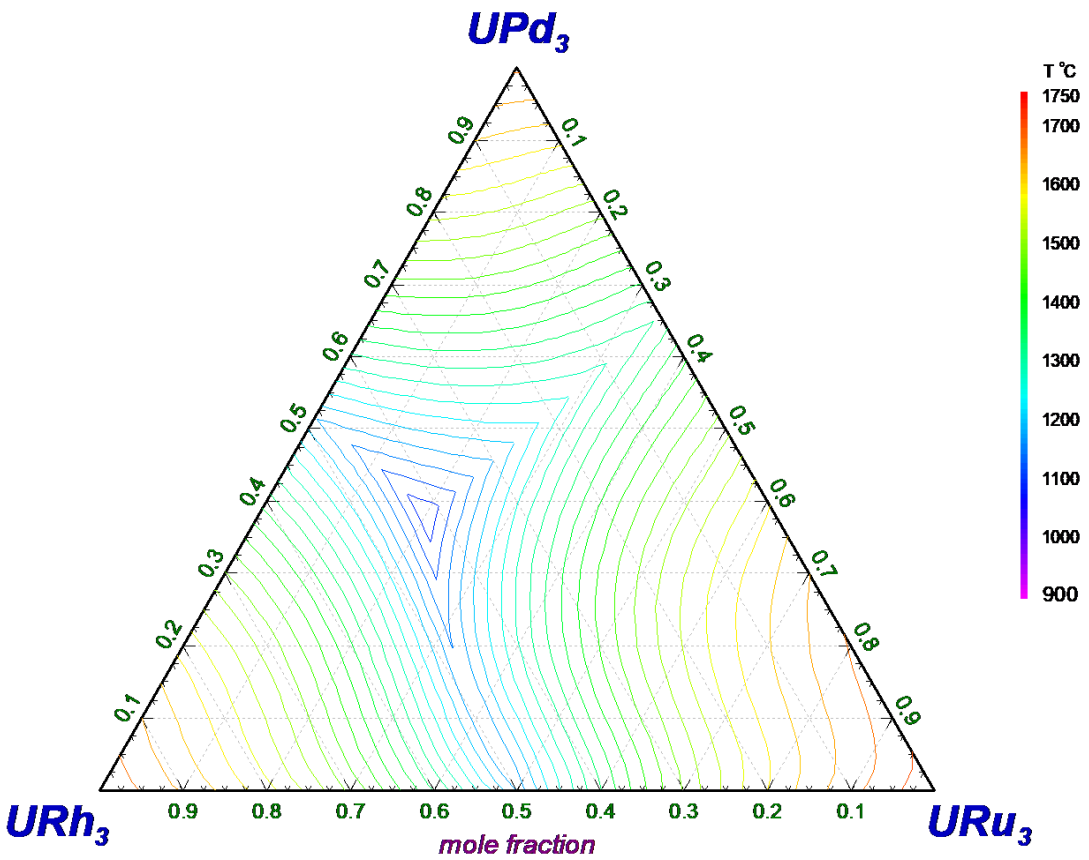

Figure 5-9. Calculated liquidus projection of the UMe_3 ternary isothermal section between 900-1750 °C and at 1 atm.

In comparison with Figure 5-8, Figure 5-9 provides the liquidus profiles at various temperatures, and the temperature interval can be changed freely.

Furthermore, the ternary eutectic point is found to be at 37.78 at.% UPd_3, 41.93 at.% URh_3, 20.23 at.% URu_3, and at 1129.85 °C (point 1 in Figure 5-10).

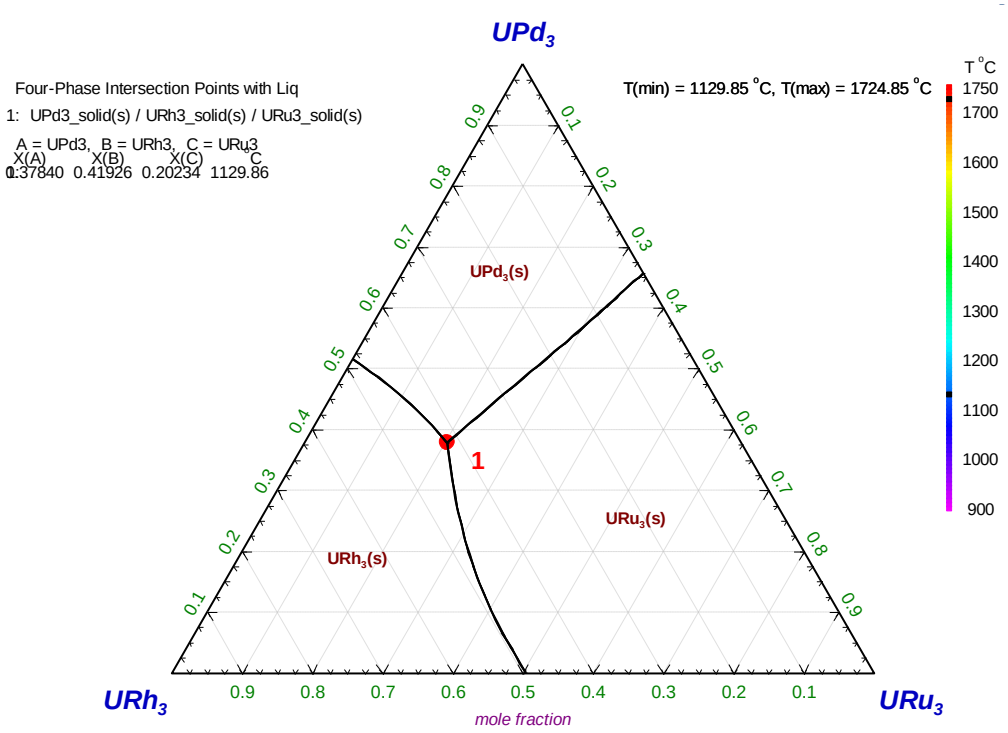

Figure 5-10. Calculation of the ternary eutectic point (1) of UMe_3 system at 1 atm.

Figure 5-10 illustrates the interpolation to the point 1 (the ternary eutectic point) and the three continuous lines represent the contracting tracks of the three binary eutectic points as the concentration of the third species increases.

5.5.4 The liquidus projections of U-Rh-Pd ternary system

By means of this quaternary thermodynamic model, liquidus projections of all the three ternary systems can be predicted. In Figure 5-11, the liquidus projection for the U-Rh-Pd system is given.

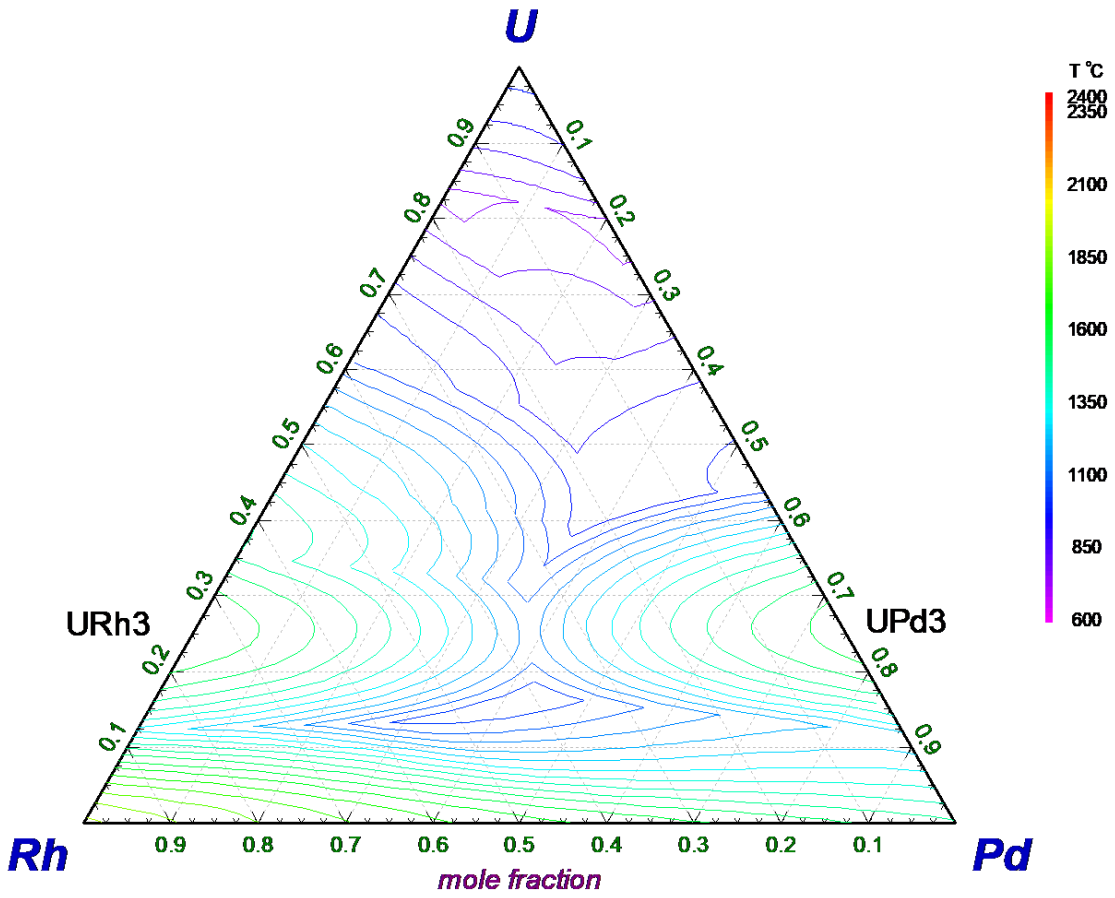

Figure 5-11. Calculated U-Rh-Pd liquidus projections from 600-2400 °C, 1 atm.

This liquidus projections show that at low temperatures (800-900 °C), Liquid phase forms at U-rich side along the U-Rh and U-Pd axes (begin from the bcc-side eutectic temperatures—the purple lines). As temperature increases, one integrated Liquid phase forms and then, due to the influences of the formation of different compounds it separates again (the blue and green lines). As U-Rh and U-Ru systems have two separate eutectic reactions, the U-Rh-Ru ternary system should have two ternary eutectic points at upper and lower parts of Figure 5-12. The liquidus projections of U-Ru-Rh and U-Ru-Pd will be shown in next section together with their isothermal sections at 1050 °C.

5.5.5 U-Ru-Pd and U-Ru-Rh systems

Currently, no experimental phase diagrams are available in the literature for these two ternary systems. From Figure 3-6 and Figure 3-5, it is known the number of compounds in the U-Ru system is larger than U-Rh system, the ternary isothermal sections are more complex than that of U-Rh-Pd system. The isothermal sections at 1050 °C are given in Figure 5-12.

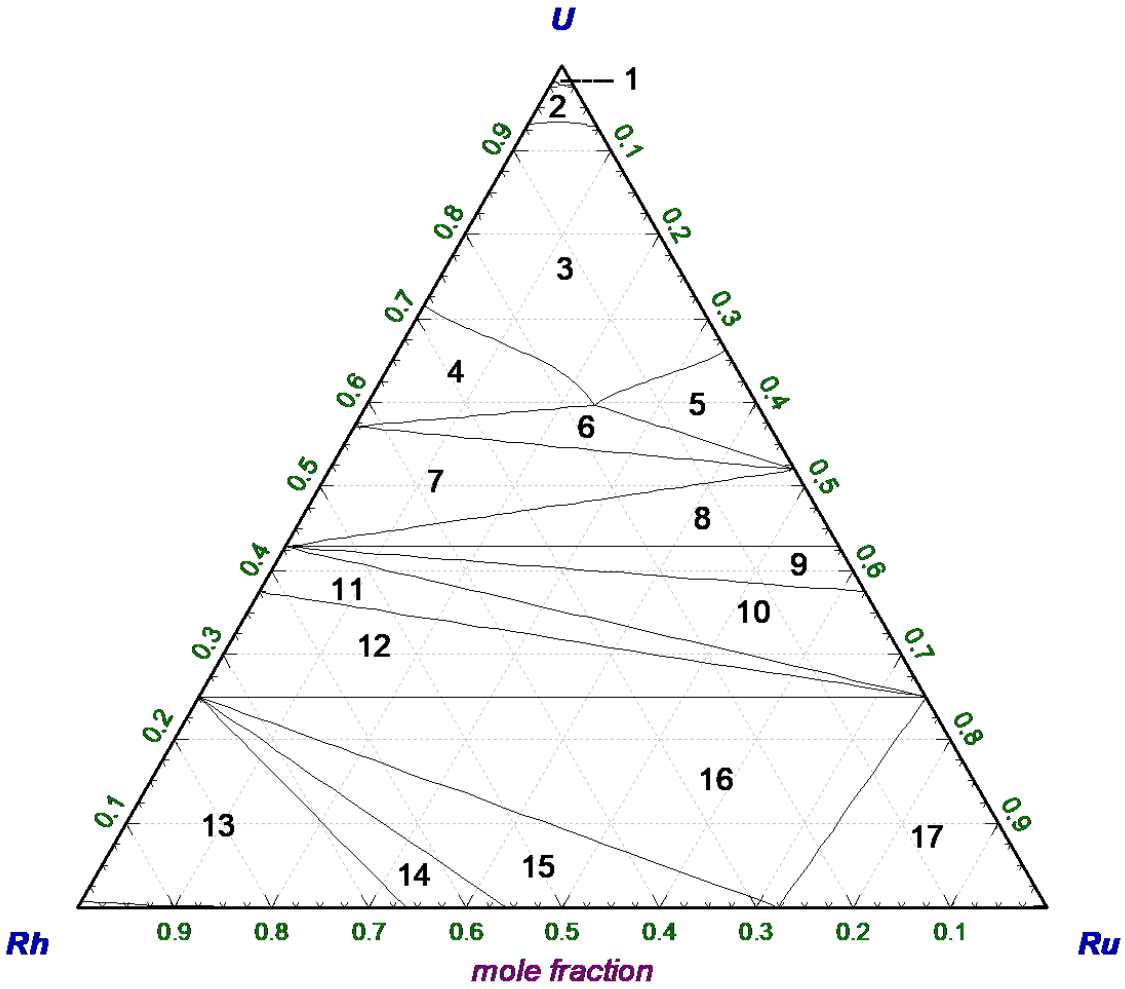

Figure 5-12. Calculated isothermal section of U-Ru-Rh system at 1050 °C, 1 atm.

The U-Ru-Rh isothermal section at 1050 °C predicted by this model is labelled by numbers and the phase in each region is listed in Table 5-16:

Table 5-16. Phase regions and phases on U-Ru-Rh isothermal section.

Phase region	Phases	Phase region	Phases
1	*bcc*	11	$URu_3 + U_3Rh_4 + U_3Rh_5$
2	*bcc* + *Liq.*	12	$URu_3 + URh_3 + U_3Rh_5$
3	*Liq.*	13	*fcc* + URu_3
4	U_4Rh_3 + *Liq.*	14	*fcc* + *hcp* + URh_3
5	*Liq.* + URu-H	15	*hcp* + URh_3
6	*Liq.* + URu-H + U_4Rh_3-H	16	*hcp* + URh_3 + URu_3
7	URu-H + U_4Rh_3-H +U_3Rh_4	17	*hcp* + URu_3
8	URu-H + U_3Rh_4 + U_3Ru_4	18	*fcc*
9	U_3Rh_4 + U_3Ru_5 + U_3Rh_4	19	*hcp*
10	URu_3 + U_3Rh_4 + U_3Ru_5		

The liquidus projection of the U-Ru-Rh ternary system is shown in Figure 5-13.

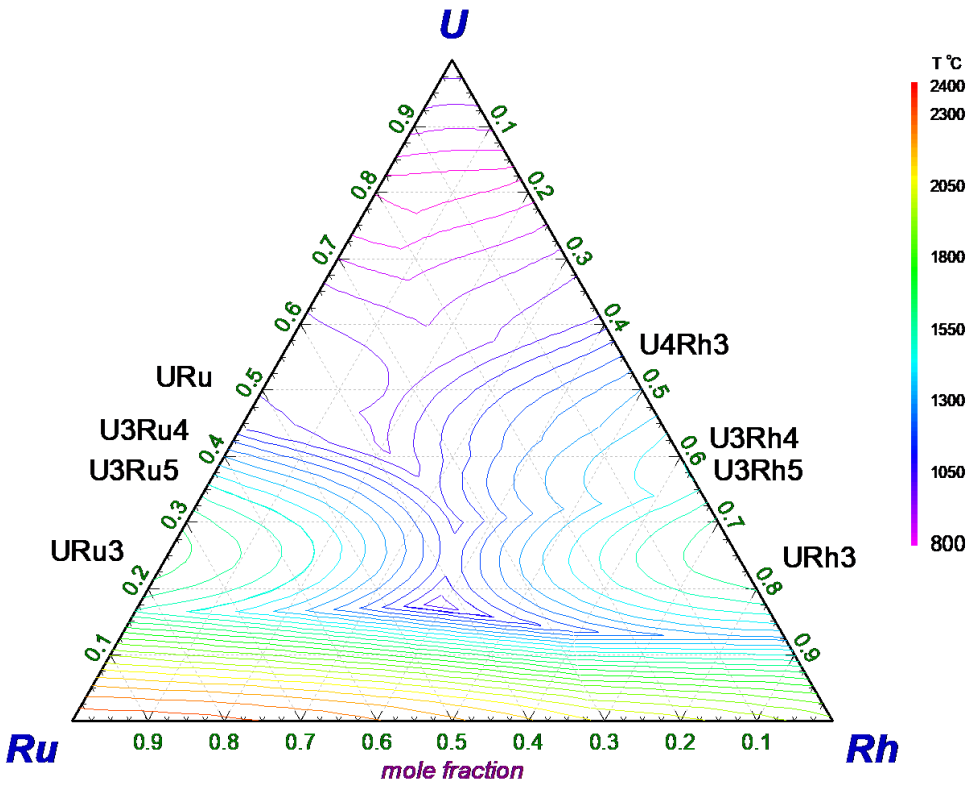

Figure 5-13. Calculated liquidus projections of U-Ru-Rh system (800-2400 °C, 1 atm).

Figure 5-14 shows the calculated ternary isothermal section of U-Ru-Pd system at 1050 °C.

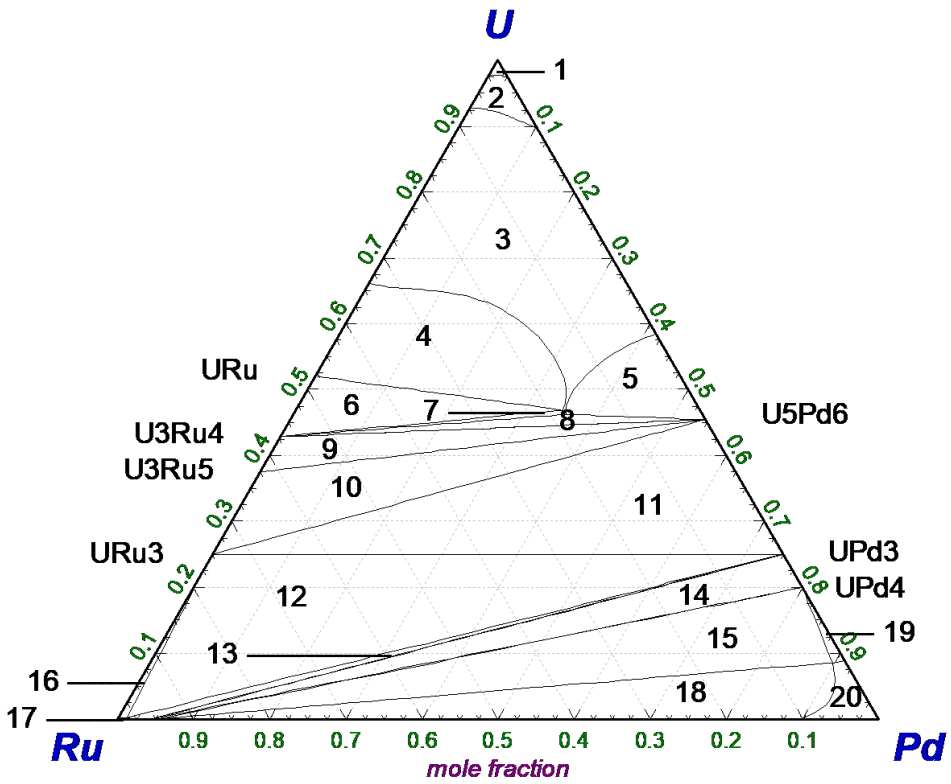

Figure 5-14. Calculated isothermal section of U-Ru-Pd system at 1050 °C, 1 atm.

The U-Ru-Pd isothermal section at 1050 °C predicted by this model is labelled by numbers and the phases in each region is listed Table 5-17.

Table 5-17. Phase regions and phases on U-Ru-Pd isothermal section.

Phase region	Phases	Phase region	Phases
1	*bcc*	11	URu_3 + UPd_3 + U_5Pd_6
2	*bcc* + *Liq.*	12	*cph* +URu_3 + UPd_3
3	*Liq.*	13	*cph* + UPd_3
4	URu-H + *Liq.*	14	*cph* + UPd_3 + UPd_4
5	*Liq.* + U_5Pd_6	15	*fcc* + *cph* + URh_4
6	*Liq.* + URu-H + U_3Ru_4	16	*cph* + URu_3
7	*Liq.* + U_3Ru_4	17	*cph*
8	*Liq.* + U_3Ru_4 + U_5Pd_6	18	*fcc* + *cph*
9	U_3Ru_4 + U_3Ru_5 + U_5Pd_6	19	*fcc* + UPd_4
10	URu_3 + U_3Ru_5 + U_5Pd_6	20	*fcc*

The predicted liquidus projection is illustrated in Figure 5-15.

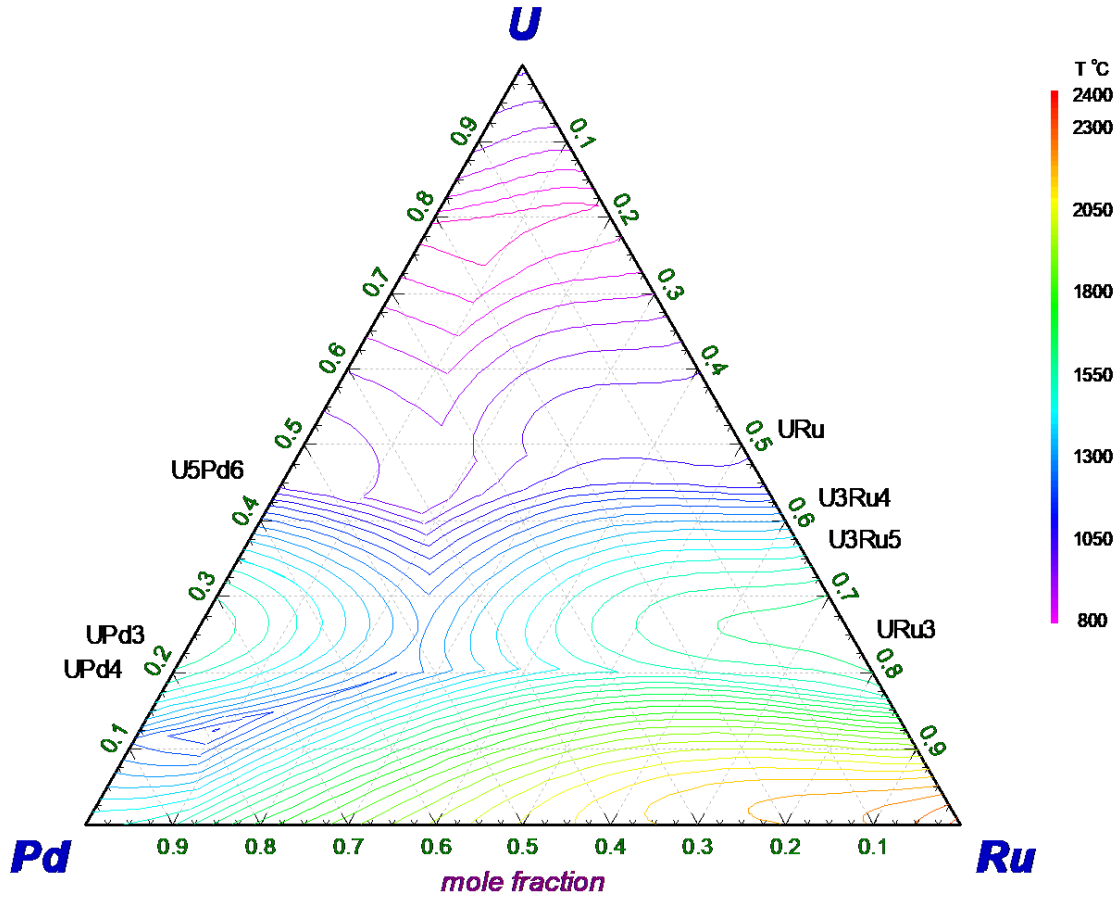

Figure 5-15. Calculated liquidus projections of U-Ru-Pd system (800-2400 °C, 1 atm).

6 Discussion

6.1 Preliminary Remarks

In evaluating the phase diagrams that were presented in Chapter 5, it was necessary to consider all the data presented in Chapter 3 and apply the methodology presented in Chapter 4. In examining the data closely, it soon becomes apparent that there are competing and conflicting results. For example, which compounds are stable? Or which eutectic temperature is the most credible and where would the eutectic composition be, and what might be the compositions at this reaction?

In this chapter, a critical review of the evaluations presented as results (in other words the evaluations to be accepted going forward) against the experimental data of Chapter 3 will be presented. Rationale will be given as to why certain data were selected and others not.

6.2 U-Pd System

During the 1950's and 1960's, among the three U-Me subsystems, the U-Pd system was the most frequently explored and it had been the most controversial one. It is controversial not only in phase diagram data, but also in thermodynamic property measurements of the compounds, *e.g.*, the enthalpy of formation of UPd_3 which is discussed in Sections 3.3 and 7.2.

When the extensively accepted U-Pd phase diagram (Figure 3-4) was compiled into the Phase Diagram Updates section of the *Journal of Phase Equilibria* in 1993 [112], the editor made three important comments:

i. The liquidus about UPd_3 is too asymmetric;
ii. The liquidus and solidus of *Liquid + fcc* region seem to cross one another when extrapolated into U-rich side; and
iii. Regarding UPd_8, an atomic ratio of 1:8 is rare for binary compounds.

In other words, some phase boundaries in this diagram are thermodynamically improbable.

Considering the instruments and methods used by different authors, *e.g.*, thermal analysis (TA), differential thermal analysis (DTA), XRD, metallography, EPMA *etc.*, the discrepancies are far beyond the ranges of random errors and/or system errors contributed by the instruments. Contamination of samples by materials from the sample containers has been reported in U-Pd phase diagram determinations [92,99]. The worst case scenario might be the co-existence of a contaminant and a catalyst, *e.g.*, when a BeO or ZrO_2 crucible and a platinum element are coexisting in the U-Me phase diagram determinations.

The purpose of a thermodynamic evaluation is not just to imitate an experimental phase diagram, but also to validate it. When the lattice stabilities used in such an evaluation are reliable, the evaluation results may be used to identify experimental contradictions. In this work, an alternative optimizing scheme is adopted and used for identification of a few major experimental fallacies. No one can perform a measurement without a container for the sample, but a reliable thermodynamic model can predict the result without the interference of the beryllium existing in experiments. This is why thermodynamic evaluations are beneficial in such complicated systems.

In the following sub-sections, phase boundary features will be discussed in detail.

6.2.1 The liquidus

Liquidus data in the U-Pd system were provided either partially or over the full range of the composition by four groups of scientists. The U-rich part will be discussed in detail in Section 6.2.3. The liquidus between 50-75 at.% by Park *et al.* [99] are higher in temperature than that of Catterall *et al.* [92] in the range of 50-75 at.% Pd, but about the same beyond 75 at.% Pd. In the range of 75-100 at.% Pd, Terekhov *et al*. [93] gave a very complicated liquidus profile (Figure 3-14), but it is unreliable because parts of the liquidus violate thermodynamic principles. It is doubtful that they could use thermocouples at the temperature limits of the application of thermocouples and produce data with very small errors. Moreover, there seems to be no contamination effect in their experiments as most other scientists had confronted. In thermodynamic assessments, the calculated liquidus in the range of 75-83 at.% Pd are very smooth, showing peritectic behaviour, instead of a eutectic reaction with a deep valley on the hypo-stoichiometric side of UPd_4. In their thermal analysis experiments, thermocouples were used even at temperatures above 1600 °C. The minimum temperature difference of the liquidus and solidus was shown as small as 25 °C, which is a very small uncertainty range. This defies all the difficulties in temperature measurement confronted by other experimentalists of U-Me phase diagrams.

Figure 6-1 and Figure 6-2 are comparisons of the calculated U-Pd phase diagram (this work) with experimental data from various sources.

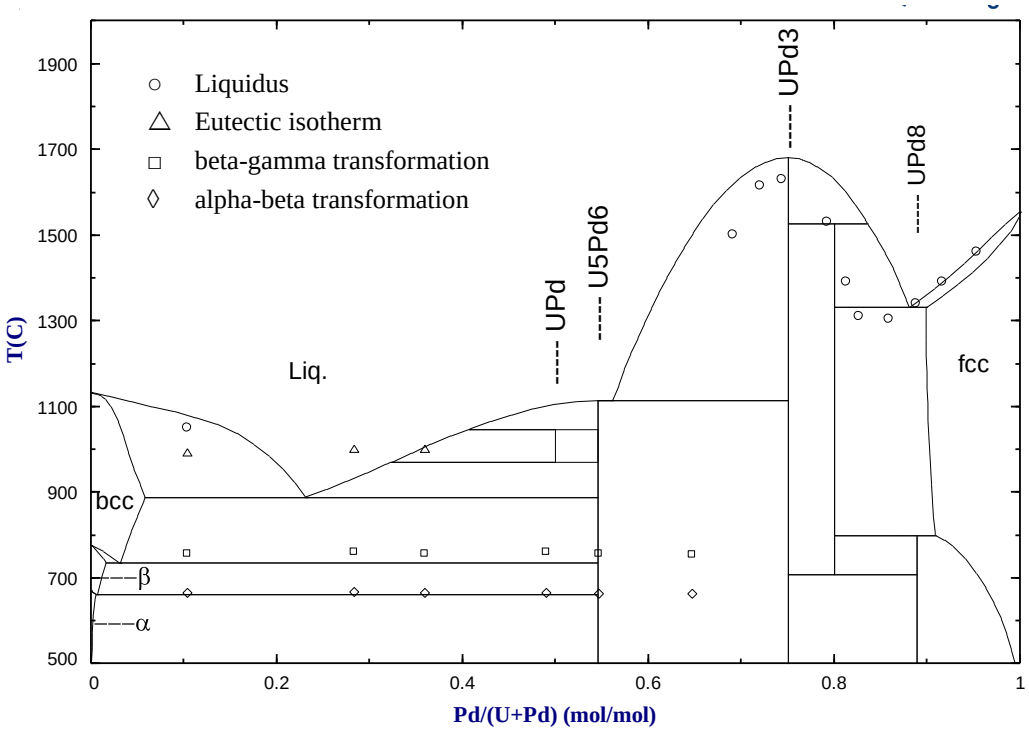

Figure 6-1. Calculated U-Pd phase diagram with Catterall *et al*. [92] data at 1 atm.

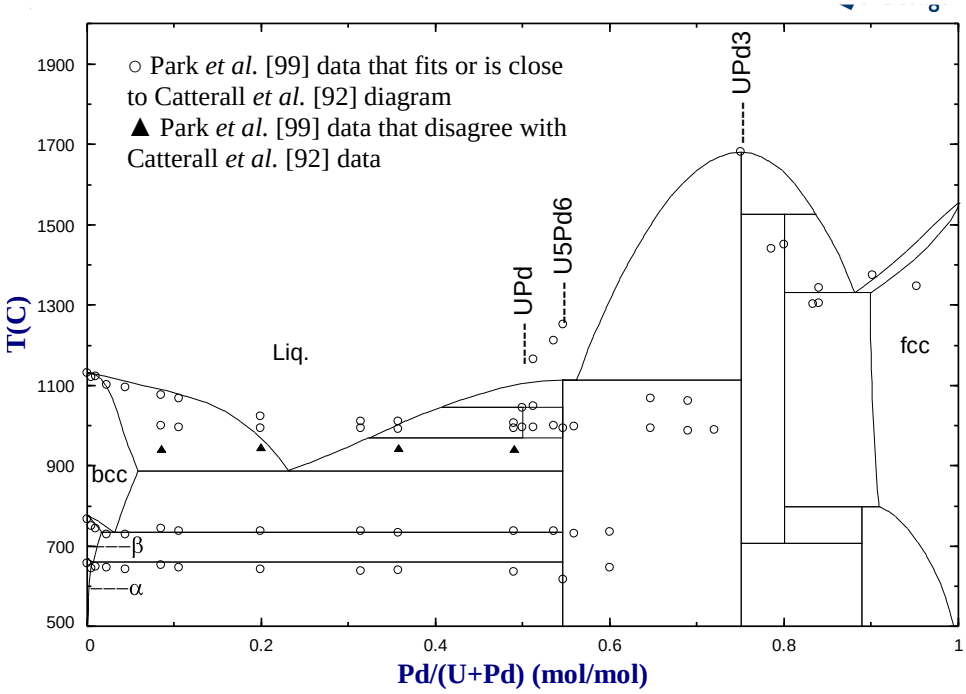

Figure 6-2. Calculated U-Pd phase boundaries with Park *et al*. [99] data.

As can be clearly seen from the diagrams of Park *et al.* [99] and Catterall *et al.* [92], the data points of the liquidus and solidus between 85 – 100 at.% Pd are sparse. Both of these groups changed from thermocouples to pyrometers at high temperatures. In the partial phase diagram by Terekhov *et al.* [93] the experimental points are so neatly distributed (see Figure 3-14) that it gives people an impression that the error of the measurements is very small, as small as less than ±5 °C. By means of the new optimization scheme, the calculated liquidus is between that of Park *et al.* [99] and that of Catterall *et al.* [92] at Pd-rich side (See the black circles and the red circles (liquidus data) in the range of 45-75 at.% Pd in Figure 6-3). In Figure 6-3, phase boundary data from Terekhov *et al.* [93] and Pells [100] are included.

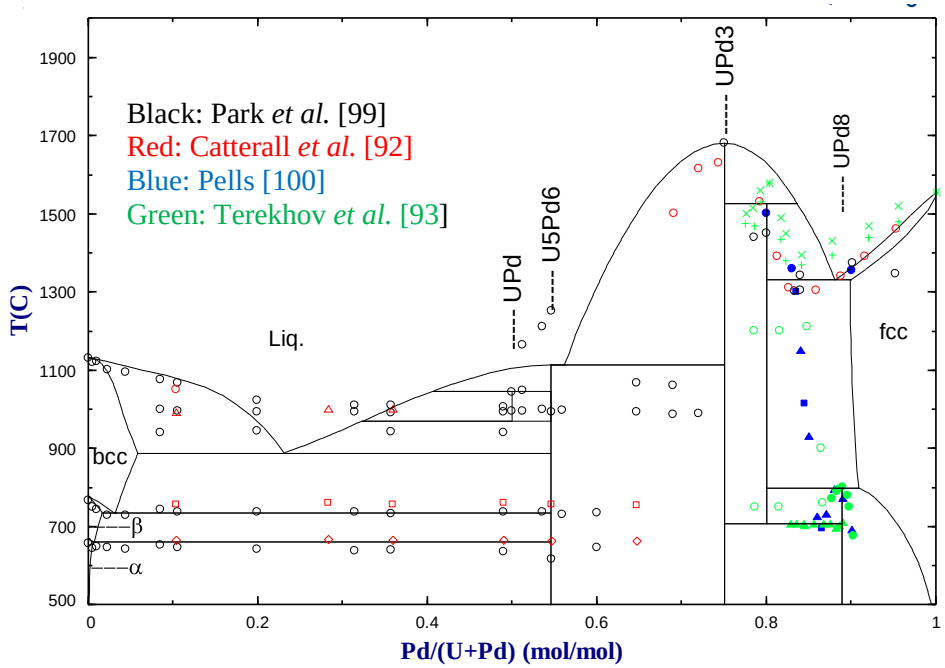

Figure 6-3. Calculated U-Pd diagram with experimental data from different authors [92,93,99,100].

The calculated figures show that the liquidus and solidus (metastable parts) about the *fcc* + *Liquid* region do not cross over each other as they are extrapolated into U-rich side in this model.

Table 6-1 lists typical liquidus data from the four groups of experimentalists and the results of the thermodynamic assessment in this work showing the obvious experimental discrepancies. The predicted values by thermodynamic evaluation are included for comparison.

Table 6-1. Liquidus data of U-Pd system from different groups [92, 93, 99, 100].

	Liquidus Temperature (°C)				
x_{Pd}	**Catterall *et al.* [92]**	**Park *et al*. [99]**	**Pells [100]**	**Terekhov *et al*. [93]**	**This work**
0.1	1050	1060			1085
0.2	1020	1015			961
0.3	1010	1010			943
0.4	1015	1030			1035
0.5	1070	1140			1106
0.6	1250	1380			1308
0.7	1540	1600			1631
0.75	1640	1680	1620	>1500*	1680
0.8	1505	1500	1515	1570	1634
0.85	1300	1302	1310	1390	1475
0.9	1360	1390	1360	1460	1361
0.95	1470	1485	-†	1520	1453

6.2.2 Solubility limit of U in Pd (*fcc* solid solution phase)

The *fcc* phase plays a very important role in U-Pd system, as well as in U-Rh-Pd ternary system. Unlike the *fcc* phase in U-Rh system and the *cph* phase in U-Ru system where the solubility of U in Rh or Ru are less than 2 at.%, the solubility of U in Pd in U-Pd system was determined to be 22 at.% U (Catterall *et al.* [92]), 15 at.% U (by Pells [100])

* Accurate data not available because the composition range does not include this composition in the phase diagram.
† Data not available because the composition range does not include this composition in the phase diagram.

and 11 at.% U (by Park *et al*. [99]), respectively. This thermodynamic evaluation shows that the limit is close to 10 at.% U.

6.2.3 U-rich side eutectic composition and temperatures

For ease of comparison, the measured eutectic properties are listed in Table 6-2.

Table 6-2. Different results in U-rich-eutectic property measurements of U-Pd phase diagram.

Author(s)	Composition (at.%Pd)	Temperature (°C)	Figure No.	Year
Catterall *et al.* [92]	37.4	998	Figure 3-11	1956
Park and Buzzard [98]	25.0	996	NA	1956
Park *et al.* [99]	23.5	1008	Figure 3-12	1963
Calculated value	23.1	888	Figure 5-1	2014

The considerable discrepancies among the different measurements can be shown pictorially in Figure 6-4, where both the data of maximum U solubility in Pd (the *fcc* solid solution) and the U-rich side eutectic point from different groups of researchers are displayed using different color. The horizontal lines on the U-rich side (about 10-50 at.% Pd) represent the controversial eutectic isotherms obtained in different experiments; the vertical lines (black, blue, purple, maroon, and green) on the Pd-rich side (80-100 at.% Pd) represent inconsistent solubility determinations. It is shown that some of the vertical lines are either longer or shorter than a phase boundary on the upper side because the phase transition temperature measured by different authors were slightly different.

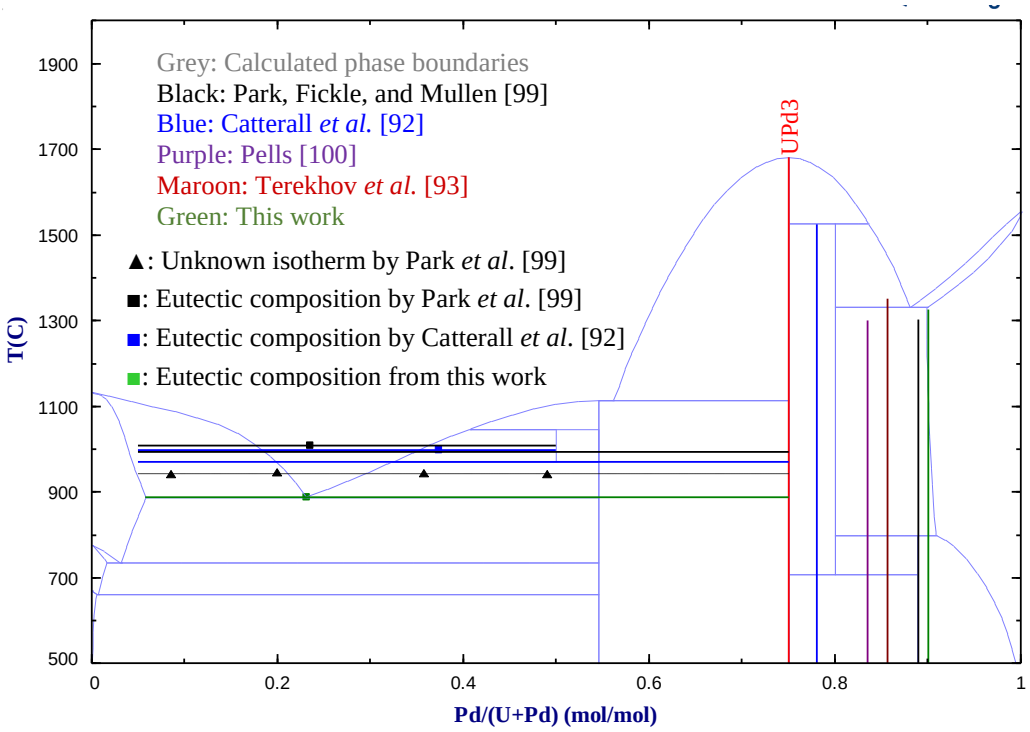

Figure 6-4. Typical experimental discrepancies in U-Pd phase diagram determinations and the thermodynamically assessed phase boundaries (grey lines) at 1 atm.

The maximum difference in the eutectic composition between the experiments was 13.9 at.%. A similar problem occurred in U-Rh system, but not as much as this. These discrepancies cannot be accounted for only by random error or systematic error in measurements, but are believed to be due to the beryllia crucible contaminations. Both Park *et al.* [99] and Catterall *et al.* [92] mentioned the contamination of BeO and ZrO_2 crucibles in their experiments. Although some compromising were adopted, the effect persisted. Comparing the phase diagrams of nine U-transition metals (Fe, Ru, Os, Co, Rh, Ir, Ni, Pd, and Pt), a conclusion can be drawn that U reacts with Be and a very stable compound with high melting point (UBe_{13}) is formed with Pd as a catalyst (a catalytic mechanism is proposed in Section 6.6.2.3.3). This makes the U-Pd phase diagram determination not a true binary system. This conclusion is based on the following facts:

1. Catterall *et al.* [92] pointed out that chemical analysis revealed the contamination of the samples by crucible materials, including zirconia crucibles and beryllia crucibles, and they believed that the latter is better than the former. Park *et al.* [99] also mentioned the "rapid reaction with the crucible materials used" within 40-80 at.% Pd, but still, they had underestimated the reaction outside of this range. Beryllia crucible were used by both groups.
2. R.W. Buzzard, the co-author of Park on "*Constitution of Uranium and Platinum Metals*" [98], proposed the U-Be binary phase diagram (Figure 6-5) in 1953 [113], in which he showed that U reacts with Be and form a γ-U + UBe_{13} eutectic isotherm at 1090 °C. The melting point of UBe_{13} is extremely high: about 2000 °C. The formation of this compound, with coexisting catalytic elements like Rh, Pd, and Pt, may have raised the eutectic temperature. The isotherm is not that of a binary system anymore. An experimental U-Be-Pd phase diagram would be helpful in solving this problem, but one is unavailable.

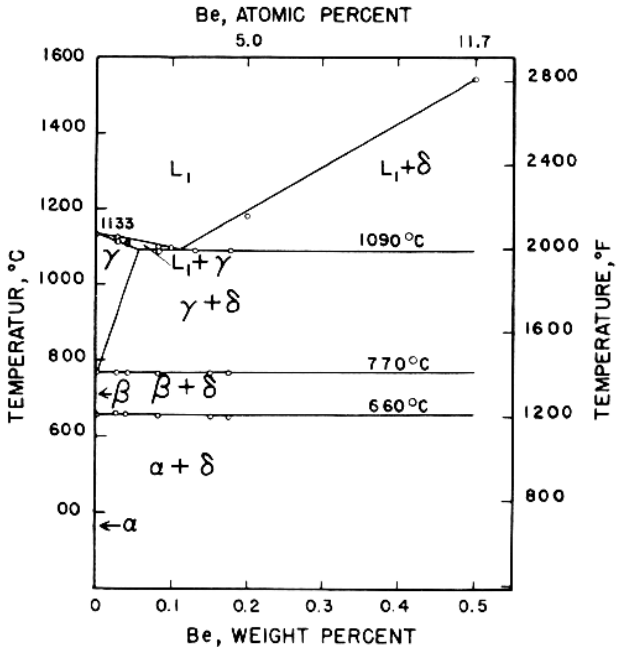

Figure 6-5. U-rich part of U-Be phase diagram by Buzzard [113].

3. The instruments used in determining eutectic points need to be improved. Park *et al.* [99] used thermal analysis alone which had caused difficulty in determining the U-rich side eutectic point in U-Rh system: without phase

identification they attributed a nearby liquidus point (20.5 at.% Pd, 897 °C) to the left side of the "eutectic point" *they* decided, and led to a higher eutectic composition and a concave liquidus that are not supported by thermodynamic evaluations. Catterall *et al.* [92] adopted microscopic observation, which cannot determine the chemical substances in the samples, but depends on the magnification of the microscope and expertise of the observers. For instance, the method may fail to identify the existence of UBe_{13} as a contaminant that may exert non-negligible heat effect, and therefore, interfere the eutectic temperature measurement. To improve the results, more factors have to be considered and more advanced techniques should be explored.

4. The trend of the eutectic composition and temperature change can be summarized by means of a comparison of the uranium-main platinum metal phase diagrams in the middle part of periodic table (Table 6-3). In comparison, the eutectic temperatures and compositions of the U and group 10 elements are obviously higher than that of U and group 8 and group 9 elements.

Table 6-3. A comparison of U-Me′ systems in terms of U-rich side eutectic features.

Group 8 Elements.

System (U-Me′)	Eutectic Composition (In terms of Me′)		Eutectic Temperature	Other Features	Source
	at.%	wt.%	°C		
U-Fe	32.62	10.2	725	Compounds on both sides	[60]
U-Ru	18.5		876		[17]
	18.5		886		[42,95]
	18.5		882		This work
U-Os	21.37*	18.0	970	Compounds on both sides	[60]

* Comparing with other group elements, this value should be less than 20%, or in a range of 15-18.5%.

Group 9 Elements.

System (U-Me′)	Eutectic Composition (In terms of Me′)		Eutectic Temperature	Other Features	Source
	at.%	wt.%	°C		
U-Co	~30		<900	Estimated from a ternary phase diagram at 900 °C. Should be lower than 865 °C.	[114]
U-Rh	24.5		865		[42,95]
	17.5		865		This work
U-Ir	15.03	12.5	914		[60]

Group 10 Elements.

System (U-Me′)	Eutectic Composition (In terms of Me′)		Eutectic Temperature	Other Features	Source
	at.%	wt.%	°C		
U-Ni	33.39	11.0	740		[60]
U-Pd	37.4		998		[92]
	23.5		1008*		[99]
	23.1		888		This work
U-Pt	12.0		1005		[98]

*Comparing with eutectic temperature of U-Ni and U-Pt, this value is too high

5. The experimental eutectic temperature features of Pd and Pt are extremely similar (*i.e.*, both of them have a typical double-isotherm around 1000 °C (Table 6-4)) and very different from other uranium-platinum phase diagrams. In all these approaches, beryllia crucibles were used.

Table 6-4. Comparison of eutectic properties of U-Pd and U-Pt systems.

System	Eutectic temperature (°C)	UMe* decomposition temperature (°C)	Reference
U-Pd	998	950	[98]
	1008	994	[99]
U-Pt	1005	961	[98,115]

* Here, Me = Pd or Pt

Based on these facts and the thermodynamic evaluation, the discrepancies in these systems should have been caused by the contamination of the crucible materials, *i.e.*, the reaction of U with Be and the reactant is UBe_{13}.

The contamination is not limited to the eutectic determination and *fcc* boundary determination. It exerts influence in the whole range of composition and temperature of this system in different degrees. Therefore, there is a potential need in analysis and clarification of the contamination reaction and its mechanism (See Section 6.6.2).

6.2.4 The Compounds

6.2.4.1 UPd and U_5Pd_6

Park and Buzzard [98] did not detect these two compounds (UPd and U_5Pd_6) in 1956. Park pointed out clearly in their 1963 report that "the contamination present in the metallographic specimens interfered with the collection of reliable X-ray data." [99]. Although they confirmed the existence of the two compounds first established by Catterall *et al*. [92], but "with some mental reservations." Catterall *et al.* [92] acknowledged that the existence of these two compounds was established by *microscopy*[*] (only) because the unsatisfactory nature of the samples defied phase identification as well as X-ray diffraction

[*] In most cases, microscopy is relatively a "primitive" tool in phase identification because the premise of the method is to know what atoms or molecules or other particles are in the samples. A microscope cannot be used to identify these particles without verification by other methods.

analysis. The structures of these two compounds were listed as unknown on the summary by Okamoto in 1993 [112]. In 1994, in order to measure the magnetic properties of these compounds, Nishioka *et al.* [116] attempted to prepare the UPd and U_5Pd_6 samples in their laboratory, and they failed in synthesis of the UPd samples. Nevertheless, they successfully obtained "a single phase of U_5Pd_6" and carried out measurements of magnetic susceptibility, magnetization, electricity resistivity and heat capacity of U_5Pd_6 at very low temperatures, *e.g.*, for high-field magnetization isotherms within 4.2-14 K.

Nishioka *et al.* [116] were fully aware of the fact that, in the accepted U-Pd phase diagram, U_5Pd_6 is not stable below 980 °C, but they acknowledged that they successfully obtained another similar compound (UAu_3) that is unstable at low temperatures [117] and can be kept for a very long time in another research. However, the so-called UAu_3 was later found to be $U_{14}Au_{51}$ in 1988 by Palenzona and Cirafici [118] and it is shown in the new U-Au phase diagram to be stable down to 0 °C. For U_5Pd_6, similar phenomenon can occur: it might be another species nearby and **is** stable down to 0 °C (Figure 6-6). Or, it simply does not exist in the U-Pd system. In addition, on the Be-Pd phase diagram [119], the compound BePd and Be_3Pd_4 have the same or very similar atomic ratios as UPd and U_5Pd_6.

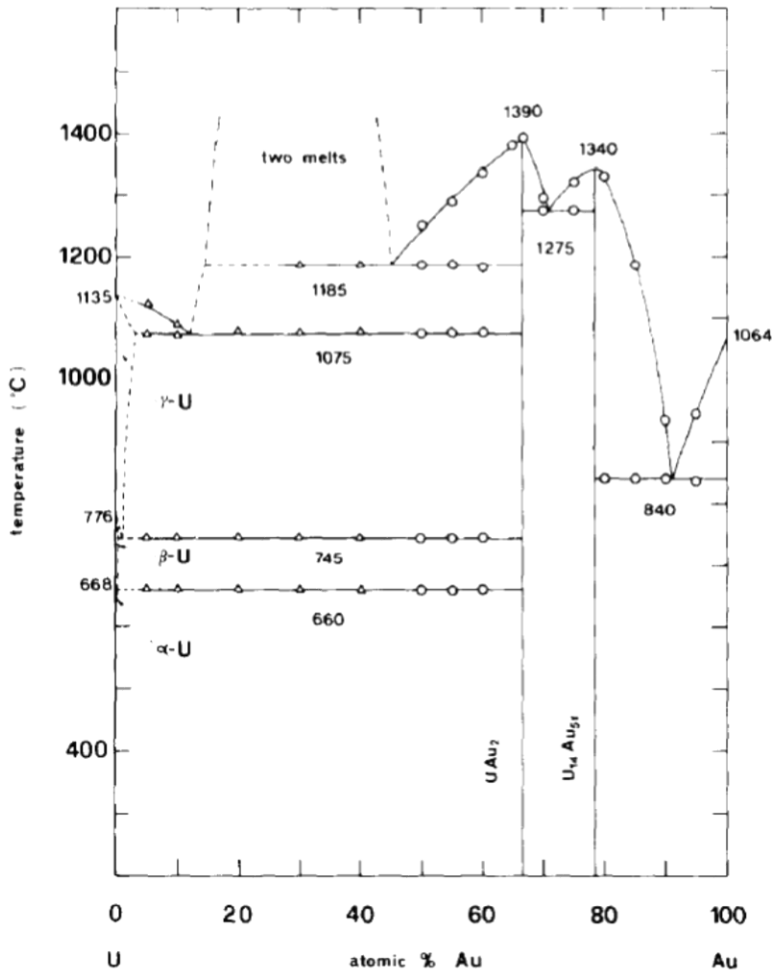

Figure 6-6. U-Au phase diagram in which UAu_3 had been replaced by $U_{14}Au_{51}$ that is stable above 0 °C [118].

In the approach by Okamoto and Massalski [117], they tried two possible solutions for the problematic liquidus shown in Figure 6-7 by adding an unknown compound between Au_3U_2 and U in Figures 13 and 14 of their paper, and in both of the figures UAu_3 is predicted to be stable above 700 °C. In addition, Okamoto and Massalski [117] concluded that thermodynamic modelling revealed improbable features in phase diagrams and clarified "subtle changes in the shape of phase boundaries which would be quite difficult to detect experimentally." The case of U_5Pd_6 here is very similar to that of UAu_3.

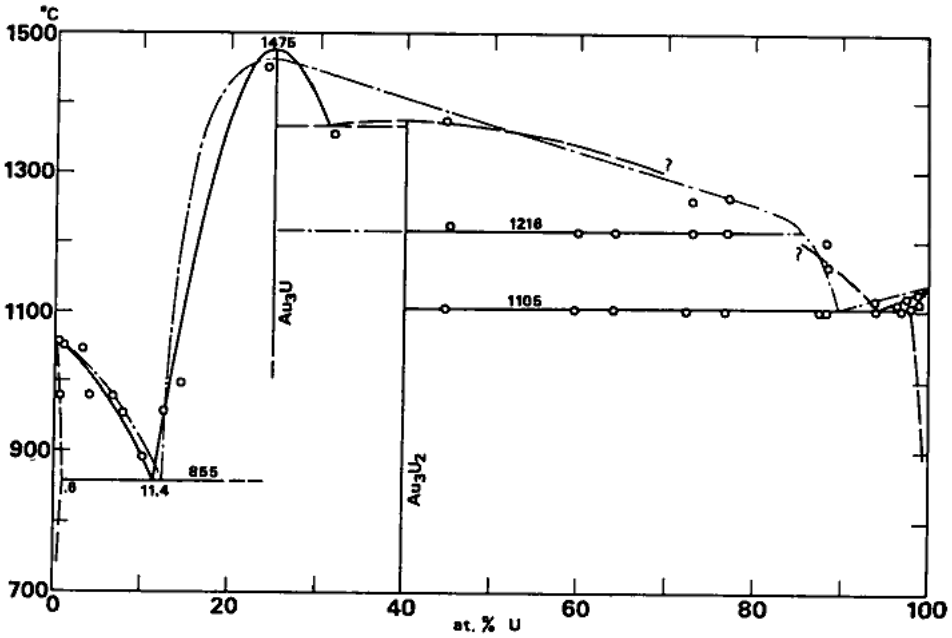

Figure 6-7. Au-U phase diagram in which Au_3U is shown unstable below about 1000 °C [117].

Kleykamp and Kang [37], who combined the available parts of the phase diagrams by Catterall *et al.* [92] and Terekhov *et al.* [93] into the presently "accepted" U-Pd phase diagram, failed in accommodating U_5Pd_6 in their experimental determinations of the U-Rh-Pd ternary isotherm at 1050 °C (see Section 3.6.1). Thermodynamic calculation in this work shows that the calculated enthalpy of formation of U_5Pd_6 is unreasonably negative in comparison with other compounds existing in this system (See Table 6-5) and the alleged U_5Pd_6 is stable down to 0 K. Moreover, although Nishioka *et al.* [116] successfully obtained the single phase sample, they acknowledged that, like Catterall *et al.* [92] and Park *et al.* [99], they failed in determining the crystal structure due to the low degree of symmetry of the crystal structure of the sample.

The calculated enthalpy of formation of U_5Pd_6 in this work is unexpectedly more negative than all the other compounds existing in this system (underlined in Table 6-5).

Table 6-5. Calculated thermodynamic properties of U-Pd system.

	UPd	**U_5Pd_6**	**UPd_3**	**UPd_4**	**UPd_8**
ΔH^0_{298K} **($J \cdot mol^{-1}$)**	-165,500	-1,110,000	-210,500	-236,200	-407,700
S^0_{298K} **($J \cdot mol^{-1}\ K^{-1}$)**	39.45	85.00	176.35	192.50	200.00

To summarise, the existence of UPd and U_5Pd_6 needs to be re-examined by carefully planning new experiments with adequate materials and technology.

6.2.4.2 UPd_3

This compound certainly exists. However, its experimental enthalpy of formation data is uncertain. Thermodynamic evaluation of this value is lower than all existing data, but still reasonable in comparison to values for URu_3 and URh_3 (See 7.2).

6.2.4.3 UPd_4

The compound has a broad range of homogeneity according to Pells [100] and Terekhov *et al*. [93]. However, in the experimental re-examination by Park, Fickle, and Mullen [99], the compound is stoichiometric. For the sake of a clear illustration of phase relationships, especially in ternary isothermal sections, and considering Park, Fickle, and Mullen [99] had treated it as a line compound, it is treated as a stoichiometric compound in this work. There have been no arguments on its existence; however, in the calculated phase diagram in this work it is found to be unstable at low temperatures.

6.2.4.4 UPd_8

UPd_8 was first detected by Pells [100] and later confirmed by Terekhov *et al.* [93], but it had never appeared in phase diagrams by Park *et al.* [98,99]. Although the thermodynamic properties are missing, the new model can predict the values and they can serve as a guide for future studies.

6.2.5 Compound models

U-Me systems contain many compounds. In U-Ru and U-Rh systems, all the compounds are stoichiometric; however, in U-Pd system, the results from different groups of scientists are controversial. As will be discussed in Section 6.6.2, potential contamination effects have been identified in this work based on analyses of different phase diagrams, their experimental conditions, related phase diagrams (such as U-Be, U-Pt, *etc.*), and the thermodynamic evaluation results. Therefore, it is important to wisely choose stoichiometric compound models so that they meet both the requirements of evaluation precision and the simplicity of the model. In addition to the newly established optimizing scheme (Figure 4-2), balanced choices are also made on the basis of the dependability of the work done by the different groups, justification through all the comparisons, analyses and thermodynamic evaluations during this work.

6.2.5.1 Binary compounds in U-Ru, U-Rh, and U-Pd systems

In the three U-Me subsystems, U_2Ru, URu, U_3Ru_4, U_3Ru_5, URu_3 (in U-Ru system); U_4Rh_3, U_3Rh_4, U_3Rh_5, URh_3 (in U-Rh system) are recognized as stoichiometric compounds by the experimentalists, and accordingly, they are treated as stoichiometric compounds in this work. In U-Pd system, however, UPd, U_5Pd_6, and UPd_3 were first identified as compounds with narrow homogeneities by Catterall *et al*. [92] in 1956, but failed to identify the compounds beyond 75 at.% Pd. Instead, they concluded that the *fcc* solution phase extends from 78 to 100 at.% Pd. In 1963, Pells [100] studied the Pd-rich side of the phase diagram and specified the existence of the following compounds: UPd_3, UPd_4, UPd_5, U_2Pd_{11}, and U_2Pd_{17}, of which, UPd_4 and UPd_5 were identified as non-stoichiometric. In 1968, Terekhov *et al*. [93] re-examined the Pd-rich part U-Pd phase diagram and denied

the existence of UPd_5, U_2Pd_{11}, and U_2Pd_{17} while confirming the existence of UPd_4 and UPd_8. In this phase diagram, UPd_3 and UPd_8 are stoichiometric, but UPd_4 is not.

A group of American scientists had been working on experimental U related phase diagrams since the 1950s and many phase diagrams were published during the 1950s and 1960s, including U-Ru, U-Rh, U-Pt, and U-Pd systems. Park and Buzzard [98] published tentative phase diagrams of several U related systems in 1956, including the U-rich part of U-Pd system. In this phase diagram, no UPd and U_5Pd_6 were detected in the region that these two compounds appeared in Catterall *et al*. [92] phase diagram. The existence of these two compounds was discussed in detail in Section 6.2.4. In 1963, Park, Fickle, and Mullen [99] submitted a detailed report re-examining the whole composition range of the U-Pd phase diagram, on which both UPd_3 and UPd_4 were treated as stoichiometric compounds. Some data in this report are unique and important because they are consistent with the thermodynamic evaluation results obtained before this forgotten report was found. Some phase boundary data or isotherm temperatures in other experimental phase diagram could not be validated by thermodynamic calculations at all, such as the solubility of U in Pd (the *fcc* solid solution on the Pd-rich side) and the U-rich side eutectic composition. Based on this new discovery [99], all the four compounds in U-Pd system are treated as stoichiometric compounds in this work.

6.2.5.2 Comments on the existence of ternary compounds

Experimental ternary phase diagrams related to U-Pd-Rh-Ru quaternary system are rarely found. For this work, the only available ternary phase diagram is the U-Rh-Pd isothermal section at 1050 °C published in 1991 by Kleykamp and Kang [37]. In the hand-drawn phase diagram in their paper, four, very small, three-phase regions were specified,

but each of them were determined uses only one data set. The experimental data are very precious, but need to be re-evaluated. It is found during thermodynamic evaluation that the demarcation of the phase boundaries in the phase diagram by Kleykamp and Kang [37] is questionable because some phase regions obviously violate the phase law.

In Table 6 of their paper, Kleykamp and Kang [37] used the following chemical formulae to represent the compound phases: UM_2, U_3M_4, U_3M_5, and U_4M_3 (where M=Rh + Pd). It seems that these are ternary compounds but the ratio of Rh and Pd is not specified. In the ternary phase diagram (Figure 4 in the original paper; Figure 3-20 in this thesis), however, only the terminal compounds are labelled. This suggests that the four horizontal lines in the figure represent ternary compounds, but UM_2 and U_4M_3 are not shown on the phase diagram. On the contrary, the longest horizontal line is between URh_3 and UPd_3 without UM_3 detected in Table 6 in [37]. According to the tie lines between the U_3M_4 horizontal line and the URh_3 - UPd_3 horizontal line, the "two-phase" equilibrium should be between U_3M_4 and UM_3 ternary compounds, but in Table 6 of the paper no U_3M_4 is shown, which should be in equilibria with UM_3. All these phenomena illustrate that some of the experimental data were misinterpreted by the authors.

It is still a mystery why these compounds lose metallic character when the size of the unit cell of a metallic compound increases. The complex intermetallics show apparent localization of electronic states, loss of conductivity, opening of gaps, softening with no work hardening *etc.* [120]. In short, the crystal cells of CMAs (Complex Metallic Alloys) become so large that non-metallic properties overwhelm the metallic properties. For such large crystal cells, it is common to have "room" for accommodating free atoms in the

system. Therefore, the "ternary compounds" identified by Kleykamp and Kang [37] might not be true ternary compounds, but binary in nature.

In order to discuss the concept of ternary compounds in the U-Me systems, some confusions in using terms like solution, *phase* and *inclusion* need to be elaborated. The main points are as follows:

1. An inclusion in used nuclear fuel does not necessarily mean that the inclusion is a single uniform phase or solution at any specific temperature. An inclusion can be a coagulation of some smaller particles with similar properties. In other words, an inclusion may contain different phases.

2. Compounds with same crystal structure (*e.g.*, Cu_3Au) may not dissolve into each other at all temperature or composition ranges.

3. The definition of a phase is the substance that has a unique X-ray spectrum profile. URu_3, URh_3, and UPd_3 have their own unique X-ray spectrum profiles [38].

According to thermodynamic evaluation results, URh_3 and UPd_3 do not exist as one solution phase below 1354 °C.

Recently, Dshemuchadse and Steurer [121] performed a statistical study on ternary intermetallic compounds. They concluded that not all so-called ternary compounds have been well studied. They pointed out that:

> *Indeed, a considerable number of structure types of ternary intermetallics are* ***binary****. These ternary compounds are partially inherently disordered if the binary structure types can be described with only two independent Wyckoff positions in the respective space group, e.g., cF24-*Cu_2Mg*,* ***cP4-*Cu_3Au***[*], cP2-CsCl etc.* [121]

[*] The cP4-Cu_3Au space group is directly related to the structures of UMe_3 compounds studied in this work. The bold font in the quotation is used by the author for the sake of emphasis.

In addition, it is notable that URh_3 and UPd_3 do not have the same crystal structure ($TiNi_3$ for UPd_3 and Cu_3Au for URh_3).

To conclude, the U-Pd phase diagram is not one that has been well studied experimentally. The experimentalists had misinterpreted or over classified the phase boundaries. The experimental methods used failed to detect some of the trace amount phases or with weaker X-ray diffraction patterns. Because of these experimental problems, the thermodynamic model does not exactly replicate the only experimental phase diagram for U-Rh-Pd [37], but instead calculates the phase boundaries according to the compound formulae in the corresponding binary phase diagrams. In this way an overall relationship of phases on the ternary phase diagrams was obtained. Furthermore, the thermodynamic evaluation results prove that the calculated U-Rh-Pd phase diagram is reasonable in all aspects: no violation of the phase rule, and the four three-phase data set obtained by Kleykamp and Kang [37] fall into the four calculated three-phase regions respectively. Undeniably, there are possibilities that in XRD determinations of the samples by Kleykamp and Kang, signals of some phases might had been shielded by other strong signals in the sample and led to many "would be" three-phase equilibrium regions were misinterpreted as two-phase equilibria. According to all these facts, ternary compounds are not considered, or to be accurate, are denied in this work.

6.3 U-Rh System

In contrast to U-Pd and U-Ru systems in which different experimental approaches were carried out on the Ru-rich side and the high temperature part of the phase diagrams, disputes on U-Rh phase diagram are focused on the U-rich side. To eliminate the

discrepancies (shown in Table 6-6), the experimental results need to be examined by thermodynamic evaluation and then by further experimental explorations guided by the thermodynamic results:

Table 6-6. Main discrepancies in U-Rh binary system.

Author(s)	Eutectic composition (at.%)	U-rich side compounds	Year	Reference
Chiswik *et al*.	~18	U_2Rh + URh	1958	[94]
Park	24.5	α-U_4Rh_3 + β-U_4Rh_3	1965	[42]
Naraine and Bell	--	U_2Rh + URh	1974	[96]

The phase diagram from Park [42] is taken as the blueprint of U-Rh model. However, it is found that it is thermodynamically improbable to set the U-rich eutectic composition to 24.5 at.% Rh in this assessment. The calculated value is as low as 17.5 at.% Rh, but it is very close to the value given in [94]. Figure 6-8 is a comparison of the calculated phase diagram with experimental data by Park.

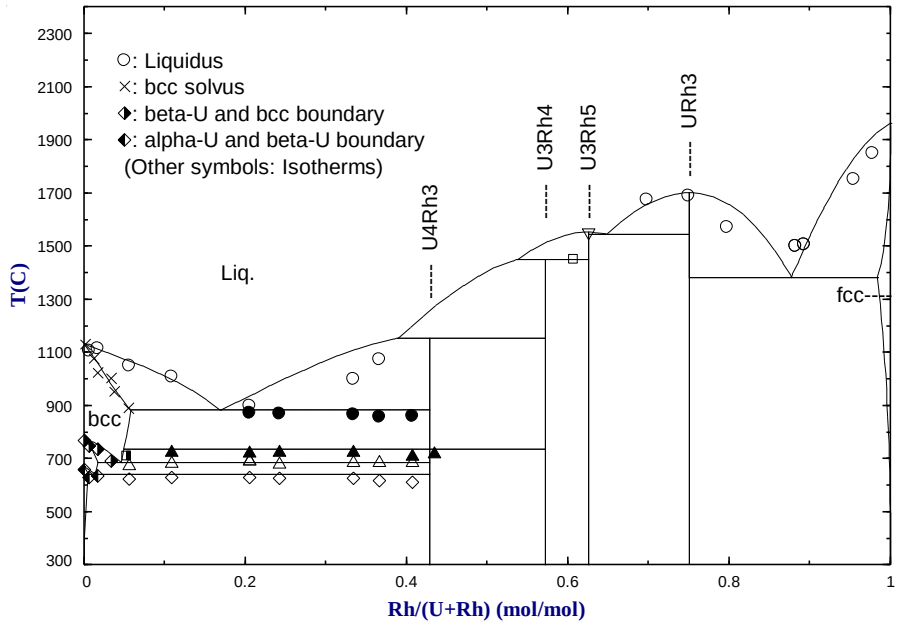

Figure 6-8. A comparison of calculated curves with experimental data of Park [42].

It can be seen that the calculated *bcc* liquidus fits well with most experimental data, but very poor for the liquidus on the right side of the eutectic point. In phase diagram from Park [42,64] (Shown in Figure 3-5), the liquidus datum close to the eutectic isotherm was attributed to the left part of liquidus of the eutectic point he designated (24.5 at.% Rh), whereas according to thermodynamic evaluation (this work), it should be part of liquidus on the right side of the eutectic point (17.5 at.% Rh). In the thesis and papers by Park, this disputed point (20.5 at.% Rh, 897 °C) was listed as any other "fusion" (liquidus) points obtained by thermal analysis. His treatment of this datum led to a **concave** liquidus that seems thermodynamically improbable under the constraint of present lattice stabilities because to obtain such a liquidus the interaction parameters must be much less negative or even positive and the equilibrium of the liquidus to neighbouring phases will be greatly changed. In addition, to realize such a concave liquidus, the thermodynamic properties, *e.g*., enthalpy of formation and entropy of the compounds, will be not comparable to the experimental data, and the interaction parameters of *Liquid*, *bcc*, and *fcc* solution phases will not be comparable with those of the U-Ru and/or U-Pd systems. Practically, for this important point, some effective phase identification experiments should be carried out to better characterize the eutectic point. Unfortunately, these kinds of supporting evidence were missing in both Park's thesis and the published paper. According to the experimental assessments of U-Pd system, there may be intrinsic difficulties in phase identification in the U-rich region as well, because of the contamination problems.

Regarding the five-compound configuration by Naraine and Bell [96], a thermodynamic evaluation was carried out in this work to examine if their results were thermodynamically reasonable. The calculated phase diagram is illustrated in Figure 6-9.

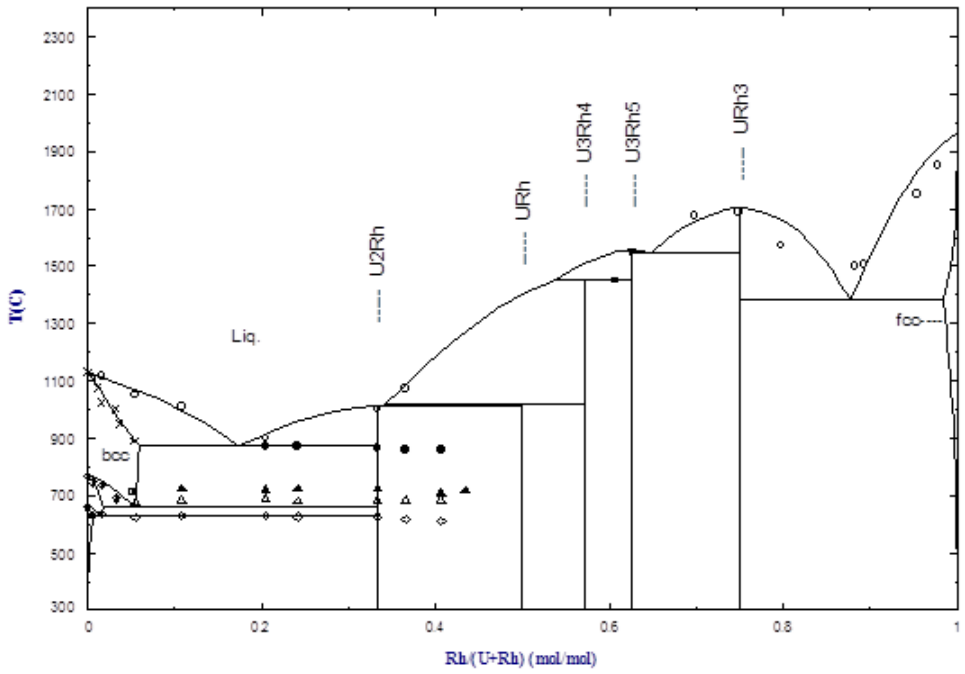

Figure 6-9. Calculated U-Rh phase diagram of the five-compound configuration with the experimental data from Park at 1 atm. [42].

Some important features of this model are the following:

1. Although the fitting of liquidus on the right side of the eutectic point is almost perfect, U_2Rh is stable up to 1011 °C, which is much higher than 755 °C [94] and 705 °C [96]. That is, these low peritectic melting temperatures are thermodynamically unlikely. Thus the "γ + URh" region shown in [94] is thermodynamically unstable;
2. The thermodynamic model cannot explain the extra experimental points for the isotherms in the field of "U_2Rh + URh".

Therefore, the five-compound configuration was rejected in this work.

6.4 U-Ru System

From the phase diagrams shown in Section 3.5.3, it can be seen that the different features of the high temperature profiles from different sources are non-negligible. For

example, in U-Ru system the calculated eutectic temperature at Ru-rich side is 1576 °C (1849 K), which is 274 °C lower than the peritectic temperature from Park [42]. In the diagram proposed by Mason and El-Genk [4], although the two possible L/*cph* liquidus separate as far as a magnitude of about 230 °C at 87 at.% Ru, the eutectic isotherm is well defined by the experimental data. The eutectic composition by Mason and El-Genk (77.5 at.% Ru) [4] is supported by metallurgical analysis and observations by Edwards *et al.* [76]. The calculated eutectic composition by Berche *et al.* [17] is 83.8 at.% Ru, which is 6.3 at.% higher than the experimental data. The reason is not provided by Berche *et al.* [17]. As part of this work [59], the fit of the calculated phase boundaries with the experimental data was attempted; however, the eutectic composition by Mason and El-Genk [4] was proved to be another scenario that is thermodynamically improbable. On the contrary, the calculated result by Berche *et al*. [17] proved to be reasonable.

The isothermal temperatures of the two reaction types (peritectic and eutectic) affect the position of the *cph* phase field. This phase was estimated by Park without giving experimental data [42]. Figure 6-10 follows Berche *et al*. [17] calculation which shows the U-Ru phase diagram with metastable solution phases, without giving a hypothetical *cph*-U lattice stability (therefore, the *cph* phase is missing). Therefore, this diagram shows several abnormal phenomena, even on the metastable phase diagram: first, the *bcc + Liquid* phase liquidus in Ru-rich region does not reflect a true liquidus; second, the *bcc + Liquid* region is separated from the β-U + *bcc* region; third, the minimum point of the *bcc + Liquid* region does not have any physical meaning, *e.g.*, it is not a eutectic point; finally, the eutectic isotherms of α/β and β/γ transformations are not shown. All these mean that the metastable phase diagram is not a reasonable one.

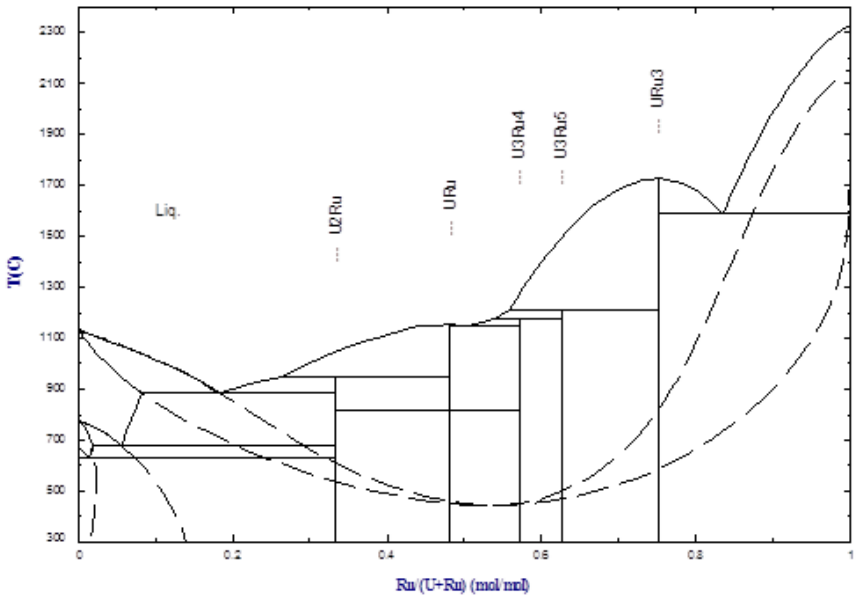

Figure 6-10. Re-calculated phase diagram with metastable solution phases without *cph* phase (Referencing for *bcc* Ru see Table 3-1) at 1 atm.

The re-assessed enthalpy of formation ($\Delta H^{\circ}_{298\,K}$) of URu_3 is -144,700 J·mol^{-1}, similar to experimental results by Wijbenga and Cordfunke [91] (-153,200 J·mol^{-1}) and Jung and Kleppa [74] (-124,000 J·mol^{-1}). In the model of energy effects of alloys [73], the value is -152,000 J·mol^{-1}. Closer assessment of enthalpy of formation of URu_3 is significant in estimating enthalpy values of other compounds in this system.

Figure 6-11 illustrates the recalculated phase diagram with published experimental data by Park [42] and Mason and El-Genk [4].

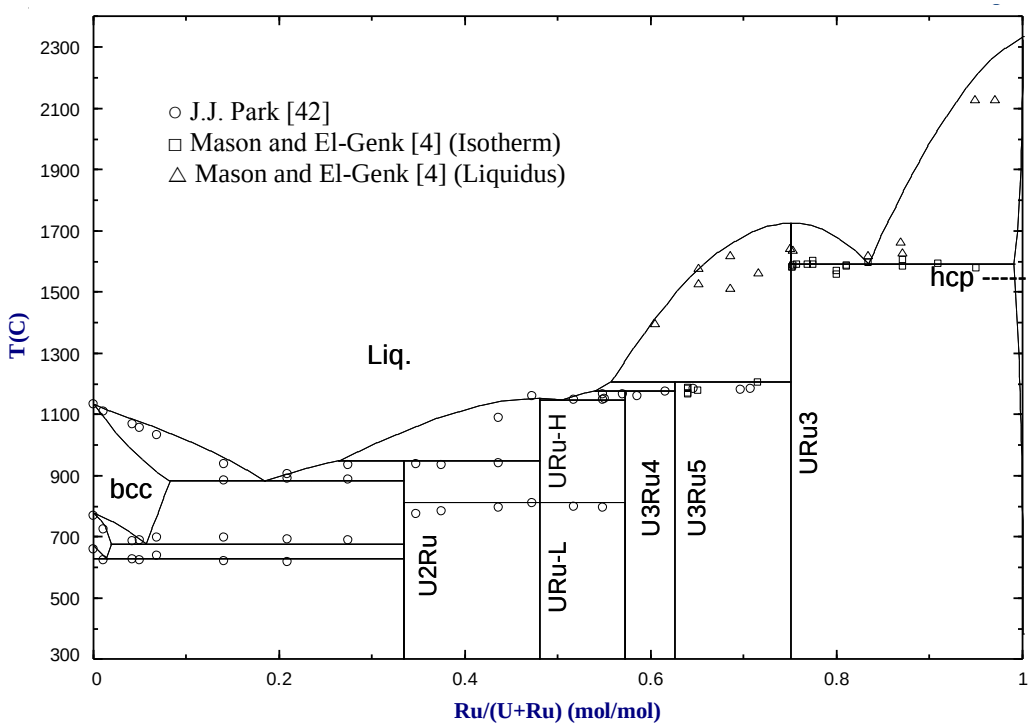

Figure 6-11. Re-calculated U-Ru phase diagram with published experimental data at 1 atm. [4,42]

6.5 Ternary, Pseudo Binary, and Pseudo Ternary Phase Diagrams

It is necessary to examine the experimental errors in existing U-Me phase diagrams and problems found in the only experimental U-Rh-Pd ternary phase diagram before the detailed discussion of the ternary and pseudo phase diagrams in this section.

6.5.1 Error Analysis Related to Binary and Ternary U-Me Systems

Thermodynamic evaluations are based on thermodynamic principles, that is, theories. All theories come from experimental observations where systematic and random errors are usually introduced. Occasionally, the design of an experiment can be imperfect or even incorrect; in some circumstances, there may be no perfect technical instruments or methods available for a specific purpose. For instance, there may be difficulty in choosing a suitable crucible material to avoid contamination of samples at high temperature

measurements. Another example is the difficulty in determining liquidus boundaries at high Me concentrations and at high temperatures. These phenomena are not uncommon in U-related transition metal phase diagram determinations.

Studies of the experimental phase diagrams determined by Park, *e.g.*, U-Ru, U-Rh, and U-Pd systems by [42,95,99], no error analysis or error bars were provided or labelled. On these phase diagrams, parts of the liquidus are represented by dash-lines showing considerable uncertainty in experimental determinations at that particular temperature and composition range. Re-examinations by other authors showed that the uncertainty of liquidus determinations at high temperatures can be as high as to a temperature difference of about 300 ºC [4] for these systems. Due to these challenges, few data points are usually available in the high concentration ranges of Me elements. As a result, it is difficult to conduct precise error analysis for these parts of the phase diagrams.

Some typical sets of experimental data in the U-Rh phase diagram investigation by Park [42] are examined here. Park provided neither error information nor error bars, although all the data sets for U-Ru and U-Rh systems were listed. As data for liquidus and solidus vary with composition and no repeated data sets were provided, no average value of the data can be calculated, therefore, no error bars can be plotted on the phase diagrams. However, the data points for isotherms below 50 at.% Me are multiple and the average temperatures of the determinations can be evaluated. Even for the four isotherms on the U-rich side of the U-Rh system, a clear descending trend of the points can be observed showing that, as Rh concentration increases, the temperature value shows a gradual decrease. The calculated average, and the upper-limit and lower-limit temperatures for the four isotherms are listed in Table 6-7.

Table 6-7. Error analysis of the U-rich side isotherms based on the U-Rh phase diagram by Park [42]

Isothermal Transition	Average Temperature (°C)	Uncertainty	
		Upper-limit	Lower limit
Eutectic	865	+7	-9
Allotropic	720	+5	-12
γ→β	683	+1.5	-0.5
β→α	623	+3	-13

For the other four isotherms above 1000 ºC (42.29-100 at.% Rh), there is only one point for the U_3Rh_4 peritectic isotherm at 1450 ºC. The others were solely determined by estimations of the temperatures of the peritectic or eutectic reactions. The reasons for the difficulty in determining the liquidus boundaries are complex. For example, in a thermal analysis or differential thermal analysis, when the heat effect of the liquid-solid transformation is too small, there may be no obvious change in the cooling or heating curve. Even if the heat effect is high enough, when contamination of the sample by crucible material occurs, the sample is no longer pure and the formation of some unknown compound or alloy may make the observation even more difficult. In addition, at very high temperatures, thermocouples are no longer applicable for the liquidus determinations. The application of pyrometers, however, has proved to be not ideal in the observation of the phase transition, which is another reason why the liquidus data are inaccurate.

The problems in high temperature determinations are not only shown in studies by Park, or Park with his co-workers, but also shown in other research. For example, in the U-Ru phase diagram by Mason and El-Genk [4], the differences in melting point determinations of URu_3 are as much as 185 ºC (*i.e.*, the congruent melting point is 1665 ºC and the peritectic melting point by Park is 1850 ºC). The measurement uncertainties in Mason and El-Genk studies were listed in several uncertainty categories, but not point by

point. Because of their difficulty in observing the phase transitions, they provided two possible liquidus with a maximum temperature difference up to about 300 ºC at high temperature ranges of the U-Ru and U-Re phase diagrams, which cannot only be accounted for by the uncertainty ranges they listed.

For the U-Rh system, Park is the only scientist who provided a relatively complete phase diagram. In contrast, for the U-Pd system, several groups of scientists produced very different phase diagrams, in which discrepancies exist not only in terms of temperature measurements, but also in terms of composition measurements. For instance, the experimentally obtained *fcc* phase boundaries vary in by an unacceptable magnitude of 11 at.%, which was derived from 22 at.% by Catterall, Grogan, and Pleasance [92]; 15 at.% by Pells [100] and Terekhov *et al*. [93]; and 11 at.% by Park, Fickle, and Mullen [99].

To conclude, in U-Pd-Rh-Ru related phase diagram determinations, not only random and systematic errors were involved, but also maybe some other detrimental factors, such as contamination by the crucible materials and misinterpretations of experimental data in determining some of the phase boundaries. Based on these facts and for the sake of the clarity of pictorial illustrations, no error bars will be used in the calculated phase diagrams in this thesis.

6.5.2 Problems Found in the Experimental U-Rh-Pd Ternary Phase Diagrams

Some of the problematic phases in the phase diagram shown in Figure 3-20 were labelled with numbers. Table 6-8 lists these regions and associated problems.

Table 6-8. Problematic regions on the phase diagram by Kleykamp and Kang [37].

Region	Phase(s) suggested by Kleykamp and Kang	Problem(s) to be elaborated
1	α1 + α2 (ternary miscibility gap of *fcc* phase)	The miscibility gap is larger than the calculated one; the α phase specified in region 2 seems to be another independent phase; it seems that there are three different phases in regions 1 and 2; the "closed region" appears based on nominal compositions of the alloys instead of equilibrium data.
2	α (*fcc* solid solution of Rh and Pd in U)	If region 1 consists of two immiscible phases with common *fcc* structure, the α should be one of them, *i.e.*, it should be either α1 or α2 instead of α.
3	Single-phase region consisted of three compounds	UMe_3 compounds are found in UO_2, UN and $(U, Pu)O_2$ fuels as a distinctive inclusion but not necessarily as a single-phase. URh_3, UPd_3 and UPd_4 on this diagram have different crystal structures and different X-ray diffraction patterns, which are features of different phases.
4	γ(URh_3)+UM_2+U_3M_5(U_3Rh_5); The compositions at three corners of the three phase region are $U_{0.38}Rh_{0.61}Pd_{0.01}$, $U_{0.33}Rh_{0.64}Pd_{0.03}$ and $U_{0.25}Rh_{0.71}Pd_{0.04}$*	Because the lower corner of the three phase region is not located at $X_{Pd} = 0$ but at the common boundary of URh_3 and UPd_3, why UPd_3 is not included is unknown. By drawing the small three phase regions, the formation of three ternary alloys (not identified in the paper) are assumed. Regions 4, 5, and 6 share a phase boundary representing UM_2.
5	No datum is given; U_3Rh_4, $U_{0.38}Rh_{0.59}Pd_{0.03}$ and $U_{0.32}Rh_{0.59}Pd_{0.09}$	Again, they are assuming the formation of another two ternary alloys.
6	γ(URh_3)+UM_2+U_3M_5(U_3Rh_4); $U_{0.43}Rh_{0.50}Pd_{0.07}$, $U_{0.33}Rh_{0.51}Pd_{0.16}$ and $U_{0.25}Rh_{0.28}Pd_{0.47}$	Again, they are assuming the formation of another three ternary alloys.
7	ε+U_3M_4+*Liquid*; $U_{0.43}Rh_{0.30}Pd_{0.27}$, $U_{0.46}Rh_{0.23}Pd_{0.31}$(*Liquid*) and $U_{0.25}Rh_{0.07}Pd_{0.68}$	In this case, they are assuming the formation of another two ternary alloys.
8	*Liquid* + UPd_3	Kleykamp and Kang [37] were the first to combine the Catterall *et al*. [92] diagram (left side of UPd_3) and that of Terekhov *et al*. [93] (right side of UPd_3). They recognized U_5Pd_6 in the range of 980-1110 ºC. However, at 1050 ºC they did not detect the compound and made no comment.
9	γ + ε + U_3M_4; $U_{0.43}Rh_{0.30}Pd_{0.27}$, $U_{0.25}Rh_{0.23}Pd_{0.31}$ and $U_{0.25}Rh_{0.10}Pd_{0.65}$	The nomenclature of the phases by these authors are also confusing. For instance, they use the horizontal lines *a* and *b* to represent ternary compounds of U_3M_4 and UM_2 respectively, but the horizontal line *c* is represented by two Greek symbols: γ and ε, the two terminal compounds.

The problems highlighted in the table can affect the reasonability of adjacent regions, in what might be termed a ripple effect. The authors tried to validate the "closed region" by estimating binary interaction parameters in a ternary regular solution model, but

* The composition of the ternary metallic compounds are estimated from Figure 3-20.

thermodynamically there should be a single binary interaction parameter for a specific phase in a ternary system. The miscibility gap should be a function of temperature instead of the binary interaction parameters. As a matter of fact, in such a ternary system, the miscibility gap is defined not only by the binary interaction parameter of U-Pd, but also by that of the U-Rh. In addition, the simplification of Equation (12) from Kleykamp and Kang [37] is not adequate because of the unreasonable omission of α_{12}.

6.5.3 Calculated Ternary U-Rh-Pd Phase Diagrams

In this work, the U-Pd-Rh-Ru quaternary thermodynamic model has been successfully established and compared with the only set of existing experimental ternary data: the U-Rh-Pd system at 1050 °C. The model cannot only "describe" the isothermal diagram, but can also be used to reinterpret some misinterpretations of the data and reasonably predict the feature of the "closed region" discovered in the experiments by Kleykamp and Kang [37].

As mentioned before, the ternary isothermal section constituted by Kleykamp and Kang [37] is the only available experimental data for this quaternary system. Therefore, the set of data can be used as reference in validating this thermodynamic model, and at the same time, subject to the evaluation and reinterpretation in reference of the new results based on thermodynamic principles.

The first step is to determine if the quaternary system needs any adjustments and how it should be adjusted. Figure 6-12 shows the calculated isothermal section of U-Rh-Pd at 1050 °C, where at least the following discrepancies can be observed:

1. parts of liquidus (at the upper part of the diagram) are not complete;

2. the *fcc*+*fcc*#2 region (at the lower part of the diagram) is crossed in the middle by the *fcc* phase boundary.

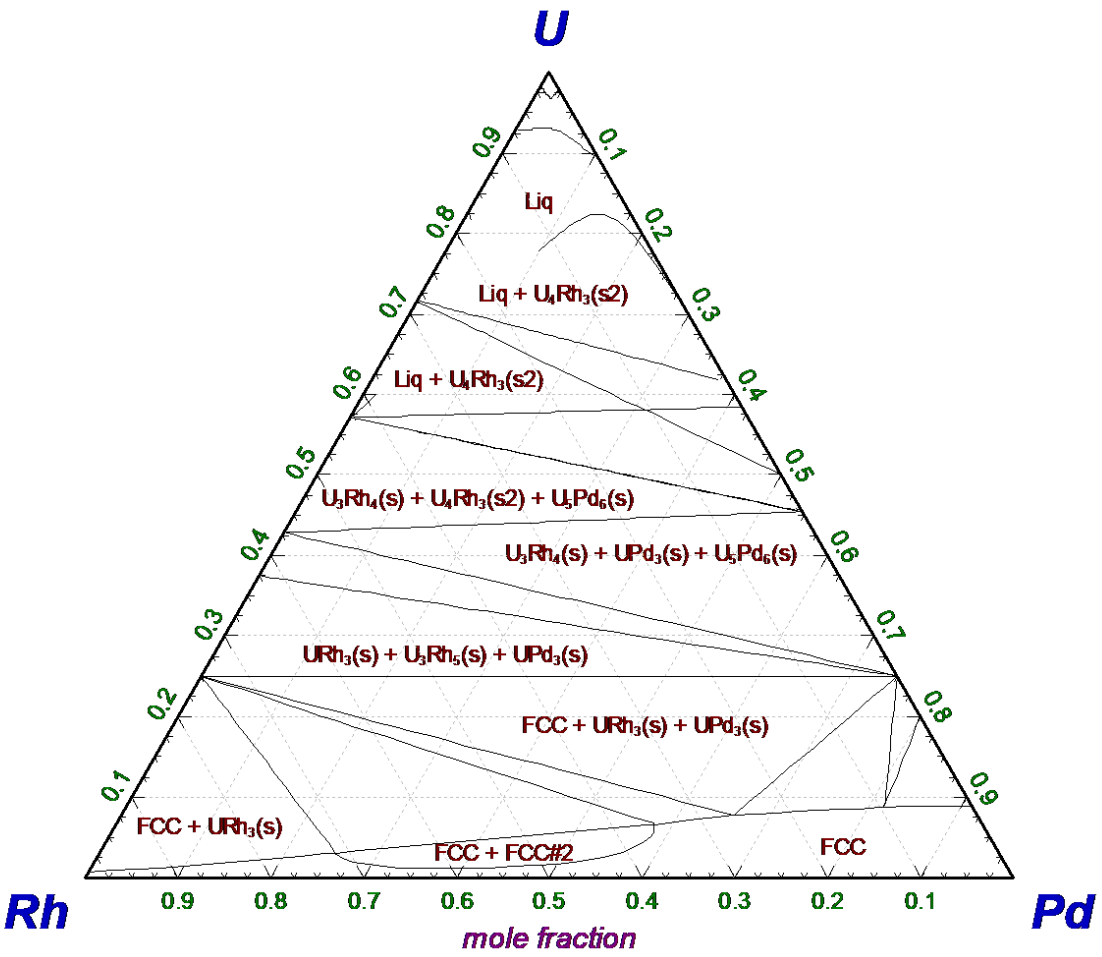

Figure 6-12. Calculated U-Rh-Pd phase diagram at 1050 °C, and 1 atm without adjustments of ternary parameters.

The *Liquid* phase and *fcc* phase are dominant solution phases in this system, therefore, necessary corrections are needed. Note that the adjustment is not based on the experimental phase diagrams because those phase diagrams are binary and with discrepancies. The principle of the adjustment is the same as presented in Section 3.45.2. It is based on the solution phase equilibrium, but it is now used for a ternary system.

The second step is to compare with the data by Kleykamp and Kang [37]. In their paper, the data are listed in two separate tables and are not classified into specific phases. This is not only confusing to the reader, but also have misled the authors themselves in plotting the phase diagram. For convenience of analysis and comparison, Table 4 in their paper is reorganized in Table 6-9 (The nominal composition is not included because the equilibrium composition is emphasized here).

Table 6-9. Phase relations in experimental data of Kleykamp and Kang [37].

Type of α phase	**In equilibrium with**	**Lattice parameter (a in pm)**	**Range of a (in pm)**	**Composition (at.%)**		
				U	**Rh**	**Pd**
α1	α2	381.1	381.1-384.7	0.5	86.5	13.0
	α2	384.6		0.9	56.4	42.7
	α2	383.9		0.6	65.8	33.6
	α2	382.1		2.1	89.4	8.5
	α2	381.8		0.6	89.5	9.9
	α2	384.7		0.8	58.1	41.1
	α2	381.4		0.5	88.5	11.0
α2	α1	392.0	390.8-395.6	10.3	53.7	36.0
	α1	395.6		11.2	19.8	69.0
	α1	391.1		4.8	19.6	75.6
	α1	394.7		10.4	20.0	69.6
	α1	393.9		9.3	17.7	73.0
	α1	390.9		5.0	17.0	78.0
	α1	390.8		5.8	15.4	78.8
α		396.2	383.1-403.3	11.1	9.5	79.4
	γ	-		15.6	24.8	59.6
	γ	396.0		-	-	-
	γ	396.1		16.5	19.8	63.7
	γ	401.1		15.0	0	85.0
		-		18.4	9.5	72.1
	γ	392.9		12.4	55.8	31.8
		394.1		12.0	45.7	42.3
		395.2		14.8	32.6	52.6
		400.9		15.4	4.8	79.8
	γ	390.8		11.1	65.3	23.6
	γ	383.1		3.4	93.3	3.3
	γ	394.9		14.2	40.8	45.0
		403.3		17.6	8.0	74.4
	γ	391.4		11.9	60.3	27.8
		387.8		8.8	69.9	21.3
γ	α	399.6	399.5-408.8	21.9	57.7	20.4
	α	399.6		21.4	46.5	32.1

Type of α phase	In equilibrium with	Lattice parameter (a in pm)	Range of a (in pm)	Composition (at.%)		
				U	Rh	Pd
		402.7		21.2	32.9	45.9
		406.2		20.2	1.9	77.9
	α	399.5		22.6	60.3	17.1
	α	399.5		24.2	70.0	5.8
	α	399.5		22.3	54.1	23.6
	α	399.6		22.3	58.8	18.9
	α	-		21.4	28.8	49.8
	α	400.9		20.8	34.2	45.0
γ	α	401.7	399.5-408.8	20.5	29.5	50.0
	ε	408.8		23.2	8.3	68.5
		404.7		21.6	17.3	61.1
	α	404.7		19.1	0	80.9
		402.5		-	-	-
		400.6		-	-	-
		405.4		-	-	-
		403.6		-	-	-
		-		23.2	16.4	60.4
		-		23.4	36.5	40.1
	ε	407.4		21.6	0	78.4
γ(+α)		403.0		19.5	12.1	68.4
		403.9		19.5	8.7	71.8
ε	γ	a=578.6 c=943.7		24.5	7.0	68.5
	γ	a=576.3 c=954.1		23.3	0	76.7

The experimental data from Table 6 of Kleykamp and Kang [37] is organized here as Table 6-10.

Table 6-10. Phase classified U-Rh-Pd experimental data for X_U>0.25 (Table 6 in paper by Kleykamp and Kang [37]).

Phase (M = Rh,Pd)	Exp. No.	Nominal composition (mole fraction)			Phase(s) calculated	Analysed composition (mole fraction)			Lattice parameter (pm)	
		U	Rh	Pd		U	Rh	Pd	a	c
γ	46	0.27	0.365	0.365	URh_3	0.25	0.305	0.445	405.8	-
	47	0.40	0.30	0.30		0.248	0.103	0.649	409.5	-
	48	0.255	0.08	0.665		0.252	0.076	0.672	410.1	-
	52	0.30	0.65	0.05		0.254	0.656	0.090	400.3	-
	57	0.32	0.655	0.025		0.25	0.72	0.03	399.5	-
	63	0.31	0.59	0.10		0.25	0.59	0.16	401.4	-
	66	0.35	0.40	0.25		0.26	0.27	0.47	-	-
	67	0.35	0.35	0.30		0.258	0.197	0.545	-	-
	68	0.27	0.655	0.075		0.253	0.660	0.087	400.1	-
	69	0.31	0.59	0.10		0.25	0.59	0.16	400.9	-
	70	0.36	0.50	0.14		0.26	0.26	0.48	-	-

Phase (M = Rh,Pd)	Exp. No.	Nominal composition (mole fraction)			Phase(s) calculated	Analysed composition (mole fraction)			Lattice parameter (pm)	
		U	Rh	Pd		U	Rh	Pd	a	c
ε	48	0.255	0.08	0.665	UPd_3	0.25	0.065	0.685	578.8	874
	49	0.330	0.05	0.620		0.254	0.024	0.722	-	-
	50	0.350	0.13	0.52		0.254	0.044	0.702	-	-
	54	0.480	0	0.52		0.247	0	0.753	-	-
	58	0.40	0	0.60		0.248	0	0.752	577.5	965.4
	74	0.40	0.22	0.38		0.246	0.058	0.696	-	-
UM_2	46	0.40	0.30	0.30	U_3Rh_5	0.426	0.335	0.239	-	-
	52	0.30	0.65	0.05		0.326	0.632	0.042	534.3	869.4
	53	0.375	0.575	0.05		0.340	0.580	0.080	-	-
	57	0.32	0.655	0.025		0.325	0.650	0.025	534.3	866.6
	63	0.31	0.59	0.10		0.328	0.587	0.085	536.0	871.1
	65	0.34	0.63	0.03		0.333	0.627	0.040	-	-
	68	0.27	0.655	0.075		-	-	-	531.9	871.8
	69	0.31	0.59	0.10		0.324	0.608	0.068	534.4	867.4
	70	0.36	0.50	0.14		0.331	0.499	0.170	537.7	869.4
U_3M_4	47	0.27	0.365	0.365	U_3Rh_4	0.325	0.531	0.144	540.8	874
	48	0.255	0.08	0.665		0.430	0.302	0.268	-	-
	49	0.330	0.05	0.620		0.435	0.116	0.449	-	-
	50	0.350	0.13	0.52		0.426	0.194	0.380	-	-
	53	0.375	0.575	0.05		≈ 0.44	≈ 0.56	0	-	-
	56	0.46	0.30	0.24		≈ 0.45	≈ 0.29	≈ 0.26	-	-
	64	0.375	0.60	0.025		0.43	0.57	0	-	-
	66	0.35	0.40	0.25		0.422	0.491	0.087	-	-
	67	0.35	0.35	0.30		0.436	0.446	0.118	-	-
	70	0.36	0.50	0.14		0.423	0.514	0.063	-	-
	72	0.50	0.45	0.05		≈ 0.43	≈ 0.41	≈ 0.16	-	-
	74	0.40	0.22	0.38		0.427	0.261	0.312	-	-
U_4M_3	56	0.46	0.30	0.24	U_4Rh_3	≈ 0.55	≈ 0.43	≈ 0.02	-	-
	72	0.50	0.45	0.05		≈ 0.51	≈ 0.44	≈ 0.05	-	-
U_3M_5	57	0.32	0.655	0.025	U_3Rh_5	0.375	0.610	0.015	-	-
	64	0.375	0.60	0.025		0.380	0.600	0.020	-	-
	65	0.34	0.63	0.03		0.380	0.589	0.031	-	-
Liquid	54	0.480	0	0.52	U_5Pd_6 + *Liquid*	≈ 0.64	0	≈ 0.36	-	-
	55	0.47	0.10	0.43		0.45	0.12	0.43	-	-
	58	0.40	0	0.60		≈ 0.5	0	≈ 0.5	-	-
	59	0.47	0.10	0.43		0.47	0.10	0.43	-	-
	74	0.40	0.22	0.38		0.431	0.322	0.247	-	-

For the sake of clarity, data of different phases are distinguished by different colors. It is noted that the following important features can be observed in Figure 6-13:

1. As Kleykamp and Kang [37] found in their experiments, a closed region (miscibility gap) does exist within *fcc* region; however, the calculated miscibility gap is much smaller than the one shown in Figure 3-20.

2. Careful labelling of the diagram shows that Kleykamp and Kang [37] had mistaken the two different *fcc* phases (*fcc* and *fcc*#2) as three phases because they labelled: α1 (*fcc*#1), α2 (*fcc*#2) and α (*fcc*). The reason for this is that they were misled by the larger uranium solubility in palladium (about 15 at.% as in Pells [100] and Terekhov *et al.* [93] phase diagrams) they accepted when combining the phase diagram, and they attributed the *fcc* crystal phase (*i.e.*, the black diamonds in Figure 6-13) in equilibrium with URh_3 and UPd_3 compounds (URh_3+*fcc* and UPd_3+*fcc* two phase regions). This is obviously unreasonable because in their accepted U-Pd and U-Rh phase diagrams *fcc* phase is not in equilibrium with these compounds.
3. In Figure 3-20, Kleykamp and Kang used the nominal composition data (added in Figure 6-13 on the calculated curves for comparison) in mapping the phase boundaries, while only using parts of the "available" equilibrium data (measured data) for establishing some binary tielines. With other measured data, they were lost in how to use them to determine the phase boundaries except for binary ones. The seven *fcc* (α1+ α2) data points are not shown which one is the so-called α1 or α2 phases and where are their specific positions in the region. However, the reclassified equilibrium data by us (Figure 6-14) can serve the purpose. According to their experiment, the *fcc* region has three different phases (α (black circles in Figure 6-14), α1 and α2), which is a conceptual mistake and violate the phase law.

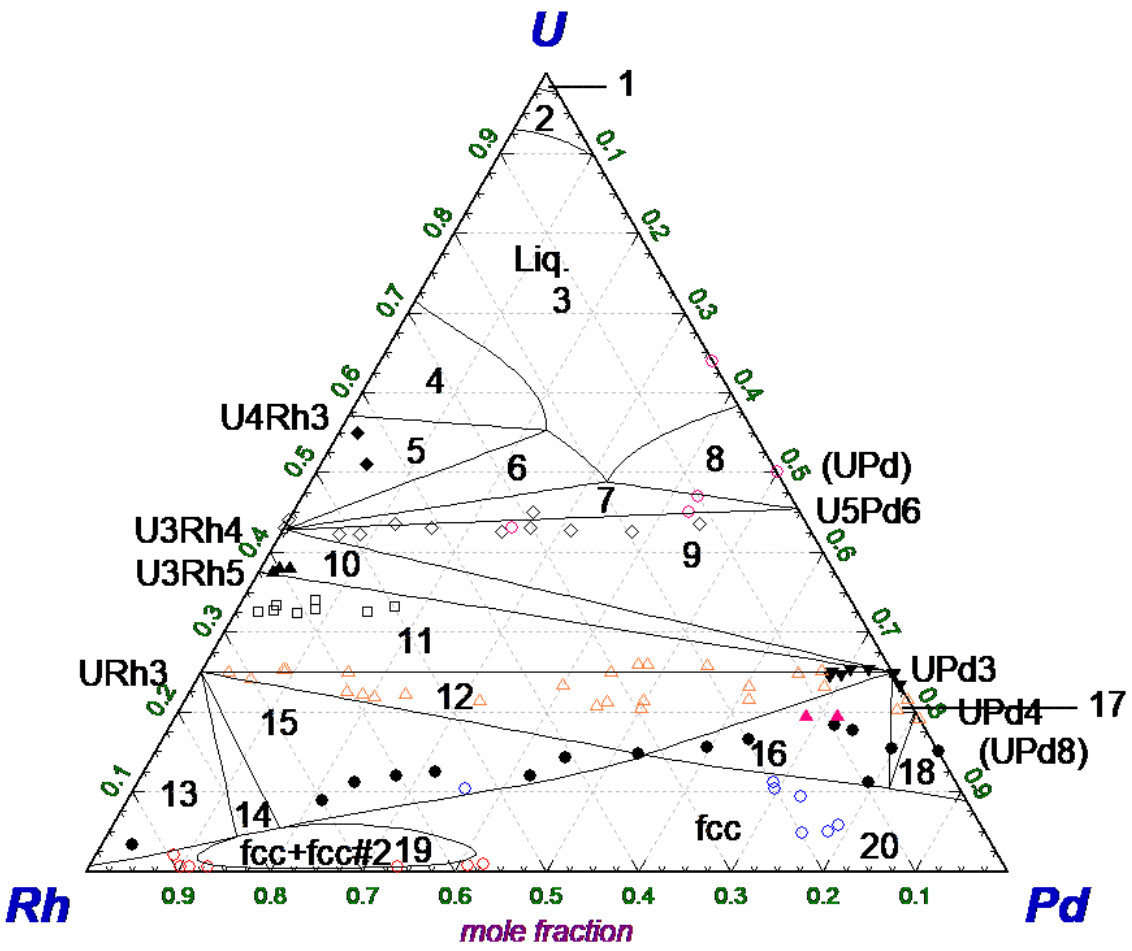

Figure 6-13. Calculated phase diagram with experimental data from Kleykamp and Kang [37] at 1050 °C and 1 atm.

Table 6-11 lists the calculated phases in equilibrium and the total phases detected by Kleykamp and Kang [37] in their hand-drawn phase diagram with accompanying symbols.

Table 6-11. Phase field classification and experimental symbols used in Figure 6-13.

No.	Phases	Experimental data from Kleykamp and Kang (K&K) [37]
1	*bcc*	None
2	*bcc* + *Liquid*	None
3	*Liquid*	○: Liquidus data
4	U_4Rh_3 + *Liquid*	None
5	U_4Rh_3 + U_3Rh_4 + *Liquid*	♦: U_4M_3 (M = Rh, Pd)
6	U_3Rh_4 + *Liquid*	None
7	U_3Rh_4 + U_5Pd_6 + *Liquid*	◊: U_3M_4; ○: Liquidus data
8	U_5Pd_6 + *Liquid*	○: Liquidus data (K&K failed to identify U_5Pd_6)
9	U_5Pd_6 + U_3Rh_4 + UPd_3	◊: U_3M_4; ○: Liquidus data
10	U_3Rh_4 + U_3Rh_5 + UPd_3	▲: U_3M_5;▼: UPd_3 (ε)
11	U_3Rh_5 + URh_3 + UPd_3	□: UM_2; Δ: URh_3 (γ)
12	URh_3 + UPd_3 + *fcc*	Δ: URh_3; ▼: UPd_3 (ε)
13	URh_3 + *fcc*	●: *fcc* (α)
14	URh_3 + *fcc* + *fcc*#2	None
15	URh_3 + *fcc*	●: *fcc* (α); ○: *fcc*
16	UPd_3 + *fcc*	▲: γ (+α) ; *fcc* (α)
17	UPd_3 + UPd_4 + *fcc*	Δ: URh_3; ●: *fcc* (α)
18	UPd_4 + *fcc*	●: *fcc* (α)
19	*fcc* + *fcc*#2	○: *fcc*#2
20	*fcc*	○: *fcc*#2; ○: *fcc*

4. Because of the missing of U_5Pd_6, the detected liquidus data are incorrect. In fact, Kleykamp and Kang [37] had acknowledged the difficulty in experimental determination of the phase boundaries in U-rich part of the isothermal section. In addition, except for Park *et al.* [99] and Catterall *et al.* [92], Kleykamp and Kang once again confronted the difficulty in phase boundary determinations, especially on the U-rich side. The same phenomena actually occurred in the determination of the eutectic points in U-Rh and U-Pd binary systems. The cause, for the former is misinterpretation of a liquidus datum point; and for the latter is the crucible contamination.
5. In the middle part of the phase diagram, Kleykamp and Kang [37] made the phase boundaries far more complex (Figure 3-20) than those predicted by the thermodynamic assessment (Figure 6-13). The possible reasons are: (1) XRD technique has been proven not effective in phase identification in the U-Pd subsystem, so the week signal of a less abundant species might have been

shielded by the strong signals of some more abundant species. As a result, some three-phase equilibria have been recognized as two-phase equilibria and too many two-phase regions were added on the isothermal section. Figure 6-14 shows a calculated phase diagram with tie-lines recognized by the experimentalists as two-phase regions. Obviously, most of the tie-lines are crossing over one phase region except for those of *fcc*+*fcc*#2 (these are actually located in *fcc* region as a miscibility gap). (2) Longer annealing time is needed for most of the samples.

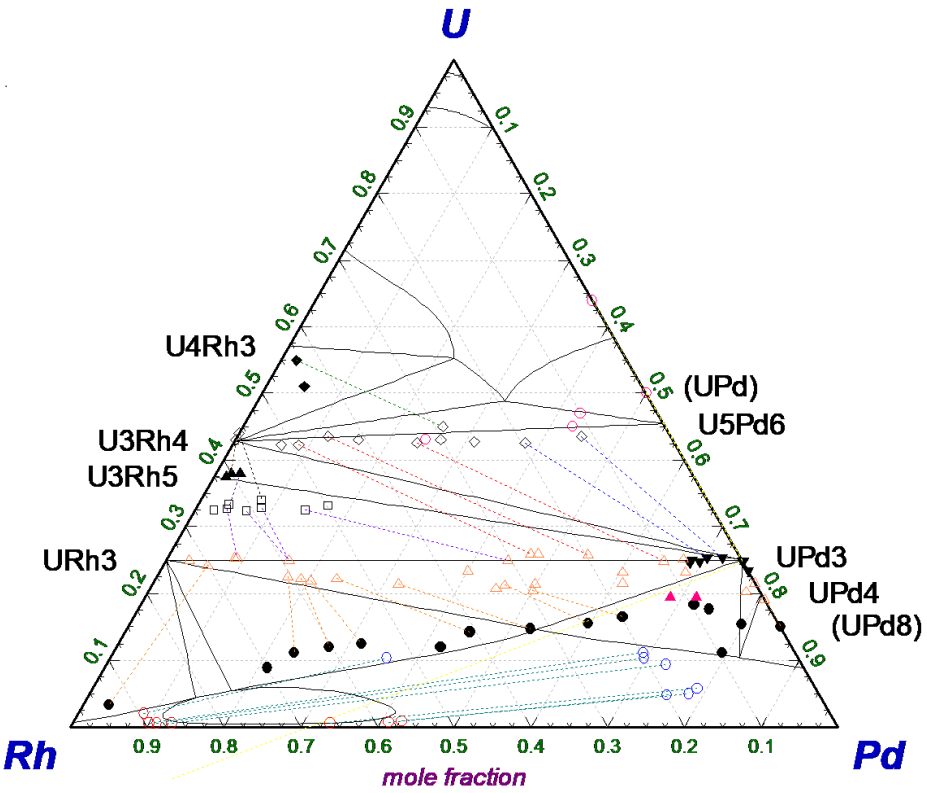

Figure 6-14. Calculated phase diagram with tie-lines drawn according to "equilibrium composition" data in [37] (1050 °C, 1 atm).

Taking the *fcc*/*fcc*#2 (α1/α2 as labelled by Kleykamp and Kang [37]) equilibrium as an example, the authors stated that the three week annealing time gave no significant X-ray diffraction pattern so they doubled the annealing time. But is this enough? The thermodynamic evaluation says "No". As the annealing time increases, the tie-lines will

get shorter and shorter and finally, the equilibrium compositions at both sides should all be located on the predicted miscibility gap boundary in accordance with the lever rule. That is, it is very slow for these samples to reach the equilibrium points. Therefore, the "closed region" should be much smaller than it is shown in Figure 3-20.

Table 6-12 shows a list of calculated phase numbers and detected phase numbers by Kleykamp and Kang [37]. The differences between the numbers represent some phase or phases were not detected experimentally due to their relatively weak signals.

Table 6-12. A comparison of calculated phase numbers and the maximum numbers of different phase regions on Kleykamp and Kang's* [37] U-Rh-Pd isothermal section.

No. of phase field	Calculated maximum phase No.	Name(s) of phases in the field (Calculated)	Maximum No. of phases in the field (K&K by nominal composition)
1	1	*bcc*	NA
2	2	*bcc* + *Liquid*	NA
3	1	*Liquid*	1
4	2	U_4Rh_3 + *Liquid*	2
5	3	U_4Rh_3 + U_3Rh_4 + *Liquid*	2
6	2	U_3Rh_4 + *Liquid*	NA
7	3	U_3Rh_4 + U_5Pd_6 + *Liquid*	3
8	2	U_5Pd_6 + *Liquid*	1
9	3	U_5Pd_6 + U_3Rh_4 + UPd_3	3
10	3	U_3Rh_4 + U_3Rh_5 + UPd_3	3
11	3	U_3Rh_5 + URh_3 + UPd_3	3
12	3	URh_3 + UPd_3 + *fcc*	2
13	2	URh_3 + *fcc*	2
14	3	URh_3 + *fcc* + *fcc*#2	NA
15	2	URh_3 + *fcc*	2
16	2	UPd_3 + *fcc*	2
17	3	UPd_3 + UPd_4 + *fcc*	NA
18	2	UPd_4 + *fcc*	1
19	2	*fcc* + *fcc*#2	2
20	1	*fcc*	1

* Simplified as K&K in the table.

6.5.4 Calculated UMe_3 binary phase diagrams

As described in Section 3.6.2, Kurosaki and Uno [38] tried to construct a ternary isothermal section of URu_3-URh_3-UPd_3 without any knowledge of the binary quasi phase diagrams involved in the system because these phase diagrams were missing. Experimental determinations of these refractory compounds are difficult if not impossible. Calculations of the UAl_3-USi_3 phase diagram for the *fcc* phase using *ab initio* methods were reported [122] in which phase variations exist only at very low temperatures (*i.e.*, below 362 K or 89 °C) (see Figure 6-15).

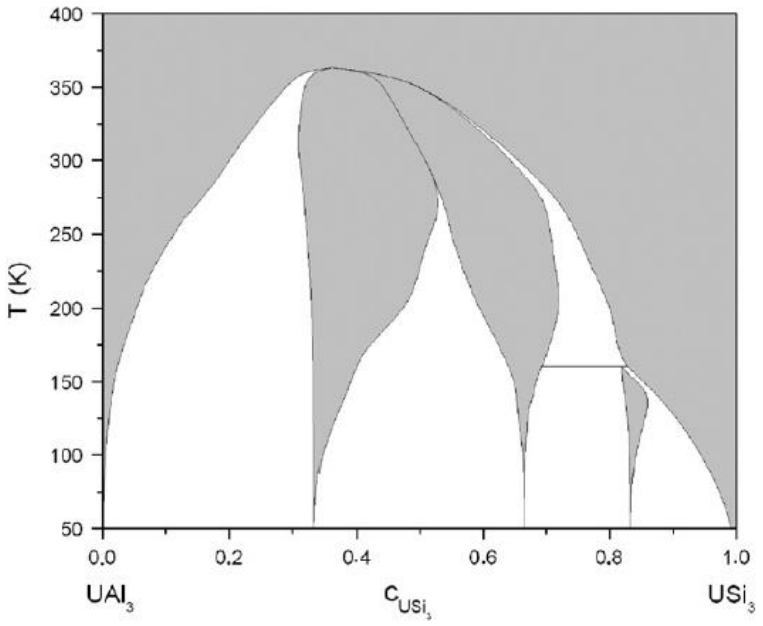

Figure 6-15. A calculated UAl_3-USi_3 phase diagram by ab initio method [122].

The most recent result of thermodynamic modelling is shown in Figure 6-16, which is much more informative and phase transformations at higher temperatures were predicted [123]. However, as these two compounds melt via a peritectic reaction, the feature of the calculated phase diagram is very different from congruent experimental phase diagrams.

For example, the liquidus is strange and the compounds have no distinctive solid/liquid melting points.

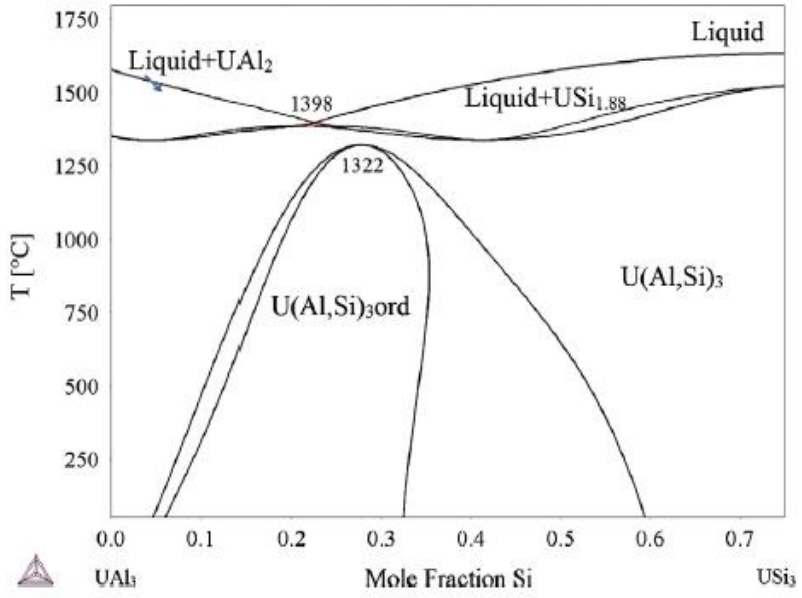

Figure 6-16. A recent calculated UAl_3-USi_3 phase diagram [123].

In this work, the binary quasi phase diagrams can be obtained directly from the well-established U-Pd-Rh-Ru quaternary system. Because all of the three UMe_3 compounds melt congruently, the binary phase diagrams show typical eutectic features.

6.6 Effects of the Two Phenomena Found in Thermodynamic Evaluation

In Chapter 5, the thermodynamic evaluation results were presented and analysed. However, for some specific phenomena and topics, extended discussions are needed. This is the purpose of this section.

6.6.1 Feature of the "closed region" of *fcc* immiscibility

A detailed discussion on the diffusive aspect of the "closed region" is given above, and now a detailed study on the temperature effect is necessary, *i.e.*, the behaviour of the *fcc* phase as temperature changes. Figure 6-17 illustrates the *fcc* boundary projections between 700-1250 °C.

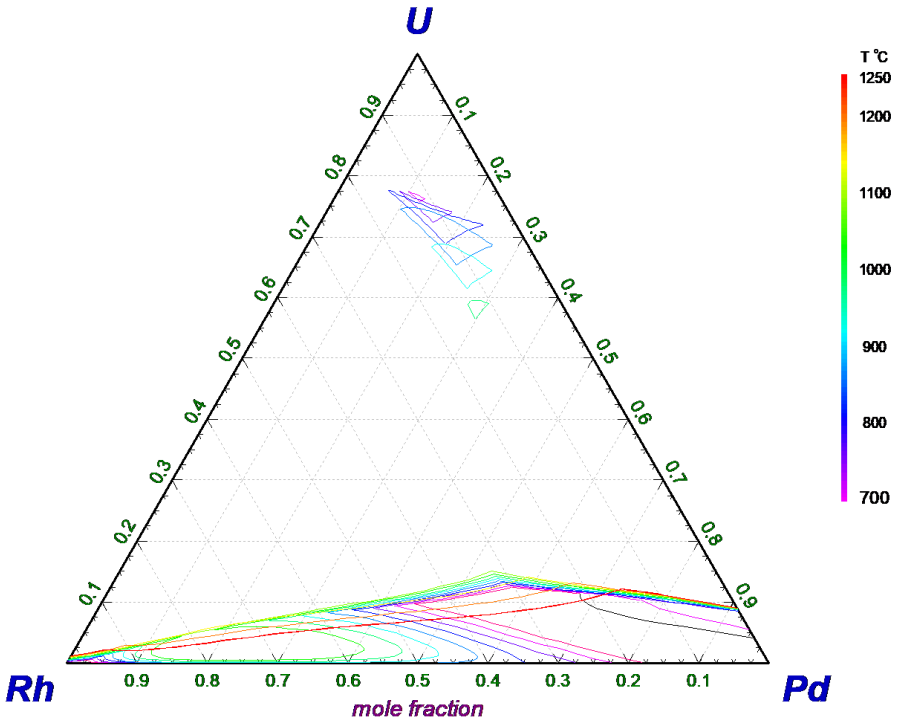

Figure 6-17. The *fcc* boundary projections between 700-1250 °C.

In the Rh-Pd binary system, the miscibility gap is shown to be lower than 845 °C (1118 K) in [37] or 910 °C (1183K) in [15]. As the uranium content increases, a separate "closed region" forms around 900 °C and contracts as temperature increases to about 1050 °C on the U-rich side. When the temperature increases a few more degrees above this value, the overall *fcc* region contracts toward low U content side, and for some unknown reasons, the software cannot show the contour of the diminishing "closed region." In fact, even at 1050 °C, the *fcc* + *fcc*#2 region is not "closed", but intersects with

the URh_3 + *fcc* + *fcc*#2 three phase region. This gives a false impression that the ternary critical temperature is very close to 1050 °C and the ternary miscibility gap is a "plateau." Nevertheless, thermodynamic calculations of different isopleths show that this is not true. For example, the isopleth at $X_U = 0.025$ provides a profile of the "closed region" shown in Figure 6-18 with a maximum temperature (1144 °C) across this plane.

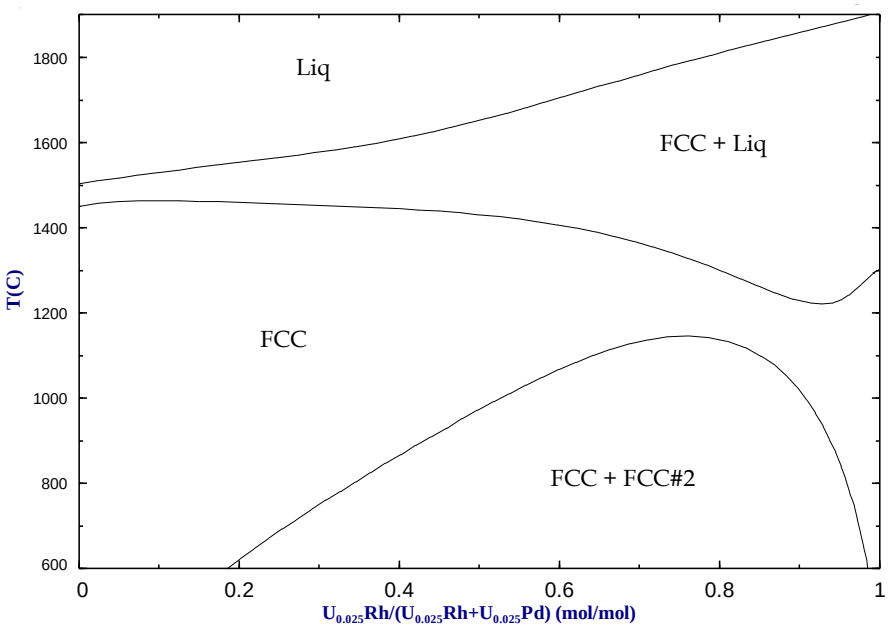

Figure 6-18. Calculated isopleths at Xu=0.025 with a maximum miscibility-gap temperature of 1144 °C (1 atm).

Figure 6-18 also shows the lowest solidus temperature at which the *Liquid* phase exists. Figure 6-19 provides another side view of the *fcc* + *fcc*#2 miscibility gap along the plane of URh_3-$Rh_{0.9}Pd_{0.1}$ with a maximum temperature of 1138 °C.

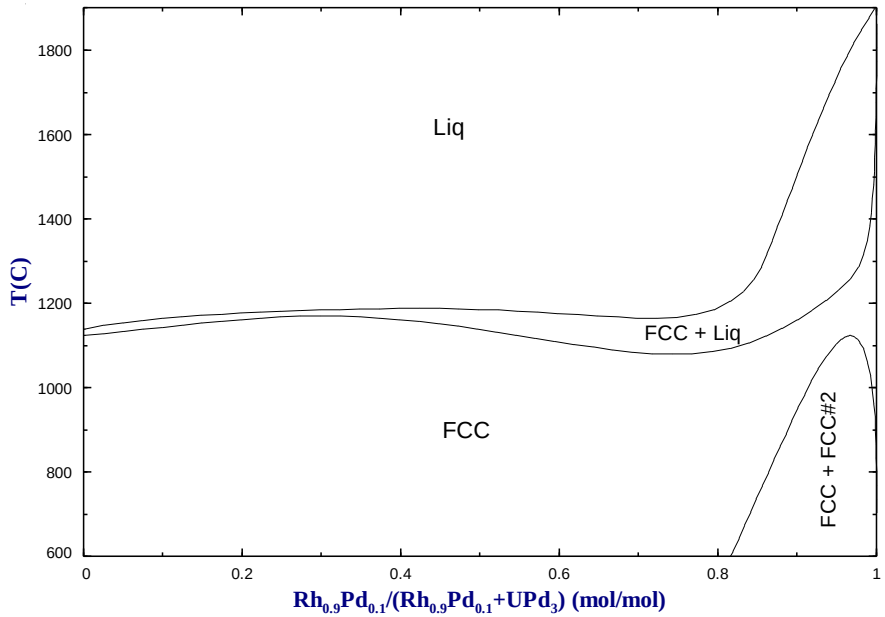

Figure 6-19. A side view of the *fcc*+*fcc*#2 miscibility gap (lower-right corner) at 1 atm.

Considering the fact that the starting points for establishing of this model are the binary sub-systems, and they are aimed to be as close to the experimental phase diagrams as possible, the extra *fcc* phase regions are kept on Figure 6-17 and the ternary interaction parameters are not changed. This means that the U solubility in Pd could be less than 11 at.% suggested by Park *et al.*[98], which is the smallest value among the experimental results. To check this, future experimental work should be conducted according the feedback information provided in this work (See Chapter 8).

6.6.2 The contamination reaction and its mechanism

6.6.2.1 Contamination in U-Me phase diagram determinations

The relevance of an experimental result depends on the method, the reliability and precision of the instruments, accurate data recording, and the system being free of contamination. Here, the last is not the least: in phase diagram determinations the existence of any foreign material affects the readouts of composition and temperature of the sample,

which usually form the two axes of a temperature-composition phase diagram. The catalytic efficiency of light platinum metals increases in the order of Ru→Rh→Pd. In the U-Ru phase diagram, there are no disputes on the U-rich side eutectic point[*], but there are disagreements on the Ru-rich side where the reaction type has been changed from a peritectic reaction to a eutectic one based on a later observation [4]. For U-Rh phase diagram, there is only one complete version of it [42] and an incomplete version [94]. The thermodynamic evaluation in this work shows that the U-rich side eutectic composition should be lower than that determined in [42] but in agreement with [94]. In both of these two systems, the experimentalists did not explicitly declare the contamination effect of the crucible material used in the experiments. In the U-Pd phase diagram determinations, nevertheless, both Park *et al*. [99] and Catterall *et al*. [92] declared explicitly the strong contamination effect by the crucible materials used. They were not aware of the same effect on the Me-rich side eutectic determinations. Thermodynamic evaluation (this work) found that for the U-Pd system, the attack on BeO (*i.e.*, the material of beryllia crucibles used in the experiments) increased both the eutectic composition and temperature in U-rich side eutectic determinations (see Section 6.2.3). The U-Be phase diagram illustrates that eutectic isotherm of γ-U with a very stable compound with a high melting point, UBe_{13}, forms at 1090 °C. In addition, Park *et al*. [99] detected an unknown isotherm below the "eutectic isotherm" (1008 °C) when re-examining U-Pd phase diagram, which implies that the false eutectic isotherm may have been an isotherm with contamination by a third

[*] The reason is so far there is only one set of experimental data in the U-rich part of the U-Ru phase diagram [42]. However, this work conforms to the result.

component (UBe_{13}). As a result, the measured eutectic isotherm is one in a ternary system, *i.e.*, U, UBe_{13}, and UPd.

Although dozens of types of catalytic reactions have been studied, no catalytic mechanism of metallic reactions, such as the one between U and BeO with existence of Pd, has been explored, neither experimentally nor theoretically. To explain the contamination effect and validate the thermodynamic evaluation, a mechanism is proposed in this work based on the physical and chemical properties of the elements involved, and the results of thermodynamic analysis.

6.6.2.2 A proposed mechanism of the contamination reactions

The intrinsic reason that accounts for the discrepancies within high Pd composition range is Be contamination. As temperature rises, more BeO molecules are available. This increases the contaminant in the samples and makes the phase identification extremely difficult, including the determination of the liquidus, the solubility of U in Pd, and the identification of the possible intermetallics.

The crucibles used in U-Pd phase diagram determinations by Park *et al*. [99] and Catterall *et al*. [92] were both made of BeO, although the latter tried ZrO_2 as well. Most crucibles are made of metal oxides because they have very high melting points.

The metal oxides with high-melting points are illusive for many people to think that they are absolutely stable under their melting temperatures. However, this is not true. CaO and MgO have higher melting points, but they do not appear in the list of recommended crucibles in Evaporation Guide for the Elements [124]. BeO and Al_2O_3 are most frequently recommended, but for many elements (in a sample or samples) the former is put in brackets

meaning that it has to be used with care. For Pd, both of the materials are recommended, but BeO is in brackets for this guide. For transition metal oxides, especially, their reactivity depends on the metal oxidation state and coordination environment. In most cases, the difference of electronegativity between the metal elements and oxygen makes the following statement true: metal oxides are virtually consisted of metallic cations and oxygen anions.

So far, studies on catalysis focus mainly on organic reactions, biochemical reactions or metal-organic reactions. Astruc [5] extensively summarizes these various interactions in a review, which includes dozens of reactions, such as hydrogenation reactions, C-C coupling reactions, dehydrogenation reactions, cycloaddition reactions, amination reactions, oxidation reactions, and many others. However, it is important to note that no metal-metal catalytic interactions are mentioned. An answer is needed for the studies on U-Me phase diagrams to see if there exist any catalytic functions or catalytic-like functions of the platinum metals.

6.6.2.3 Mechanism of contamination in U-Pd phase diagram determination

In the U-Ru and U-Rh binary phase diagram determinations, Park observed no crucible contamination. Mason and El-Genk [4], however, mentioned the influence of crucible materials at high temperature (Ru-rich side) measurements. The reason is that the catalytic efficiency increases from left to right for the light platinum metals in the periodic table, as well as for the heavy platinum metals. Pd and Pt, the last elements in light and heavy platinum metals, are both catalysts with extremely high efficiency. It is interesting that in U-Pd and U-Pt binary phase diagrams, similar U-rich side eutectic temperatures are observed (see Table 6-4). This implies that beryllium contamination (the crucibles used

for determination of U-Pt phase diagram were also beryllia (BeO) crucibles) happened in U-Pt phase diagram determination too.

Pd is extensively used as nanoparticle catalysts, therefore, its catalytic characteristics must be emphasized in this context. Recent research shows that even in used nuclear fuels Pd nanoparticles exist [125]. Therefore, it is possible that Pd helps in lowering activation energy of some other co-existing species during the U-Pd phase diagram determination.

6.6.2.3.1 Sample environment in thermal analysis (TA) or differential thermal analysis (DTA)

In binary phase diagram construction, thermal or differential thermal analysis is one of the best tools to map the temperature-composition relations of the various phases in a phase diagram. To avoid oxidation of the sample, a high vacuum or an inert gas pursing should be maintained. The process involves relatively high temperatures and contact with a third species—the crucible material. In the case of U-Pd phase diagram determination, ZrO_2 and BeO crucibles were used and Catterall *et al*. [92] found that the contamination effect was not acceptable. They tried to improve the result by changing the procedures, and they believed the amount of Be became very small. However, the chemical analysis method for Be analysis they used was not provided. If it was the similar to the method for Pd analysis, the precipitated UBe_{13} compound might not be detected. The same effect was also found by Park *et al*. [99], but both of them were not aware the influence of the contamination on the U-rich side eutectic determinations. Base on this analysis, the mechanism of the contamination reactions is focused on the following four elements: U, Pd, Be and O.

6.6.2.3.2 The electronic structure and orbital energies of U, Pd, Rh, Ru, Be and O

The occurrence of a chemical bonding is determined by mainly two factors:

1. Symmetry of the electronic structure of the reactants
2. Energy level of orbitals of the elements involved in a reaction

Each element has its characteristic symmetrical configurations of the electronic orbitals. For some elements, there exists a unique symmetry. For the transition elements, more symmetrical configurations are possible. An effective bonding occurs only when the two interactive atoms have similar orbital energies and the bonding of the two orbitals are allowed in respective of symmetry.

Physical Measurement Laboratory in NIST calculated the ground-state orbital energies of 92 elements by four standard approximations that use the exchange-correlation energy function of Vosko, Wilk, and Nusair [126,127]:

i. the local-density approximation (LDA);
ii. the local-spin-density approximation (LSDA);
iii. the relativistic local-density approximation (RLDA);
iv. the scalar-relativistic local-density approximation (ScRLDA).

Although the data are ground-state orbital energy values, they give useful information on possible bounding of the co-existing elements. Nevertheless, it is difficult to compare all the allowable symmetry of the co-existing elements. In spite of this, the smaller values of active orbital energy indicate that the orbitals are active at certain conditions. For example, the 5f orbitals of uranium have a relatively high (less negative)

energy and they are found to be responsible for the heavy-Fermi characteristics of UBe_{13} at low temperatures [128].

6.6.2.3.3 The contamination mechanism

With reference of U-Be phase diagram, we suggest that the experimental eutectic temperatures (998 °C by Catterall *et al*. [92]; 1008 °C by Park *et al*. [99]), which are much higher than the calculated value (888 °C, this work), are caused by the formation of UBe_{13} because of the interaction of U and Pd with the crucible material. The compound forms from very low Be concentrations with a eutectic temperature of 1090 °C in the U-Be system. The compound has a melting point of about 2000 °C and is stable over almost all the composition range of the binary system at 1100 °C. Therefore, the isotherm at 998 or 1008 °C should represent a ternary eutectic isotherm (a mixture of UBe_{13} and γ-U and UPd)as suggested in the experimental phase diagrams. One supportive evidence is that Park *et al*. [99] observed an **unknown** isotherm (~940 °C) much lower than the "eutectic temperature," but higher than the calculated one [98], which should be related with the true eutectic temperature, but was still elevated by the co-existing contaminant: a small amount of UBe_{13}. The crystal structure of this compound is shown in Figure 6-20.

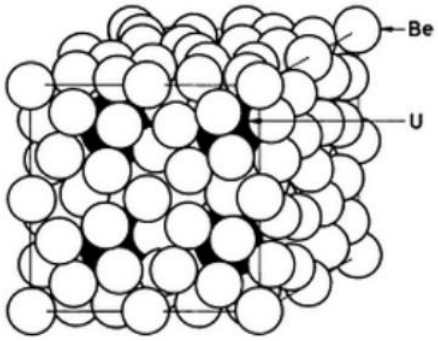

Figure 6-20. Crystal structure of UBe_{13} [128].

On the basis of a qualitative analysis of the energy gaps for various related chemical bonding, a mechanism of the contamination process is proposed:

As atoms, Pd exists in the samples for U-Pd phase diagram determination, while BeO is the material of the crucible used for the determination. Therefore, the first step of the contamination reactions is weakening of the Be-O bond by an approaching Pd atom:

$$BeO + Pd \rightarrow Be\text{-}O\text{-}Pd \quad (29)$$

At U-rich side, a large amount of free U atoms is available for the less bonded Be atoms and a competitive reaction occurs:

$$U + Be\text{-}O\text{-}Pd \rightarrow U\text{-}Be + Pd\text{-}O \quad (30)$$

U-Be is unsaturated and it picks up more ligands to form UBe_{13}, which is determined by the symmetry of U and Be atoms and their sizes. The energy gap between Pd 4d orbitals and U 6d and 7s orbitals are smaller than Be 2p orbitals; however, at U-rich side Pd concentration is relatively smaller and the atomic size of Pd (atomic radius: 138 pm) is much larger than that of Be (atomic radius: 111 pm) [129]. As a result, U-Be bonding is favorable in respective of space. At the same time, for other U atoms that are close to Pd atoms, UPd forms because of the smallest energy gap between the 4d orbitals of Pd and 6d and 7s orbitals of U:

$$U + Pd \rightarrow UPd \quad (31)$$

PdO is the only well-established oxide of Pd with a melting point of 750 °C [130]. Therefore, it is not stable above this temperature. During the cooling process, Pd-O is not stable and decomposes above 750 °C:

$$2Pd\text{-}O \rightarrow 2Pd + O_2 \quad (32)$$

The overall contamination reaction is represented by

$$15U + 26BeO \xrightarrow{Pd} 2UBe_{13} + 13UO_2 \quad (33)$$

As temperature rises, both reactivity and the catalytic activity of Pd increase. As a result, in the samples, part of Pd atoms serves as catalysts and the extra part of Pd atoms react with U at certain composition ranges.

In conclusion, some of the Pd atoms (corresponding to the amount of decomposed BeO) serve as catalyst for the formation of UBe_{13} at temperatures above 750 °C; other Pd atoms react with U. The participation of BeO in the thermal analysis process makes the experimental phase diagram not a really binary phase diagram, but Be contaminated ternary system. Consequently, deviations of the phase boundaries in different parts of the diagrams and discrepancies from different groups of scientists occurred. Under such complicated circumstances, thermodynamic evaluation becomes valuable because the contamination is almost inevitable in experimental measurements of this system.

7 Potential Improvement to a Nuclear Fuel Database or an Industry Code

As introduced at the beginning of the thesis (Chapter 1), some nuclear fuel oriented thermodynamic databases are under development, typically the Fuelbase [7,8] and the RNFTT (Royal Military College of Canada Nuclear Fuel Thermochemical Treatment) [9,11,33]. The former aims at nuclear fuel designs with multicomponent systems and the latter focuses on the study of the fission product behaviour. The establishment of the U-Pd-Rh-Ru quaternary system is a natural expansion of the RNFTT project. Therefore, enrichment of this work to the project will be discussed and then the potential improvement to industry codes such as BISON will be tentatively evaluated in this chapter.

7.1 The RNFTT treatment previous to this work

The RNFTT treatment operates with two computer codes: FactSage [131] and ORIGEN-2* [132]. The former is mainly for equilibrium calculations, although some modules for kinetic phase transformation analysis have been developed in recent years, *e.g.*, the capability in studying non-equilibrium solidification processes. To simulate kinetic nuclear fission processes, ORIGEN-2 was used to calculate chemical inventories in a simulated reactor. The thermodynamic data of the typical elements, compounds, and solutions were collected for the FactSage compound and solution databases. The calculated data are to be used in the simulation of kinetic fission processes in different conditions in a nuclear reactor. By this means, the RMCC team calculated the CANDU

* The CANDU version is called SCALES-5.

fuel inventory at a typical burnup* [10] which confirmed the presence of noble metal fission products (See Section 1.1).

The RNFTT thermodynamic fuel model dealt with many types of fission products generated in CANDU reactor during operation, *e.g.*, the non-stoichiometry phenomenon in the UO_2 phase solute oxides, noble metal inclusions, the other metallic inclusion (U(Ru-Rh-Pd)$_3$), zirconate and uranate solutions as well as some other minor solid phases and volatile gaseous species. By establishing the U-Pd-Rh-Ru quaternary system at equilibrium, this discussion on the RNFTT fuel model is focused on the enrichment of this work to the model.

In the RNFTT database prior to this work, elemental thermodynamic data for U, Ru, Rh, and Pd elements were included, but the binary U-Pd, U-Rh, and U-Ru systems were not thermodynamically optimized. Therefore, the intermetallic compounds in the compound database of these three systems were very limited and no ternary interaction parameters were established. In fact, among the fourteen compounds involved in the three subsystems only three UMe_3 compounds were included in the database. In addition, no equilibrium relationships in these three systems were described in the original RNFTT model. As discussed in Section 3.3, the measured enthalpy values for URh_3 and UPd_3 from different authors varies extraordinarily and it is found that the enthalpy of formation values used in the original RNFTT treatment were the one from Wijbenga [72], which are extremely negative. All the data for the other 11 compounds involved in U-Me phase diagrams were missing. As a result, the original RNFTT fuel model could not calculate

* Bin#10, power 980.3 kW(f)·bundle^{-1}, irradiated for 143 days, burnup 140 MWdays, and neutron flux = 2.16×10^{14} n·cm^{-2}·s^{-1}.

the inventories below the highest melting point of the UMe_3 compounds because of the missing of the optimized Gibbs energy expressions of the related phases.

7.2 Enrichment of this work to the RNFTT treatment

In principle, a binary phase diagram can be calculated if all the thermodynamic properties in Gibbs energy expressions of various phases are known. This would have been a benchmark in determining the liquidus interaction parameters; however, the experimental values of each of the properties vary in such a broad range that it is unclear which value should be selected. Due to extraordinary difficulties in measuring thermodynamic properties for the actinide-platinum metal systems at very high temperatures and relatively low temperatures (*e.g.*, for phase transitions of solid phases below melting temperature), the available thermodynamic properties are rare, especially those of complex intermetallic compounds. Therefore, it is attractive to use the experimental enthalpies of formation and entropies of UMe_3 compounds as benchmarks in determining interaction parameters for the *Liquid* phase in U-Me systems, which may define the position of the liquidus in a binary phase diagram; then, with known thermodynamic properties of the UMe_3 compounds and the known position of the liquidus, thermodynamic properties of other compounds in the system can be easily assessed by a computational thermodynamic method. In practice, however, care must be taken in determining which set of experimental data should be chosen as the benchmarks. The extremely negative values of enthalpy of formation obtained by Wijbenga [72,91] impose obstacle to a successful modelling. As mentioned before, Huang *et al*. [77] used the value of enthalpy of formation for UPd_3 in their simulation of fission products in uranium-zirconium hydride fuel and proposed a Gibbs energy function of UPd_3. It was found in this work that the function implicitly implies an

entropy of 66.1 $J \cdot mol^{-1} \cdot K^{-1}$ for UPd_3, which is less than half of the accepted value of 176.3 $J \cdot mol^{-1} \cdot K^{-1}$. In optimizing the interaction parameters of the solution phases of U-Rh and U-Pd systems, the extremely negative values from Wijbenga were found unreasonable because they suggested very low minimum liquid-solid transition temperatures.

Accordingly, the values of enthalpy of formation of UMe_3 compounds are re-assessed in this work (See Table 7-1).

Table 7-1. A comparison of standard enthalpy of formation values from different authors with newly assessed values in this work.

Authors	ΔH°_{298} $(kJ \cdot mol^{-1})$		
	UPd_3	**URh_3**	**URu_3**
Jung and Kleppa [74]	-294.7	-278.8	-124.0
Wijbenga [72]	-524.0	-301.2	-153.2
Lorenzelli and Marcon [71]	-260.0		
de Boer *et al.* [73]	-244.0	-192.0	-152.0
Holleck and Kleykamp [75]		-256.7	-224.9
Edwards *et al.* [76]			-195.0
Wang and Kaye (this work)	-210.5	-194.0	-144.7

Figure 7-1 compares the values predicted in this work with previous experimental results, which shows that the newly calculated values are in good agreement with those by de Boer *et al.* [73]. These experimental and thermodynamically calculated results emphasise the difficulties of experimental determinations of thermodynamic properties of U-Me (including UMe_3) compounds and their phase boundaries.

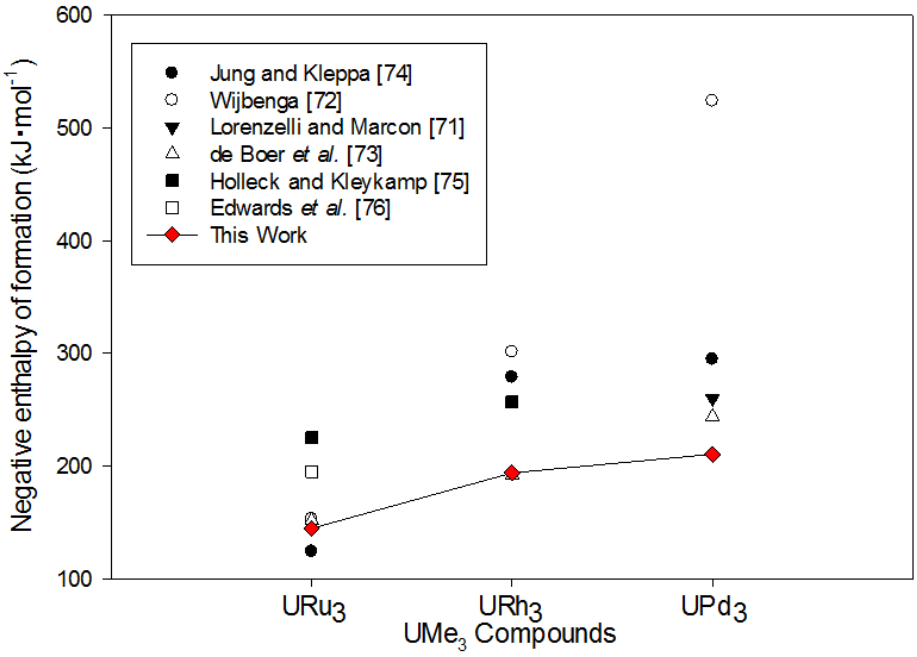

Figure 7-1. A comparison of this work with those summarised by Jung and Kleppa [74].

Gibbs energy functions of UMe_3 compounds before and after reassessments are listed in Table 7-2.

Table 7-2. Gibbs energy functions of UMe_3 compounds.

Compound		Gibbs energy function (G(T)) (J·mol^{-1})	ΔH^0_{298K} (kJ·mol^{-1})	S^0_{298K} (J·mol^{-1}·K^{-1})
Before	URu_3	-185783+541.6T-101.2TlnT-9.2x10^{-3}T^2+235907T^{-1}	-153.2	144.5
	URh_3	-335946+556.1T-104.4TlnT-9.1x10^{-3}T^2+305017T^{-1}	-302.0	152.24
	UPd_3	-553930+488.0T-98.7TlnT-5.7x10^{-3}T^2	-524.0	176.35
After	URu_3	-177240+540.8T-101.2TlnT-9.2x10^{-3}T^2+235907T^{-1}	-144.7	145.3
	URh_3	-228000+555T-104.4TlnT-9.1x10^{-3}T^2+305017T^{-1}	-194.0	153.4
	UPd_3	-240430+488.0T-98.7TlnT-5.7x10^{-3}T^2	-210.5	176.35

It can be seen that only minor changes were made for entropy values but major changes for enthalpy of formation values, especially those for URh_3 and UPd_3. Considering the discrepancies in experimental phase diagram construction of the U-Rh and

U-Pd systems, the deviations in enthalpy measurements may also be caused by the contamination of containers or other related materials.

Table 7-3 summarizes thermodynamic properties of compounds in U-Me systems calculated in this work.

Table 7-3. A summary of thermodynamic properties of U_xMe_y compounds.

System	Compound	ΔH^0_{298K} (kJ·mol^{-1})	S^0_{298K} (J·mol^{-1}·K^{-1})
U-Ru	URu-L	-597.66	25.16
	URu-H	-597.70	25.16
	URu_3	-144.7	145.3
	U_3Ru_4	-375.88	196.3
	U_3Ru_5	-389.22	241.9
	U_2Ru	-123.77	103.4
U-Rh	URh_3	-194.00	153.4
	U_3Rh_4	-461.18	196.1
	U_3Rh_5	-508.54	226.6
	U_4Rh_3-L	-442.74	190.75
	U_4Rh_3-H	-442.74	190.69
U-Pd	UPd	-165.50	39.45
	UPd_3	-210.50	176.35
	UPd_4	-236.20	192.5
	UPd_8	-407.70	200.0
	U_5Pd_6	-1110.0	85.0

In addition, heat capacities, enthalpies and entropies of many U_xMe_y compounds were unknown before this research. By establishing the U-Pd-Rh-Ru quaternary system, these thermodynamic properties were calculated and illustrated in Figure 7-2 to Figure 7-4. The temperature range is specified as the melting points of the UMe_3 compounds; as a

result, the heat capacities of other compounds (with melting points below UMe_3) become constant above their melting points. The U-Ru is depicted first in Figure 7-2. The experimental data on the three figures are from [86,87].

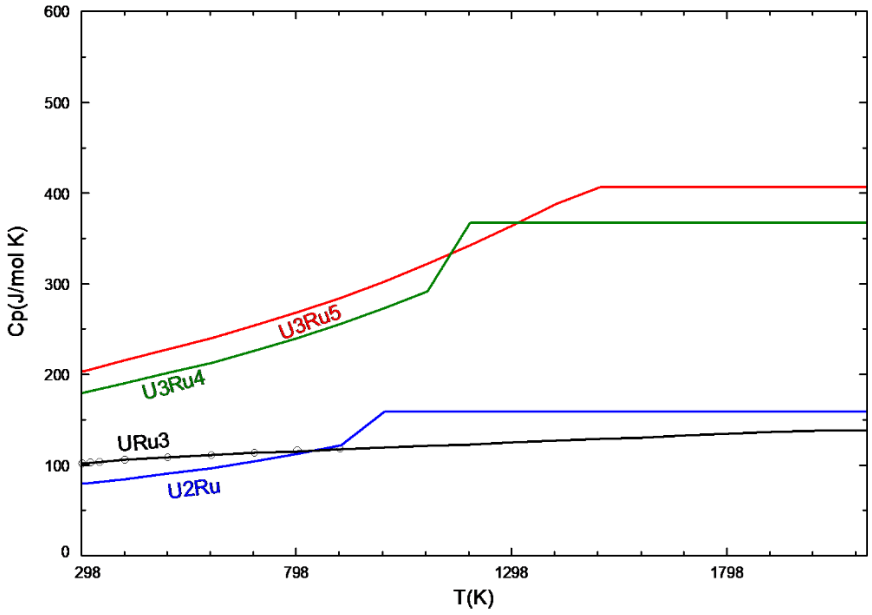

Figure 7-2. Calculated and experimental C_p curves for compounds in U-Ru system.

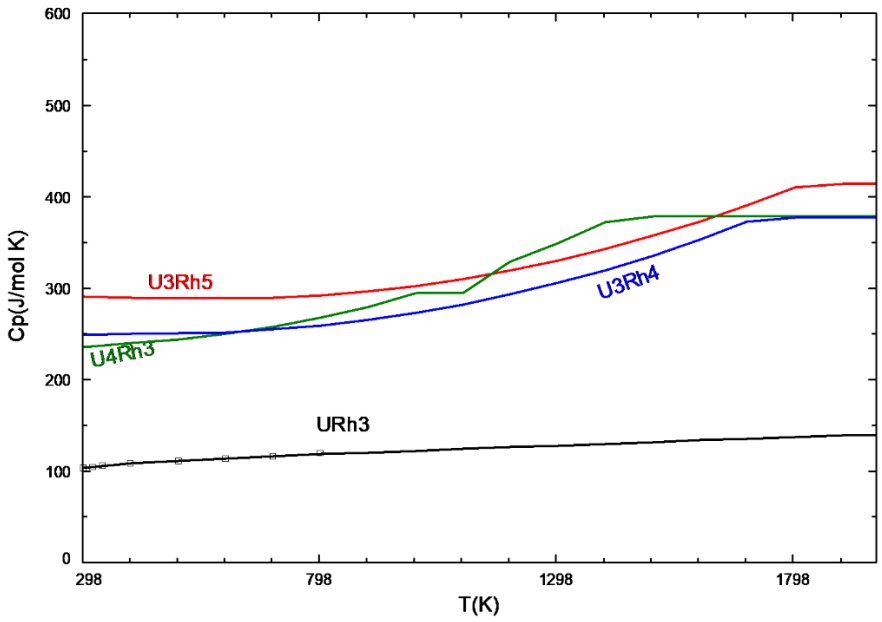

Figure 7-3. Calculated and experimental C_p curves for compounds in U-Rh system.

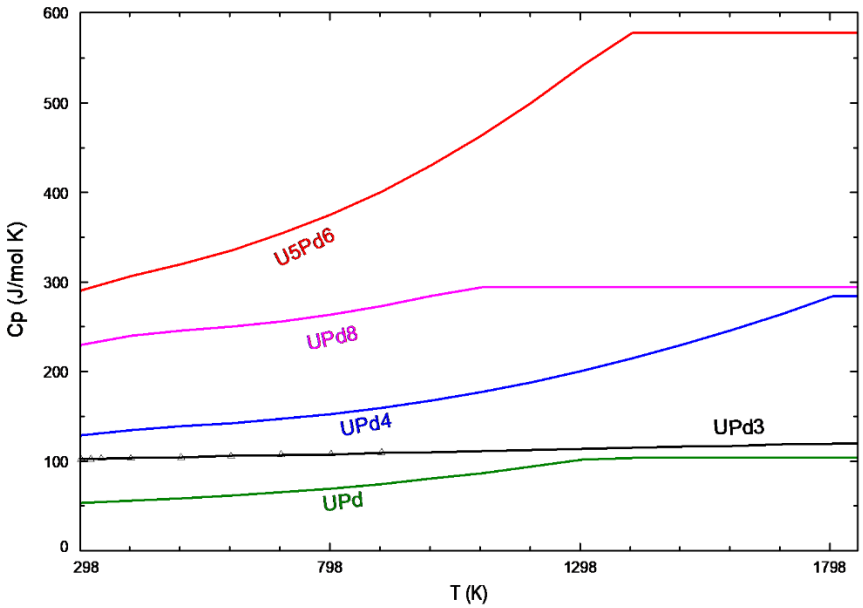

Figure 7-4. Calculated and experimental C_p curves for compounds in U-Pd system.

7.3 Efforts in improvement of industry codes

The BISON code is one of the newest industry codes for this purpose. As summarized in Chapter 1, the code is based on a series of coupled non-linear partial differential equations and no thermochemical databases are coupled in the code. In fact, thermodynamic databases such as Fuelbase [7,8] and RNFTT [9-11] are themselves under development so there is no sophisticated and complete databases to be coupled with BISON. The trend of development of nuclear industry codes during the past decade show that, in order to account for the deformation of the fuel and the cladding caused by the formation of the solid fission products, a perfect code can only be achieved after establishing a complete thermochemical database with all related species and phases. The establishment of the U-Pd-Rh-Ru quaternary system and its incorporation into the RNFTT are part of indispensable efforts in improving the developing nuclear fuel industry codes.

Conclusions

Starting from a thermodynamic reassessment of U-Ru system based on Berche *et al*. [17] work, U-Rh and U-Pd binary systems were evaluated thermodynamically for the first time. In this process, difficult choices had to be made due to the disagreements upon some important experimental data from different groups of scientists, and therefore, a new strategy in optimizing this type of systems was established. The new strategy was shown to be effective in resolving the experimental discrepancies caused by contamination from sample containers. The assessed self-consistent U-Pd-Rh-Ru quaternary thermodynamic model successfully predicted the *fcc* miscibility gap found in experimental U-Rh-Pd ternary isothermal section by Kleykamp and Kang [37] and some misinterpretations of their data were identified and analysed. The three dimensional profiles of the miscibility gap found only at the 1050 °C isothermal section were calculated and the critical temperature of the ternary miscibility gap was calculated to be 1144 °C.

Binary quasi-phase diagrams of URu_3, URh_3, and UPd_3 were calculated, the ternary eutectic temperature and composition were calculated, and an equilibrium ternary isothermal section of URu_3-URh_3-UPd_3 at 1673K (1400 °C) were predicted, which proved the existence of the liquid phase that failed to be detected in the experiment [38].

The interaction parameters and thermodynamic properties established here were incorporated into the established RMCC nuclear fuel treatment (RNFTT) for more accurate calculation of the inventory of nuclear fission products at different burnups. A more sophisticated RNFTT database improved by this research has the potential to be coupled in a standard industry code such as BISON for further perfection. Parts of these results

were presented at the annual Canadian Nuclear Society Conferences of 2015 (Saint John) [59], 2016 (Toronto) [24,25], and 2017 [133].

8 Future Work

As summarized in Chapter 0, by means of thermodynamic evaluation some experimental fallacies or misinterpretations were found in this work. It is meaningful that the results will be adopted as clues for future experimental explorations regarding the U-Pd-Rh-Ru ternary system. The research will need expensive equipment and will be extremely time consuming, but it might be a suitable project for an institution like a national nuclear laboratory.

Future experimental work can be carried out in the following three aspects:

8.1 The U-Rich Side Eutectic Composition of U-Rh System

The eutectic composition in the phase diagram of Park [42,95] is 24.5 at.% Rh (See Sections 3.3.4.2 and 5.3), but the result of thermodynamic evaluation is 17.5 at.% Rh. It is predicted in this work that the experimental datum (20.5 at.% Rh, 897 °C) of the liquidus was misinterpreted by Park [42,95]: he attributed it to the liquidus on the left side of the eutectic point resulting in a concave liquidus and a higher eutectic composition (24.5 at.% Rh). Thermodynamic validation shows that this datum (20.5 at.% Rh, 897 °C) should be attributed on the right side of the eutectic composition.

This can be verified experimentally by repeating the heating and cooling process at composition of 20.5 at.% Rh, or 79.5 at.% U – after the mixing and heating to a temperature higher than 897 °C, and determining the cooling profile at a controlled cooling speed by DTA. Then phase identifications should be conducted, *e.g.*, by means of XRD and/or EPMA. The samples annealed at 897 °C should be analyzed after being quenched to room

temperature. If the results show the solid phase in equilibrium with the liquid phase at 897 °C is U_4Rh_3, instead of γ-U, the eutectic composition should be close to 17.5 at.% Rh.

8.2 U-Rich Side Eutectic Temperature and composition of U-Pd System

Pd, Rh, and Ru can all be used as catalysts in various chemical processes and the phenomenon has also been found in the thermodynamic evaluation of the U-Pd-Rh-Ru quaternary system, especially the catalytic character of Pd in case of using beryllia crucible as a container of mixed U-Pd samples. In U-Ru and U-Rh system, the catalytic effect is not obvious at temperatures lower than 1000 °C at the U-rich side of the phase diagrams, but at high temperatures and the Ru- or Rh-rich sides the latent effect cannot be excluded. In U-Pd system, however, the Pd catalytic effect is proven to be severe by a thermodynamic evaluation at the U-rich side.

As shown in Table 6-2, the differences between experimental and thermodynamically evaluated composition and temperature values are obvious. From the perspective of thermodynamic analysis, some foreign factors must have affected the experimental results. The catalytic effect at about 45-70 at.% Pd composition range was noticed by some of the experimentalists, but not at the U-rich side. It is predicted in this work that a contamination reaction occurred during the experiments.

The challenge in verifying the contamination at U-rich side is the difficulty in choosing the right crucible. Perhaps, there may be no ideal crucibles to completely eliminate the catalytic effect in U-Pd or U-Pt phase diagram determinations (because in the

U-Pt experimental phase diagram [98] a similar pseudo eutectic isotherm was determined). However, by using crucibles other than beryllia the contamination effect may be reduced.

8.3 The Miscibility Gap in U-Rh-Pd Ternary Isothermal Section at 1050 °C

In Sections 6.5.2, 6.5.3, and 6.6.1, detailed analyses are provided on the miscibility gap or the so-called the "closed region" in the U-Rh-Pd phase diagram. The thermodynamic evaluation predicts that in the experimental construction of the ternary isothermal section at 1050 °C, the annealing time was not long enough, although Kleykamp and Kang [37] had extended it from three weeks to six weeks.

The experiment can be repeated at different annealing time scales and observe the changes of the size of the miscibility gap. It is predicted in this work that the size of the gap will be reduced to somewhere close to the calculated size.

9 References

1. D. Olander, "Nuclear fuels - Present and future", *Journal of Nuclear Materials,* **389** (2009), 1-22.
2. ASTM E230-03, "Standard Specification and Temperature-Electromotive Force (emf) Tables for Standardized Thermocouples", (2003).
3. ISA–MC96.1–1982, "Temperature Measurement Thermocouples", (12 August 1982).
4. R.E. Mason, M.S. El-Genk, "Experimental inverstigation of the ruthenium-uranium and rhenium-uranium systems", *Journal of Nuclear Materials*, **217** (1994), 304-321.
5. D. Astruc, "Transition-metal Nanoparticles in Catalysis: From Historical Background to the State-of-the Art", in Nanoparticles and Catalysis, Weinheim, WILEY-VCH Verlag GmbH & Co. KGaA Weinheim, (2008), 1-48.
6. A.T. Dinsdale, "SGTE data for pure elements", *CALPHAD*, **15** [4] (1991), 317-425.
7. C. Guéneau, C. Chatillon, and B. Sundman, "Thermodynamic modelling of the plutonium-oxygen system", *Journal of Nuclear Materials*, **378** (2008), 257-272.
8. A. Berche, C. Rado, O. Rapaud, C. Guéneau, and J. Rogez, "Thermodynamic study of the U-Si system", *Journal of Nuclear Materials*, **389** (2009), 101-107.
9. W.T. Thompson, B.J. Lewis, E.C. Corcoran, M.H. Kaye, S.J. White, F. Akbari, Z. He, R. Verrall, J.D. Higgs, D.M. Thompson, T.M. Besmann, and S.C. Vogel, "Thermodynamic treatment of uranium dioxide based nuclear fuel", *International Journal of Materials Research,* **98** (2007), 1004-1011.
10. E.C. Corcoran, M.H. Kaye, F. Akbari, J.D. Higgs, R.A. Verral, Z. He, J.F. Mouris, B.J. Lewis, and W.T. Thompson, "First Principles CANDU Fuel Model and Validation Experimentation", in *Proceedings of the 2007 International LWR Fuel Performance Meeting,* San Francisco CA, (2007).
11. E.C. Corcoran, M.H. Kaye and M.H.A. Piro, "An overview of thermochemical modelling of CANDU fuel and applications to the nuclear industry", *CALPHAD*, **55** (2016), 52-62.
12. IAEA, "Fuel Modelling at Extended Burnup (FUMEX-II)", IAEA-TECDOC-1687, Vienna, (2012).
13. R.L. Williamson, K.A. Gamble, D.M. Perez, S.R. Novascone, G. Pastore, R.J. Gardner, J.D. Hales, W. Liu, and A. Mai, "Validating the BISON fuel performance code to integral LWR experiments", *Nuclear Engineering and Design*, **301**, (2016), 232-244.
14. F. Cousin, K. Dieschbourg, and F. Jacq, "New capabilities of simulating fission product transport in circuits with ASTEC/SOPHAEROS v.1.3", *Nuclear Engineering and Design*, **238** (2008), 2430-2438.

15. M.H. Kaye, A Thermodynamic Model for Noble Metal Alloy Inclusions in Nuclear Fuel Rods and Application to the Study of Loss-of-Coolant Accidents, PhD Dissertation, Queen's University, Kingston, ON (2001).

16. M.H. Kaye, B.J. Lewis, and W.T. Thompson, "Thermodynamic treatment of noble metal fission products in nuclear fuel", *Journal of Nuclear Materials*, **366** (2007), 8-27.

17. A. Berche, N. Dupin, C. Guéneau, C. Rado, B. Sundman, and J.C. Dumas, "Calphad Thermodynamic Description of Some Binary Systems Involving U", *Journal of Nuclear Materials*, **411** (2011), 131-143.

18. S. Bajaj, A. Landa, P.Söderlind, P.E.A. Turchi, and R. Arróyave, "The U-Ti System: Strengths and Weaknesses of the CALPHAD Method", *Journal of Nuclear Materials*, **419** (2011), 177-185.

19 M. Kurata, "Thermodynamic assessment of the Pu-U, Pu-Zr, and Pu-U-Zr systems", *Calphad*, **23** [3-4], (1999). 305-337.

20. M. Kurata, "Thermodynamic database on U-Pu-Zr-Np-Am-Fe alloy system I — re-evaluation of U-Pu-Zr alloy system", *IOP Conference Series: Materials Science and Engineering*, **9** (2010), 1-8.

21. A. Perron, P.E.A. Turchi, A. Landa, P. Söderlind, B. Ravat, B. Oudot, F. Delaunay, and M. Kurata, "Thermodynamic re-assessment of the Pu-U system and its application to the ternary Pu-U-Ga system", *Journal of Nuclear Materials*, **454** (2014), 81-95.

22. A. Berche, T. Alpettaz, S. Chatain, C. Blanc, S. Gossé, and C. Guéneau, "Thermodynamic Study of the Uranium–Vanadium System", *Journal of Chemical Thermodynamics*, **43** (2011), 458-466.

23. S. Gossé, N. Dupin, C. Guéneau, J.-C. Crivello, and J.-M. Joubert, "Thermodynamic assessment of the Pd-Rh-Ru system using CALPHAD and first-principles methods", *Journal of Nuclear Materials*, **474** (2016), 163-173.

24. M.H. Kaye and L. Wang, "U-Ru-Rh-Pd quaternary system: Thermodynamic calculations and experimental explorations", in *Proceedings of the 36th Annual Conference of the Canadian Nuclear Society*, Toronto, 2016.

25. M.H. Kaye and L. Wang, "An alternative strategy for thermodynamic evaluations of experimental U-Me phase diagrams to resolve considerable experimental discrepancies", in *Proceedings of the 36th Annual Conference of the Canadian Nuclear Society*, Toronto, 2016.

26. L. Wang and M.H. Kaye, "The Other Metallic Phase in Spent Nuclear Fuel - A Complete Thermodynamic Evaluation of the U-Pd-Rh-Ru System", *Proceedings of the 13th International Conference on CANDU Fuel*, Kingston, ON, (2016).

27. S.G. Prussin, D.R. Olander, W.K. Lau, and L. Hansson, "Release of Fission Products (Xe, I, Te, Cs, Mo, and Tc) from Polycrystalline UO_2", *Journal of Nuclear Materials*, **154** (1988), 25-37.

28. H. Kleykamp, "The chemical state of the fission products in oxide fuels", *Journal of Nuclear Materials*, **131** (1985), 221-246.

29. H. Kleykamp, "The Chemical State of the Fission Products in Oxide Fuels within the Different Stages of the Nuclear Fuel Cycle", High Tech Ceramics, edited by: P. Vincenzini, Elsevier Science Publishers, Amsterdam, (1987), 2769-2783.

30. H. Kleykamp, "The chemical state of fission products in oxide fuels at different stages of the nuclear fuel cycle", *Nuclear Technology*, **80** (1988), 412-422.

31. P.G. Lucuta, R.A. Verrall, Hj. Matzke, and B.J. Palmer, "Microstructural Features of SIMFUEL- Simulated High-Burn-up UO_2-based Nuclear Fuel", *Journal of Nuclear Materials*, **178** (1991), 48-60.

32 D. Olander, "Chapter 12-Behaviour of solid fission products in oxide fuel elements", in Fundamental Aspects of Nuclear Reactor Fuel Elements, Springfield, National Technical Information Service US Department of Commerce, (1976), 172-198.

33. B.J. Lewis, B.J. Corse, W.T. Thompson, M.H. Kaye, F.C. Iglesias, P. Elder, R. Dickson, and Z. Liu, "Low volatile fission-product release and fuel volatilization during severe reactor accident conditions", *Journal of Nuclear Materials*, **252** (1998), 235-256.

34. B.J. Lewis, W.T. Thompson, F. Akbari, D.M. Thompson, C. Thurgood, and J. Higgs, "Thermodynamic and kinetic modelling of fuel oxidation behaviour in operating defective fuel", *Journal of Nuclear Materials*, **328** (2004), 180-196.

35. J.D. Higgs, B.J. Lewis, W.T. Thompson, and Z. He, "A conceptual model for the fuel oxidation of defective fuel", *Journal of Nuclear Materials*, **366** (2007), 99-128.

36. Oak Ridge National Laboratory, "SCALES-5", Radiation Safety information Computational Center, Oak Ridge, 2005.

37. H. Kleykamp and S.G. Kang, "The Constitution of the Uranium-Palladium and Uranium-Rhodium-Palladium Systems", *Zeitschrift für Metallkunde*, **82** (1991), 544-552.

38. K. Kurosaki and M. Uno, "Phase Equilibria in the Ternary URu_3-URh_3-UPd_3 System", *Journal of Alloys and Compounds*, **271–273** (1998), 641–644.

39. J.O.A. Paschoal, H. Kleykamp, and F. Thümmler, "The Constitution of the Ru-Rh System", *Journal of the Less-Common Metals*, **98** (1984), 279-284.

40. E. Raub, "Metals and Alloys of the Platinum Group", *Journal of the Less-Common Metals*, **1** (1959), 3-18.

41. A.A. Rudnitskii and R.S. Polyakova, "The Palladium-Ruthenium System", *Russian Journal of Inorganic Chemistry*, **4** [6] (June 1959), 631-636.

42. J.J. Park, "Uranium Phase Diagrams and a Solid Solubility Correlation", PhD Dissertation, University of Maryland, College Park, MD (1965).

43. M.H. Kaye, K.M. Jaansalu, and W.T. Thompson, "Phase Equilibrium in Metallic Systems", *Canadian Metallurgical Quarterly*, **42** (Oct. 2003), 393-410.

44. M. Margules, "Über die Zusammensetzung der gesättigten Dämpfe von Mischungen", *Sitzungsberichte der Kaiserliche Akadamie der Wissenschaften Wien Mathematisch-Naturwissenschaftliche Klasse*, **104** (1895), 1243-1278.

45. O. Redlich and A.T. Kister, "Algebraic representation of thermodynamic properties and the classification of solutions", *Industrial & Engineering Chemistry*, **40** (1948), 345-348.

46. Y.-M. Muggianu, M. Gambino and J.-P. Bros, "Enthalpies de formation des alliages liquides bismuth-étain-gallium à 723 K – choix d'une représentation analytique des grandeurs d'excès intégrales et partielles de mélange", *Journal de Chimie Physique*, **72** [1] (1975), 83-88.

47. F. Kohler, "Zur Berechnung der thermodynamischen Daten eines ternären Systems aus den zugehörigen binären Systemen", *Monatshefte für Chemie*, **91**, (1960), 738-740.

48. G.W. Toop, "Predicting Ternary Activities Using Binary Data", *Transactions of the Metallurgical Society of AIME*, **233** (1965), 850-855.

49. N. Saunders and A.P. Miodownik, CALPHAD: A Comprehensive Guide, Oxford: Elsevier Science Ltd., (1998).

50. L.S. Darken, "Application of the Gibbs-Duhem Equation to Ternary and Multicomponent Systems", *Journal of the American Chemical Society*, **72** (1950), 2909-2914.

51. C. Wagner, Thermodynamics of Alloys, London: Addison-Wesley Press, (1952).

52. R. Schuhmann, Jr., "Application of Gibbs-Duhem equations to ternary systems", *Acta Metallurgica*, **3** [3] (1955), 219-226.

53. N.A. Gokcen, "Application of Gibbs and Gibbs-Duhem Equations to Ternary and Multicomponent Systems", *Journal of Physical Chemistry*, **64** [4] (1960), 401-406.

54. M. Hillert, "Empirical methods of predicting and representing thermodynamic properties of ternary solution phases", *CALPHAD*, **4** [1] (1980), 1-12.

55. I. Ansara, C. Bernard, L. Kaufman, and P. Spencer, "A comparison of calculated phase equilibria in selected ternary alloy systems using thermodynamic values derived from different models", *CALPHAD*, **2** (1978), 1-15.

56. A.D. Pelton, "The Polynomial Representation of Thermodynamic Properties in Dilute Solutions", *Metallurgical and Materials Transaction B*, **28B** (1997), 869-876.

57. P. Chartrand and A.D. Pelton, "On the choice of 'Geometric' thermodynamic models", *Journal of Phase Equilibria*, **21** [2] (2000), 141-147.

58. D.A. Porter and K.E. Easterling, Phase Transitions in Metals and Alloys, Wokingham, VNR International, (1981).

59. L. Wang and M.H. Kaye, "A re-examination of thermodynamic modelling of U-Ru phase diagram", in *35th Annual Conference of the Canadian Nuclear Society*, Saint John, (2015).

60. H. Baker and H. Okamoto (Editors), ASM Handbook, Materials Park, Ohio: ASM International, (1992).

61. E.H.P. Cordfunke and R.J.M. Konings, Thermochemical Data for Reactor Materials and Fission Products, Elsevier Science Publishers, Amsterdam, (1990).

62. D.D. Wagman and F.D. Rossini, "Selected Values of Chemical Thermodynamic Properties", National Bureau of Standards Series 270, U.S. Department of Commerce, Washington, D.C., (1968-1971).

63. I. Barin, O. Knacke, and O. Kubaschewski, Thermochemical Properties of Inorganic Substances, Springer-Verlag, Berlin, (1977).

64. T.B. Massalski, Binary Alloy Phase Diagrams, **1** & **2**, American Society for Metals, Metals Park, Ohio, (1986).

65. R. Hultgren, R.L. Orr, D. Anderson, and K.K. Kelley, Selected Values of Thermodynamic Properties of Metals and Alloys, John Wiley and Sons, New York, New York, (1974).

66. R. Gürler, "A Computer Assessment of the Molybdenum-Palladium Phase Diagram", *Journal of Alloys and Compounds*, **191** (1993), 83-86.

67. R. Gürler, L.A. Cornish, and J.N. Pratt, "Computer Assessment of the Palladium-Rhodium System", *Journal of Alloys and Compounds*, **191** (1993), 165-168.

68. R. Gürler, "A Computer Assessment of the Ru-Rh and Ru-Pd Systems", *Journal of Alloys and Compounds*, **191** (1993), 31-35.

69. M.H. Rand and P.E. Potter, "Thermodynamics and Phase Diagrams of Mo-Pd-Ru and Related Systems", *Physics*, **103B** (1981), 21-30.

70. R. Gürler and J.N. Pratt, "A Computer Assessment of the Molybdenum-Rhodium Phase Diagram", *Journal of Alloys and Compounds*, **189** (1992), 97-100.

71. N. Lorenzelli and J.-P. Marcon, "Étude thermodynamique d'un combustible UC simulant un taux de combustion de 100.000 MWJ/t par mesure de vaporisation", *Journal of Nuclear Materials*, **44** (1972), 57-63.

72. G. Wijbenga, "The Enthalpy of Formation of UPd_3 by Fluorine Bomb Calorimetry", *Journal of Chemical Thermodynamics*, **14** (1982), 483-493.

73. F.R.de Boer, W.C.M. Mattens, R. Boom, A.R. Miedema, and A.K. Niessen, Cohesion in Metals: Transition Metal Alloys, North Holland: Elsevier Science Publishers B.V., Amsterdam, (1988).

74. W.-G. Jung and O.J. Klappa, "Enthalpies of formation of Me_3U (Me = Ru, Rh, Pd) by high-temperature reaction calorimetry", *Journal of Chemical Thermodynamics*, **23** (1991), 147-153.

75. H. Holleck and H. Kleykamp, "Phasengleichgewichte und thermodynamische untersuchungen im system uran-rhodium-kohlenstoff", *Journal of Nuclear Materials*, **45** (1972/73), 47-54.

76. J.G. Edwards, J.S. Starzynski, and D.E. Peterson, "Sublimation Thermodynamics of the URu_3 Compound", *Journal of Chemical Physics*, **73** [2] (1980), 908-912.

77. J. Huang, B. Tsuchiya, K. Konashi, and M. Yamawaki, "Thermodynamic analysis of chemical states of fission products in uranium-zirconium hydride fuel", *Journal of Nuclear Materials*, **294** (2001), 154-159.

78. T. Adachi, M. Ohnuki, N. Yoshida, T. Sonobe, W. Kawamura, H. Takeishi, K. Gunji, T. Kimura, T. Suzuki, Y. Nakahara, T. Muromura, Y. Kobayashi, H. Okashita, and T. Yamamoto, "Dissolution study of spent PWR fuel: Dissolution behaviour and chemical paroperties of insoluble residues", *Journal of Nuclear Materials*, **174 (**1990), 60-71.

79. C.H. Lee, M.Y. Suh, K.S. Choi, J.S. Kim, Y.J. Park, and W.H. Kim, "Determination of Ru, Rh, Pd, Te, Mo, and Zr in spent pressurized water reactor fuels by ion exchange and extraction chromatographic separations and inductively coupled plasma atomic emission spectrometric analysis", *Analytica Chimica Acta*, **475** (2003), 171-179.

80. B. Erdmann and C. Keller, "Actinide(lanthanide)-noble metal alloy phases, preparation and properties," *Journal of Solid State Chemistry*, **7** (1973), 40-48.

81. B. Johansson, O. Eriksson, M.S.S. Brooks, and H.L. Skriver, "Theoretical studies of actinide intermetallic compounds", *Inorganica Chimica Acta*, **140** (1987), 59-66.

82. K.A. McEwen, W.G. Stirling, C.K. Loong, G.H. Lander, and D. Fort, "Crystal-field excitations in polycrystalline $U(Pd_{1-x}Pt_x)_3$", *Journal of Magnetism and Magnetic Materials*, vols. **76** & **77** (1988), 426-428.

83. K. Kurosaki, H. Kobayashi, M. Uno, and S. Yamanaka, "Thermal conductivities of uranium intermetallic compounds", *Journal of Nuclear Science and Technology*, vol. Supplement **3** (2002), 811-814.

84. S. Yamanaka, K. Yamada, T. Tsuzuki, T. Iguchi, M. Katsura, Y. Hoshino, and W. Saiki, "Mechanical and thermal properties of uranium intermetallic compounds", *Journal of Alloys and Compounds*, **271-273** (1998), 549-556.

85. A. Schenck, D. Andreica, F.N. Gygax, M. Pinkpank, K.A. McEwen, and A. Amato, "Anomalous temperature dependence of the μ^+ Knight shift and the phase diagram of UPd_3", *Physica B*, **289-290** (2000), 311-315.

86. E.H.P. Cordfunke, R.P. Muis, G. Wijbenga, R. Burriel, M. To, H. Zainel, and E.F. Westrum, Jr., "Thermodynamics of Uranium Intermetallic Compounds- I. Heat Capacities of URu_3 and URh_3 from 5 to 850 K", *Journal of Chemical Thermodynamics*, **17** (1985), 1035-1044.

87. R. Burriel, M. To, H. Zainel, E.F. Westrum, Jr., E.H.P. Cordfunke, R.P. Muis, and G. Wijbenga, "Thermodynamics of Uranium Intermetallic Compounds- II. Heat

Capacity of UPd_3 from 8 to 850 K", *Journal of Chemical Thermodynamics*, **20** (1988), 815-823.

88. H. Kopp, "Investigations of the Specific Heat of Solid Bodies", *Philisophical Transactions of the Royal Society of London*, **155** (1865), 71-202.

89. J. Leitner, P. Voňka, D. Sedmidubský, and P. Svoboda, "Application of Neumann-Kopp rule for the estimation of heat capcity of mixed oxides", *Thermochimica Acta*, **497** [1-2] (2010), 7-13.

90. R. Prasad, S. Dash, S.C. Parida, Z. Singh, and V. Venugopal, "Gibbs Energy of Formation of UPd_3 (s)", *Journal of Nuclear Materials*, **277** (2000), 45-48.

91. G. Wijbenga and E.H.P. Cordfunke, "Determination of Standard Gibbs Energies of Formation of URh_3 and URu_3 by Solid-State e.m.f. Measurements", *Journal of Chemical Thermodynamics*, **14** (1982), 409-417.

92. J.A. Catterall, J.D. Grogan, and R.J. Pleasance, "The system uranium-palladium", *Journal of the Institute of Metals*, **85** (1956), 63-67.

93. G.I. Terekhov, S.I. Sinyakova, M.V. Vendernikov, and O.S. Ivanov, "Phase diagram of the palladium side of the uranium-palladium system", in Physical Chemistry of Alloys and Refractory Compounds of Thorium and Uranium, ed. O.S. Ivanov, Academy of Sciences of the USSR, Moscow (1968); translated into English by Jerusalem, Keter Press (1972), 118-122.

94. H.H. Chiswik, A.E. Dwight, L.T. Lloyd, M.V. Nevitt, and S.T. Zegler, in *Proceeding of the 2nd International Conference on Peaceful Uses of Atomic Energy*, Geneva, (1958), 1-35.

95. J.J. Park, "Reactions of Uranium with the Platinide Elements (I and II)", *Journal of Research of the National Bureau of Standards-A. Physics and Chemistry*, **72** [1] (1968), 1-17.

96. M.G. Naraine and H.B. Bell, "Thermodynamic and phase behaviour in the U-Rh-C system", *Journal of Nuclear Materials*, **50** (1974), 83-90.

97. J.O.A. Paschoal, H. Kleykamp, and F. Thümmler, "Phase Equilibria in the Quaternary Molybdenum-Ruthenium-Rhodium-Palladium System", *Zeitschrift Fuer Metallkunde*, **74** (1983), 652-664.

98. J.J. Park and R.W. Buzzard, "Constitution of Uranium and the Platinum Metals", United States Atomic Energy Commission, Ames, (1956), 89-102.

99. J.J. Park, D.P. Fickle, and L.R. Mullen, "The uranium-palladium system", U.S. Department of Commerce: National Bureau of Standards Report 8120, Washington, DC, (1963).

100. G.P. Pells, "The Palladium-Uranium Phase Diagram up to 25 at.% Uranium", *Journal of the Institute of Metals*, **92** (1963-64), 416-418.

101. F.A. Rough and A.A. Bauer, "Constitution of Uranium and Thorium Alloys", Battelle Memorial Institute, Columbus OH, (1958).

102. A.A. Abou-Zahra and F.H. Hammad, "The uranium-rich region of the uranium-ruthenium binary system", *Journal of the Less-Common Metals*, **48** (1976), 177-181.

103. R.F. Hills, B.W. Howlett, B.R. Butcher and D. Stewart, "The effect of cooling rate and composition on the transformation of the Gamma-phase in uranium ruthenium alloys (with an appendix on ruthenium as a grain-refining element)", *Journal of Nuclear Materials,* **16** (1965), 109-128.

104. J.I. Bramman, R.M. Sharpe, D. Thom, and G. Yates, "Metallic fission-product inclusions in irradiated oxide fuels", *Journal of Nuclear Materials*, **25** (1968), 201-215.

105. M. Uno, K. Kurosaki, and A. Nakamura, "Reactions of uranium nitride with platinum-family metals", *Journal of Nuclear Materials*, **247** (1997), 322-327.

106. K. Kurosaki and M. Uno, "Formation of the Cu_3Au type solid solution of UPd_3 by doping a small amount of URu_3", *Journal of Alloys and Compounds*, **274** (1998), 222-228.

107. J. Gibbs, Scientific Papers of J. Willard Gibbs, **1 & 2**, London, New York and Bombay: Longmans, Green and Co., (1906).

108. L. Kaufman and H. Bernstein, Computer Calculation of Phase Diagrams, New York and London: Academic Press, (1970).

109. C.W. Bale, E. Bélisle, P. Chartrand, S.A. Decterov, G. Eriksson, K. Hack, I.-H. Jung, Y.-B. Kang, J. Melançon, A.D. Pelton, C. Robelin, and S. Petersen, "FactSage thermochemical software and databases – recent developments", *CALPHAD*, **33** (2009), 295-311.

110. C.W. Bale, E. Bélisle, P. Chartrand, S.A. Decterov, G. Eriksson, A.E. Gheribi, K. Hack, I.-H. Jung, Y.-B. Kang, J. Melançon, A.D. Pelton, S. Petersen, C. Robelin, J. Sangster, P. Spencer, and M-A. VanEnde, "FactSage thermochemical software and databases, 2010–2016", *CALPHAD*, **54** (2016) 35-53.

111. H. L. Lukas, S.G. Fries and B. Sundman, Computational Thermodynamics: The CALPHAD Method, Cambridge: Cambridge University Press, 2007, 110-111.

112. H. Okamoto, "Pd-U (Palladium-Uranium)", *Journal of Phase Equilibria*, **14** [2] (1993), 264-265.

113. R. Buzzard, "Beryllium and uranium system", *Journal of Research of the National Bureau of Standards,* **50** [2] (1953), 63-67.

114. V. Raghavan, "Al-Co-U (Aluminum-Cobalt-Uranium)", *Journal of Phase Equilibria and Diffusion*, **30** [3] (2009), 268-269.

115. B.A.S. Ross and D.E. Peterson, "The Pt-U (Platinum-Uranium) System", *Bulletin of Alloy Phase Diagrams,* **11** [3] (1990), 240-243.

116. T. Nishioka, K. Kimura, M. Kontani, H.A. Katori, and T. Goto, "Magnetic properties of U_5Pd_6", *Journal of the Physical Society of Japan,* **63** [7] (1994), 2503-2506.

117. H. Okamoto and T.B. Massalski, “Phase relationships and thermodynamic modelling in several binary systems based on gold”, in Noble Metal Alloys: Phase Diagram, Alloy Phase Stability, Thermodynamic Aspects, Properties and Special Features, Warrendale, The Metallurgical Society, 1986, 265-288.

118. A. Palenzona and S. Cirafici, “The phase diagram of the U-Au system”, *Journal of the Less-Common Metals*, **143** (1988), 167-171.

119. L.E. Tanner and H. Okamoto, “The Be-Pd (Beryllium-Palladium) System”, *Bulletin of Alloy Phase Diagrams*, **8** [4] (1987), 389-392.

120. J.M. Dubois, “An introduction to complex metallic alloys and to the CMA Network of Excellence”, in *Basics of Thermodynamics and Phase Transition in Complex Intermetallics*, New Jersey, London, Singapore, Beijing, Shanghai, Hong Kong, Taipei, Chennai, World Scientific, 2008, 1-29.

121. J. Dshemuchadse and W. Steurer, “More statistics on intermetallic compounds - ternary phases”, *Acta Crystallographica.*, **A71** (2015), 335-345.

122. P.R. Alonso, P.H. Gargano, and G.H. Rubiolo, “First principles calculation of the Al_3U-Si_3U pseudobinary fcc phase equilibrium diagram”, *CALPHAD: Computer Coupling of Phase Diagrams and Thermochemistry*, **38** (2012), 117-121.

123. D. Rabin, R.Z. Shneck, G. Rafailov, I. Dahan, L. Meshi, and E. Brosh, “Thermodynamic modeling of Al–U–X (X = Si,Zr)”, *Journal of Nuclear Materials*, **464** (2015), 170-184.

124. E. Graper, “Evaporation Guide for the Elements”, Lebow Corporation, Albrecht Fischer of VTS-CreaTec Gmbh, Christian Bradley of Oxford Scientific and Dietrich von Diemar of Specs Scientific, 2008. [Online]. Available: http://www.oxford-vacuum.com/background/thin_film/reference_data.pdf. [Accessed 16 7 2015].

125. E.C. Buck, E.J. Mausolf, B.K. McNamara, C.Z. Soderquist, and J.M. Schwantes, “Nanostructure of metallic particles in light water reactor used nuclear fuel”, *Journal of Nuclear Materials*, **461** (2015), 236–243.

126. S.H. Vosko, L. Wilk, and M. Nusair, “Accurate spin-dependent electron liquid correlation energies for local spin density calculations: a critical analysis”, *Canadian Journal of Physics*, **58** (1980), 1200-1211.

127. “Atomic Reference Data for Electronic Structure Calculations”, Physical Measurement Laboratory, NIST, 1997. [Online]. Available: http://physics.nist.gov/PhysRefData/DFTdata/Tables/ptable.html. [Accessed 17 7 2015].

128. H.U. Borgstedt and H. Vedemeyer, GMELIN Handbook of Inorganic Chemistry: U Supplement, Berlin: Springer-Verlag, 1989.

129. D.R. Lide, CRC Handbook of Chemistry and Physics, 81st edition, Boca Raton: CRC Press, (2000-2001).

130. C.E. Housecroft and A.G. Sharpe, Inorganic Chemistry, Harlow: Pearon Education Limited, 2005.

131. C.W. Bale, P. Chartrand, S.A. Degterov, G. Eriksson, K. Hack, R.B. Mahfoud, J. Melançon, A.D. Pelton, and S. Petersen, "FactSage thermodynamical software and databases", *CALPHAD,* **26** [2] (2002), 189-228.

132. A.G. Croff, "ORIGIN2 - A Revised and Update Version of the Oak Ridge Isotope Generation and Depletion Code", ORNO-5621, Oak Ridge, 1980.

133. M.H. Kaye and L. Wang, "A Proposed Catalytic Mechanism of Pd on the Formation of UBe_{13} in Experimental Construction of U-Pd Phase Diagrams", in *Proceedings of the 37th Annual Conference of the Canadian Nuclear Society*, Niagara Falls, (June 2017).